PERFORMANCE ANALYSIS OF 5G AND BEYOND WIRELESS SYSTEMS

A THESIS

SUBMITTED TO THE DELHI TECHNOLOGICAL UNIVERSITY

FOR THE AWARD OF THE DEGREE OF

DOCTOR OF PHILOSOPHY

IN

Computer Science & Engineering

SUBMITTED BY

MANPREET KAUR

DEPARTMENT OF COMPUTER SCIENCE & ENGINEERING

DELHI TECHNOLOGICAL UNIVERSITY

DELHI- 110042 (INDIA)

APRIL 2023

DELHI TECHNOLOGICAL UNIVERSITY

CERTIFICATE

This is to certify that the thesis entitled **"PERFORMANCE ANALYSIS OF 5G AND BEYOND WIRELESS SYSTEMS"** being submitted by Manpreet Kaur (Reg. No.: 2K19/PhD/CO/06) for the award of degree of Doctor of Philosophy to the Delhi Technological University is based on the original research work carried out by him/her. She has worked under my supervision and has fulfilled the requirements which to my knowledge have reached the requisite standard for the submission of this thesis. It is further certified that the work embodied in this thesis has neither partially nor fully submitted to any other university or institution for the award of any degree or diploma.

Dr. Rajesh Kumar Yadav
(Supervisor)
Assistant Professor,
Department of CSE,
DTU-Delhi, India

ACKNOWLEDGEMENT

ABSTRACT

With the recent advancements in wireless communication, there has been tremendous growth in the applications such as body area communication, vehicular communication and device-to-device (D2D) communication etc. In most of these future generation applications, the data is transferred from source to destination through a wireless link. The signal experience many phenomena like reflection, refraction, diffraction and scattering in its path traveling from transmitter (Tx) to receiver (Rx). These phenomena result in the fluctuations in the received signal strength which eventually degrades the quality of the signal and is termed as fading. Fading can be classified as small-scale fading and large-scale fading. To characterize the small-scale fading and large-scale fading, different mathematical models are used in literature.

The size of the mobile cells in third/fourth generation (3G/4G) wireless technologies was relatively large, thus the signal propagation scenario was thought to be outdoor propagation and various models such as Rayleigh, Rician, Nakagami, Weibull etc. were used to model that scenario.

One of the main objectives of the fifth generation (5G) wireless networks is to provide high throughput and low latency to all users anywhere within the coverage area. However, because of the high attenuation provided by the structures' walls, delivering reliable services to consumers inside the buildings remains a serious challenge. The creation of a heterogeneous cellular network, in which a macro-cell is overlaid over a number of femtocells, dedicated to providing coverage for indoor users, is an effective approach that has recently been embraced by numerous standards. Femtocells are small,

low power cellular BS, which can be installed in a small business environment or a home to provide better coverage with improved battery life for the mobile stations. Due to the small areas of the femtocells, the characterization of the signal cannot be modeled in the form of traditional outdoor propagation models.

For addressing the propagation phenomenon in 5G and beyond technology, Beaulieu-Xie (BX) and Fisher-Snedecor F (FSF) distributions are introduced. The BX fading channel has found application in the signal propagation in small buildings and fast-moving trains. FSF fading channel is a composite fading model that is used to model the signal propagation for D2D and wearable communication links.

The performance of communication system inside the densely packed small cells or femtocells with maximum ratio combining (MRC) diversity is studied. The closed-form expressions for outage probability (Pout), amount of fading (AF) and average symbol error probability (ASEP) for coherent and non-coherent modulation schemes are derived for the said channel. Further, the channel capacity (CC) analysis over different transmission policies is performed and the corresponding results are plotted. The effect of diversity on the performance measures are demonstrated.

In contrary to Shannon's ergodic capacity, the delay-constrained effective rate is used to define the maximum data rate of the real-time applications in 5G and beyond networks. We have studied the effective throughput performance of the multi-antenna system over the BX fading channel and FSF fading channel. The closed-form mathematical expressions for the effective capacity (EC) are derived in terms of Meijer-G function and the effect of different fading parameters on the effective throughput of the system is

demonstrated. The simplified asymptotic expression for high signal-to-noise ratio (SNR) and low SNR regimes is provided to gain more insight in to the system.

The intelligent reflecting surfaces (IRS) is a newer technology that is being used in 5G and beyond networks to improve the system performance. Due to this, the IRS-aided systems have been actively investigated. The application of the derived formulation for the IRS-aided system over the BX and SFS channels are studied. Interesting results of the system performance in terms of channel parameters are demonstrated.

For the expressions having infinite series representation, the truncation error has been provided wherever possible. The effect of fading parameters on the performance measures are demonstrated through analytical results. Simulation results are corroborated along with the numerical results to verify the correctness of the proposed formulations. The results presented in this study can be used in designing the communication systems for real-time applications in next-generation wireless networks.

LIST OF PUBLICATIONS

Published

1. **Manpreet Kaur,** R.K. Yadav, Performance analysis of Beaulieu-Xie fading channel with MRC diversity reception. *Transactions on Emerging Telecommunications Technology (Wiley & Sons)*, 31: e3949, 2020. https://doi.org/10.1002/ett.3949 **(SCI journal with Impact factor- 3.310).**

2. **Manpreet Kaur,** R.K. Yadav, Effective Capacity Analysis Over Fisher-Snedecor F Fading Channels with MRC Reception. *Wireless Personal Communications, (Springer)*, 121, 1693–1705, 2021. 10.1007/s11277-021-08692-w. **(SCI journal with Impact factor- 2.017).**

3. **Manpreet Kaur,** R.K. Yadav, EC Analysis of Multi-Antenna System over 5G and Beyond Networks and its Application to IRS-Assisted Wireless Systems. *Wireless Personal Communications, (Springer)*, 124, 1861-1881, 2022. 10.1007/s11277-021-09434-8. **(SCI journal with Impact factor- 2.017).**

4. S. Kumar, P. Yadav, **Manpreet Kaur**, R. Kumar, A survey on IRS NOMA integrated communication networks. *Telecommunication Systems, (Springer)*, 80, 277–302 2022. https://doi.org/10.1007/s11235-022-00898-y **(SCI journal with impact factor: 2.336**)

5. S. Kumar, P.S. Chauhan, R. Bansal, **Manpreet Kaur**, R. K. Yadav, Performance Analysis of CSS Over α–η–μ and α–κ–μ Fading Channel Using Clustering-Based Technique. *Wireless Personal Communications, (Springer)*, 126, 3595-3610, 2022. https://doi.org/10.1007/s11277-022-09880-y **(SCI journal with impact factor: 2.017**)

6. **Manpreet Kaur,** R.K. Yadav, Data rate over different applications in 5G and beyond Networks, *IEEE International Conference on Electronics and Sustainable Communication Systems (ICESC)*, Coimbatore, India, 997-1004, 2021. 10.1109/ICESC51422.2021.9532961.

7. **Manpreet Kaur,** R.K. Yadav, Throughput Analysis of RIS-Aided Wireless System over Fisher-Snedecor Composite channel, *IEEE International Delhi Section Conference (DELCON), New Delhi, India* 1-8, 2022. 10.1109/DELCON54057.2022.9753655.

Under Review

1. On the Effective throughput of Shadowed Beaulieu-Xie fading channel. (Submitted for possible publication)

2. Effective Capacity Analysis over Cascaded Rayleigh Fading Channels with Arbitrary Correlation. (Submitted for possible publication)

TABLE OF CONTENT

LIST OF TABLES

LIST OF FIGURES

LIST OF ACRONYMS

1G	1st Generation
2G	2nd Generation
3G	3rd Generation
4G	4th Generation
5G	5th Generation
6G	6th generation
ABEP	Average Bit Error Probability
ABER	Average Bit Error Rate
ACC	Average Channel Capacity
AF	Amount of Fading
ASEP	Average Symbol Error Probability
AWGN	Additive White Gaussian Noise
BER	Bit Error Rate
BS	Base Station
BX	Beaulieu-Xie
CC	Channel Capacity
CDF	Cumulative Distribution Function
CDI	Channel Distribution Information
CIFR	Channel Inversion with Fixed-Rate
CRN	Cognitive Radio Network
CSI	Channel State Information
DF	Delay-And-Forward

D2D	Device-To-Device
EC	Effective Capacity
EGC	Equal Gain Combining
FIFO	First-In-First-Out
FSF	Fisher-Snedecor F
FSO	Free-Space Optics
FTR	Fluctuating Two Rays
GSC	Generalized Selection Combining
IoT	Internet-Of-Thing
i.i.d	independent and identically distributed
i.n.i.d	independent and non-identically distributed
IRS	Intelligent Reflecting Surfaces
Kms.	Kilometers
LOS	Line of Sight
M-FSK	Multiple Frequency Shift Keying
MGF	Moment Generating Function
MHz	Mega Hertz
MIMO	Multiple Input Multiple Output
MISO	Multiple Input Single Output
M-QAM	M-ary quadrature amplitude modulation

MRC	Maximal Ratio Combining
NOMA	Non-Orthogonal Multiple Access
NLOS	Non-Line-Of-Sight
OFDM	Orthogonal Frequency-Division Multiplexing
OPRA	Optimal power and rate adaption
ORA	Optimum Rate Adaptation
PDF	Probability Density Function
PLS	Physical Layer Security
P_{out}	Outage Probability
QoS	Quality of Services
RF	Radio Frequency
RIS	Reconfigurable Intelligent Surfaces
RV	Random Variable
Rx	Receiver
SER	Symbol error rate
SC	Selection Combining
SNR	Signal to Noise Ratio
SU	Secondary User
STBC	Space-Time-Block-Codes
TIFR	Truncated CIFR
TWDP	Two Wave Diffused Power
Tx	Transmitter

UAV	Unmanned Aerial Vehicle
VANET	Vehicular Ad-Hoc Network
V2V	Vehicle-To-Vehicle
VoIP	Voice over IP
WBAN	Wireless Body Area Network
WSN	Wireless Sensor Network
W/LN	Weibull/Lognormal

LIST OF SYMBOLS

$I_0(.)$ — modified Bessel function of first kind and order zero

$\log_e(.)$ — natural log

$\log_2(.)$ — logarithm with base 2

$\Gamma(.)$ — gamma function

$\sum_{i=1}^{N}(.)$ — summation

$E[.]$ — expectation operator

$\Gamma(a,b) = \int_{b}^{\infty} t^{a-1} \exp(-t) dt$ — upper incomplete gamma function

$Y(a,b) = \int_{0}^{b} t^{a-1} \exp(-t) dt$ — lower incomplete gamma function

$_1F_1(.;.;.)$ — confluent hypergeometric function

$_0F_1(;;.)$ — confluent hypergeometric function

$(x)_n$ — Pochhammer's symbol

$Q(.)$ — Q-function

$C(d,r)$ — combination of r objects from a set of d objects

$Q_u(.;.)$ — Marcum-Q function of order u

$\exp(.)$	exponential
$L_n^{\alpha}(.)$	nth-order Laguerre polynomial
$M_{a,b}(.)$	Whittaker function
$\phi_2^{(L)}(.;.;.)$	confluent multivariate hypergeometric function
$\phi_2(.;.;.)$	confluent bivariate hypergeometric function
$G_{p,q}^{m,n}(.)$	Meijer-G function
$U(.;.;.)$	Tricomi's function
$f_\gamma(\gamma)$	distribution function of the fading channel
$B(.,.)$	beta function
$_2F_1(.,.;.;.)$	Gauss hypergeometric function
$E_i(.)$	exponential integral function
M'_{γ_D}	1st derivative of end-to-end SNR
$M(s)$	Moment generating function

CHAPTER 1

INTRODUCTION

Depending upon the dimension of the obstructions, the signal experiences different phenomenon like reflection, diffraction and scattering etc., while traveling from Tx to Rx. In the designing of a communication system, the QoS parameters are evaluated and their performances in terms of channel fading parameters are studied. For this, we need to model the wireless channel between the Tx and the Rx. Different channel models are present in literature, which are applicable to different propagation scenarios. This chapter discusses different fading channels, the measures to mitigate the detrimental effect of fading and the performance parameters of the wireless communication systems. In the final section, the main contribution and organization of thesis is elaborated.

1.1   Multipath Fading

Small-scale fading is also known as multipath fading. In this phenomenon, multiple replicas of the same transmitted information reach the Rx at different time instances. Due to multipath fading, the overall quality of the signal is degraded. The variation of fading is very in-deterministic, and hence it is difficult to have an accurate model of fading. However, many researchers have given a number of mathematical models to characterize the effect of fading. These models depend upon the different environments and can be described by different statistical distributions. Some of the common multipath fading models are described below.

1.1.1   Traditional Models

In the earlier mobile technology generations (1G-4G), the maximum distance from BS to the mobile users was large (approximately in Kms.) and the signal propagation from the BS to the mobile user was outdoor propagation. Depending upon the propagation scenario, the channel between the BS and the mobile users were modeled in the form of traditional distribution functions as discussed below.

1. **Rayleigh:** Rayleigh distribution is used to model the communication scenario, when independent scatters are very large and there is no LOS component of the signal present at the Rx. The PDF of γ following the Rayleigh distribution is given by [1] as

$$f_\gamma(\gamma) = \frac{1}{\bar{\gamma}} \exp\left(-\frac{\gamma}{\bar{\gamma}}\right), \qquad \gamma \geq 0 \tag{1.1}$$

   here $\bar{\gamma}$ is average received SNR and γ is instantaneous received SNR.

2. **Nakagami-*m*:** Nakagami-m distribution is used to model ionosphere radio land-mobile and indoor-mobile propagation links [1]. The PDF of γ following the Nakagami-*m* distribution is given by [1] as

$$f_\gamma(\gamma) = \frac{(m_{nak})^{m_{nak}} \gamma^{(m_{nak}-1)}}{\bar{\gamma}^{m_{nak}} \Gamma(m_{nak})} \exp\left(-\frac{\gamma m_{nak}}{\bar{\gamma}}\right), \qquad \gamma \geq 0, \ \frac{1}{2} \leq m_{nak} \tag{1.2}$$

   where m_{nak} is the Nakagami-m fading parameter.

3. **Nakagami-*n* (Rice):** Rice is used to model propagation path when there exists a strong LOS path component along with random weak components. The PDF of γ following the Rice is given by [1] as

$$f_\gamma(\gamma) = \frac{\left(1 + n_{nak}{}^2\right)\exp\left(-n_{nak}{}^2\right)}{\overline{\gamma}}\exp\left(-\frac{\gamma\left(1 + n_{nak}{}^2\right)}{\overline{\gamma}}\right), \qquad \gamma \geq 0, \ 0 \leq n_{nak} \qquad (1.3)$$

where n_{nak} is the Nakagami-*n* fading parameter.

4. **Nakagami-*q* (Hoyt):** This distribution is used to model the propagation channel with more severe fading conditions. The PDF of γ following Hoyt distribution is given by [1] as

$$f_\gamma(\gamma) = \frac{\left(1 + q^2\right)}{2q\overline{\gamma}}\exp\left(-\frac{\gamma\left(1 + q^2\right)^2}{4q^2\overline{\gamma}}\right)I_0\left(\frac{\gamma\left(1 - q^4\right)}{4q^2\overline{\gamma}}\right), \qquad \gamma \geq 0, \ 0 \leq q \leq 1 \qquad (1.4)$$

where *q* is the Nakagami-*q* fading parameter.

5. **Weibull:** Another important fading distribution which is used to model radio system in 800-900 MHz frequency range is Weibull distribution. The PDF of γ following Weibull distribution is given by [1] as

$$f_\gamma(\gamma) = \frac{c}{2}\left(\frac{\Gamma\left(1 + \frac{2}{c}\right)}{\overline{\gamma}}\right)^{\frac{c}{2}}\gamma^{\left(\frac{c}{2}-1\right)}\exp\left[-\left(\frac{\gamma}{\overline{\gamma}}\Gamma\left(1 + \frac{2}{c}\right)\right)^2\right], \qquad \gamma \geq 0 \qquad (1.5)$$

where c is the shape parameter.

1.1.2   5G Fading Models

With the requirements of high data rate and low latency networks in next-generation 5G technologies, the concept of densely packed small cells or femtocells is introduced to

fulfil the demand of the traffic. Femtocells are small, low power cellular BS which can be installed in a small business environment or a home to provide better coverage with improved battery life for the mobile stations [2]. Due to the small areas of the femtocells, the characterization of the signal inside the femtocells cannot be considered as outdoor propagation model. For addressing different propagation phenomenon of multiple LOS components along with the diffused power components inside a femtocell, a new fading model for indoor propagation namely BX is proposed in [3]. The PDF of γ following BX distribution is given by [3] as

$$f_\gamma\left(\gamma\right)=\frac{\eta^{\frac{m+1}{2}}\gamma^{\frac{m-1}{2}}}{(mk)^{\frac{m-1}{2}}}\exp\left(-(mk+\eta\gamma)\right)I_{m-1}\left(2\sqrt{mk\eta\gamma}\right) \tag{1.6}$$

where m, λ are severity fading parameter and non-centrality parameters.

1.2 Shadowing

Large obstacles between the Tx and Rx like buildings and towers are the main cause of shadowing. Some of the common shadowing fading models are described below.

Lognormal: There is a general consensus among the researchers that shadowing can be best modeled in the form of lognormal distribution with the PDF of γ given by [1] as

$$f_\gamma\left(\gamma\right)=\frac{1}{\sigma\gamma\sqrt{2\pi}}\exp\left(-\frac{\left(\log_e\gamma-\mu\right)^2}{2\sigma^2}\right) \tag{1.7}$$

where μ is the mean and σ is the standard deviation of RV $\log_e\gamma$.

Gamma: Representing shadowing using the lognormal PDF often leads to analytical difficulty in deriving the closed-form expressions when combined with other functions. Gamma distribution is the most acceptable approximation of lognormal distribution and is most widely used in literature to model shadowing effects. The PDF of gamma distribution is given by [1] as

$$p_\gamma(\gamma) = \frac{m^m \gamma^{(m-1)}}{\bar{\gamma}^m \Gamma(m)} \exp\left(-\frac{m\gamma}{\bar{\gamma}}\right), \qquad \gamma \geq 0 \tag{1.8}$$

Inverse Gaussian: Inverse Gaussian distribution is also used to model shadowing because of its closeness with the lognormal distribution [4].

1.3   Composite Fading

In practical wireless communication scenarios, the signal propagation is affected by the simultaneous occurrence of multipath and shadowing effects called as composite fading. Composite fading models being the more realistic channel are used for accurate modeling of wireless channels. Different composite fading channels are used in literature to study the performance of wireless systems.

1.4   Diversity Combining

Diversity is a reception combining technique which is used to overcome the effect of fading. By transmitting the signal over more than one path, the probability that each signal will receive the same deep fade is reduced. Various diversity combining techniques are popular in literature.

1.4.1   Selection Combining

SC is a diversity combining scheme in which one branch with max. SNR among all the available branches is selected [5]. The block diagram of SC scheme is shown in figure 1.1.
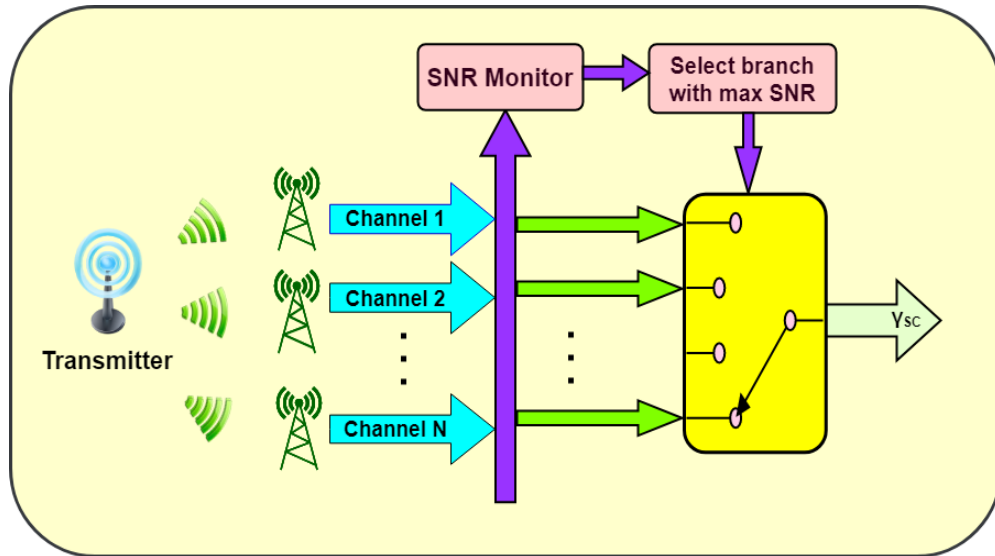
Figure 1.1 Selection Combining schematic

The branch with the highest instantaneous SNR is connected to output demodulator. SC performs detection of only one signal having the highest SNR. Therefore, it is the scheme that offers least complexity.

1.4.2   Equal gain Combining

EGC is the simplified version of the MRC technique. In this, the overall SNR at the output of the combiner is the addition of all branches SNR and the gain of all the branches are set to be one. Thus, it produces SNR at the combined output lower than that of MRC.

1.4.3   Maximal ratio Combining

In MRC technique each branch signal is multiplied with a gain weight factor which is proportional to the SNR of the channel **[6]**.
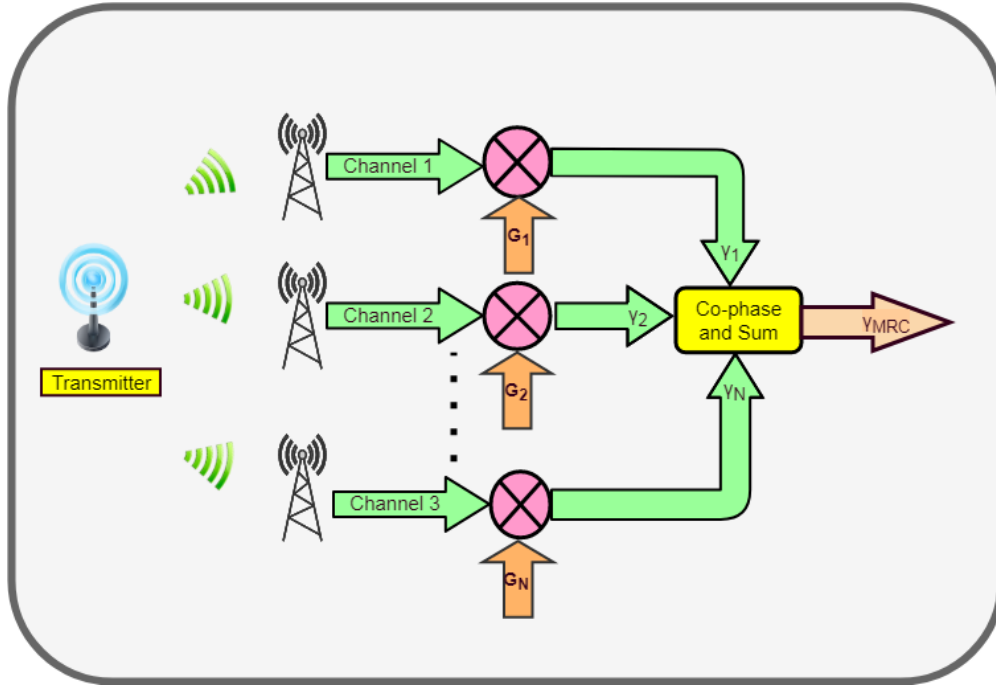
Figure 1.2 MRC Combining scheme

The channel having better fading condition shall be assigned with high weight. The pictorial representation of MRC is shown in figure 1.2. This is considered as the most complex scheme as the SNR of all the branches are optimally combined at the Rx. Here all the signals on *N* branches are weighted according to their individual SNR and then summed.

1.5   Performance Measures of the System

Outage Probability: It is the probability that the received SNR falls below a particular threshold (γ_{th}). The P_{out} can be defined as

$$Pout = \int_{0}^{\gamma_{th}} f_{\gamma}(\gamma)d\gamma \tag{1.8}$$

Amount of Fading: AF is a measure of the severity of the channel and is defined as

$$AF = \frac{E[\gamma^2]}{E[\gamma]^2 - 1} \tag{1.9}$$

ASEP/ABEP: For evaluating the performance as well as to get a better understanding of wireless communication system behavior, ASEP is widely used metrics. In case of fading channels, ASEP can be mathematically calculated out by averaging the instantaneous error probability and is given by

$$\bar{P} = E[P(\gamma)] = \int_{0}^{\infty} P(\gamma)f_{\gamma}(\gamma)d\gamma \tag{1.10}$$

where $P(\gamma)$ is the instantaneous symbol error probability, which depends upon the modulation techniques used in the communication system.

Channel Capacity: Shannon derived the CC formula and showed that reliable data transmission is possible if the transmitting rate does not exceed the CC. The reliable data transmission corresponds to achieve arbitrarily small error probability. Shannon capacity with regards to wireless channels of interest is obscure and depends on the channel condition as well as on the channel information at Tx and/or Rx. In wireless communication having the information about the channel properties of the communication link is termed as CSI. The CC model following Shannon's theorem is shown in figure 1.3.
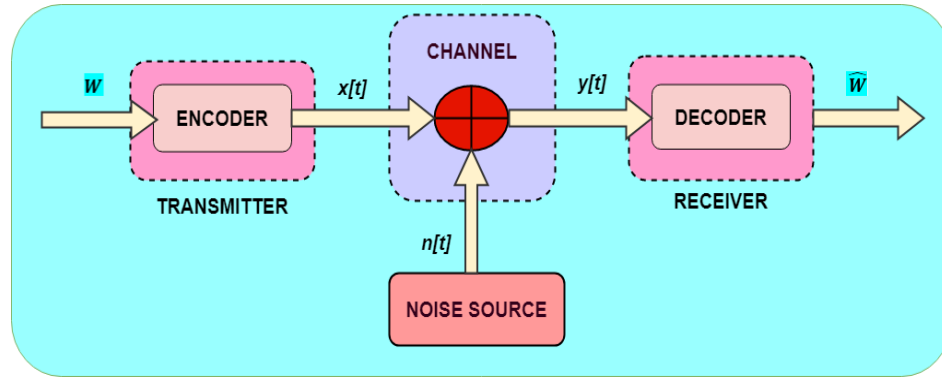
Figure 1.3 Shannon CC model

The information about the signal propagation between the Tx and the Rx and the related effect of fading can be estimated if CSI is known. The following scenarios are given to estimate the CC.

i. *CDI:* In this scheme, the channel gain distribution is known to both Tx and Rx.

ii. *Receiver CSI:* In this scheme, the CSI is known to the Rx and the channel gain distribution is known to both Tx and Rx.

iii. *CSI at both Tx and Rx:* In this case both the Tx and Rx have CSI and Tx adjusts its transmission methodology according to the CSI as shown in figure 1.4.
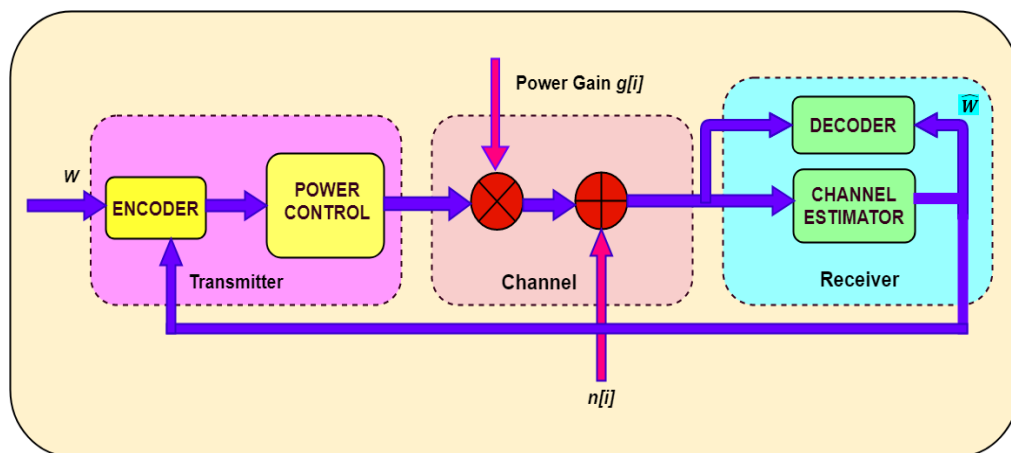
Figure 1.4 Channel with Tx and Rx CSI

Effective Capacity: In traditional communication systems, throughput was considered the only QoS parameter and ergodic capacity was used to characterize the effective data rate. Now with the emergence of real-time applications like video conferencing, smart grid network and online interactive gaming, not only the throughput but the delay sensitivity of the communication system has gain importance for the system designer. Shannon capacity is not able to characterize the effective rate of a system, when delay constraint is considered as a QoS parameter. To account for the delay performance of the real-time systems, the effective rate was proposed in [7]. EC can be defined as the maximum rate of data transfer that a wireless communication system can support with a guaranteed delay bound QoS constraint. For the fading channel, the EC that can be supported under a statistical QoS constraint can be expressed as

$$R(\theta) = -\frac{1}{A} \log_2 \left[E\left\{ (1+\gamma)^{-A} \right\} \right] = -\frac{1}{A} \log_2 \left[\int_o^\infty (1+\gamma)^{-A} f_\gamma(\gamma) d\gamma \right] \tag{1.11}$$

where *A* denotes the metric of the delay constraint and mathematically can be given a $A = \theta T B / \ln(2)$, in which θ is the delay exponent, *T* is a block length. A larger value of θ means stringent QoS whereas a smaller value of θ exhibits lenient QoS requirement and when $EC = Shannon's\, Ergodic\, capacity$. It means that the system can tolerate larger $_{\theta \to 0}$

delays when it is not bounded by the delay constraints.

1.6   Thesis Organization and Contributions

In this thesis, the performance analysis of 5G and beyond wireless systems is performed. The thesis work is divided into different chapters. Chapter wise contribution of the thesis is as follows:

Chapter 2: Literature Review

- A detailed and exhaustive literature survey is presented for the various approaches and techniques used to evaluate the performance of communication systems in different fading channels.

- Performance of various fading models in different applications of 5G and beyond networks are surveyed. Based on the literature survey, research gaps are identified, and research objective of the thesis is formulated.

Chapter 3: Performance Analysis of Beaulieu-Xie Fading Channel with MRC combining

- BX fading channel model and its performance analysis over MRC diversity is studied.

- The closed-form mathematical expressions for the performance parameters like P_{out}, AF, CC and ASEP/ABEP (coherent/non-coherent detections) over the BX fading channel are derived. The capacity performance over different transmission policies is performed.

- The effect of diversity and other fading parameters on the system performance measures are demonstrated through numerical simulations.

Chapter 4: Performance Analysis of EC over Beaulieu-Xie Fading Channel with Multi-antenna system

- The effective throughput performance of the multi-antenna system over the BX fading channel is studied.

- The simplified high-SNR and low-SNR expressions are proposed that enables direct interpretation of the system behaviour.

Chapter 5: Performance Analysis of EC over Fisher-Snedecor *F* Fading Channel with MRC diversity reception

- The EC performance of the delay sensitive communication system over FSF fading channel with maximum ratio combining is studied.

- The closed-form mathematical expressions for the EC are derived in terms of Meijer G-function and the effect of different fading parameters on the effective throughput of the system is demonstrated.

Chapter 6: RIS-aided throughput analysis over the Fisher-Snedecor *F* and Beaulieu-Xie fading channels

- Throughput performance for the RIS-aided system over the FSF and BX fading channels are derived.

- It is concluded that the effect of fading can be compensated by increasing the number of reflecting elements in the IRS-assisted system.

Chapter 7: Conclusion and Future Scope of Work

- Conclusions of proposed methods and algorithms are presented in this chapter.

- A detailed discussion of possible avenues of future scope work is presented.

CHAPTER 2

LITERATURE REVIEW

This chapter presents the summary of work done in literature for traditional fading models and 5G fading models. Various works on effective throughput of the system for SISO, SIMO and MIMO systems are thoroughly reviewed in this chapter. The performance of the system over various networks like WSN, cooperative networks, UAV networks and hybrid networks etc. are reviewed here. Based on the extensive literature review, research gaps are identified and the corresponding objectives are set. Various algorithms and methods used to model wireless communication channel and the performance evaluation of these channels present in the literature are discussed here.

2.1   Introduction

With the recent advancements in wireless communication, there has been tremendous growth in the applications such as body area communication, vehicular communication and D2D communication etc., which require a high data rate with high reliability. In most of these future generation applications, the data is transferred from source to destination through a wireless link. The signal experience many phenomena like reflection, refraction, diffraction and scattering in its path traveling from Tx to Rx [1]. These phenomena result in the fluctuations in the received signal strength which eventually degrades the quality of the signal. The multipath fading results in the rapid fluctuation in the signal amplitude and shadowing give rise to the slow variation in the signal strength

at the Rx. Therefore, the QoS offered by the wireless communication system, in turn depends on the truthful assessment of the received signal at the Rx [1]. These resultant phenomena may deteriorate the quality of radio links; reduce the overall reliability of the signal and the performance of the communication system. Apart from these deleterious effects, the general research of the communication system broadly covers the aspects of channel modeling and other signal improvement techniques. The prime-facie of any wireless communication system development is the accurate channel characterization. It helps us to acquire knowledge about the fading behavior of the channel, not only to analyze the performance but also to improve system design. Since the fading phenomenon observed in the wireless system is random, thus the effect can be modeled in terms of fundamental statistics, such as the density function, the CDF, and the MGF. Among the aforementioned, the most commonly used fundamental statistics is the PDF. The statistic can easily be used for analyzing the system with diversity and in error correction coding [1]. On the other hand, the remaining statistics also play a vital role in assessing the communication system performance metrics, namely, P_{out}, average SNR, ASEP/ABEP and CC etc.

The CC along with other performance parameters like the P_{out}, and the error probability etc. is an essential parameter of concern in the designing of a communication system, which helps system engineers to provide the QoS within the limited available spectrum to a large number of users. Also, to address the explosive traffic demands, the capacity of the fading channel is increasingly becoming a prime concern in the designing of the wireless communication system. The CC is an extremely important quantity since it allows the transmission of the data through the channel with an arbitrarily small

probability of error.

The growing demand of high data rate in the future generation networks make it important to determine the capacity limits of the underlying channels. With the exponential rise in the services of the next-generation networks, it becomes extremely important to analyze the effect of several channel perturbations on the transmission rate. Capacity analysis based on Shannon's formula is investigated in the work of literature [8] [9]. CC is often expressed as a function of the average transmitted power. This function is obtained by optimizing the mutual information over all source distribution which have their average second moment, is equal to the given power or upper bounded by this power. CC parameter governs how fast data can be transmitted through the channel; which eventually depends upon the bandwidth of the channel as well as the quality of the channel. Data transmitted over the wireless channel suffers from random fluctuations due to channel impairments which, tend to degrade the transmission capability of the channel. CC analysis of various wireless channels under different propagation conditions has been analyzed in [10] [11] [12] [13] [14] [15]. Several works in literature are available that explores and review the implementation of CC analysis in different scenarios. For instance, a review of the multipath fading models is presented in [16] where the performance comparisons of the different models are presented. A conceptual explanation of the EC towards the delay-sensitive applications is presented [17]. A survey over the secrecy capacity performance over different fading channel is performed in [18], [19] [20]. Furthermore, a survey over the new technologies for 5G and beyond networks is provided in [21], [22].

2.2 Work on Traditional Fading Channels

To model the signal propagation, various mathematical distributions are studied in the literature. To model, the multipath fading, different models are widely explored in the literature. In [23], the performance analysis of the non-identical generalized Gamma fading channel is derived. This approach provides a simpler solution for the evaluation of CC in wireless communication system. The transmitted signal often suffers from shadowing due to the terrain, building structures, and trees, which in turn degrades the signal quality. To model this effect various models such as Lognormal, gamma, inverse gamma and inverse Gaussian are used. In [24], authors have presented an asymptotic analysis of the ergodic capacity for the Lognormal shadowed channel. An alternative model of shadowing, the inverse Gaussian channel is studied in [25]. The benefits of the inverse gamma over Lognormal and gamma shadowing are discussed in [26] and its CC analysis is comprehensively studied. In [27], analysis of CC over the lognormal channel is presented and expression of CC is represented in a simpler form.

Degradation of the signal due to the simultaneous occurrence of multipath and shadowing effects is called as composite fading. The CC analysis over composite Nakagami-m/Gamma and Nakagami-m/inverse Gaussian channel is presented in [28] and [29]. The expressions of P_{out} are also derived for both the cases in [28] and [29]. Using the incomplete generalized MGF, closed-form expressions for the P_{out} of the MRC scheme are obtained over the κ-μ shadowed fading channels in [30]. Similarly, for α-κ-μ shadowed channel, ACC is analyzed in [31], using the mixture gamma distribution. Table 2.1 summarizes the review of performance parameters over different fading channels presented in the literature.

Table 2.1 Review of various performance parameters over different channels

Reference	Representation of Expression	Fading Channel	Parameter Analyzed	Comments
[32]	Meijer-G Function	η-μ and κ-μ	ACC	The expressions are presented in terms of the Meijer-G function. This function can be easily implemented in available software which makes the analysis simpler.
[33]		nakagami-*m*, rician , weibull	ACC	
[34]		α-μ	OPRA, ORA	
[35]		α-η- μ and α-κ − μ	ACC	
[36]		W/LN	ACC	
[12]		Hoyt/gamma	ORA	
[37]	Infinite series summation	Nakagami-q	OPRA, ORA, CIFR, and TIFR	The expressions are presented in the form of infinite series summation So, the truncation error need to be calculated to get the desired accuracy.
[27]		Lognormal	Ergodic CC	
[38]		Nakagami-n	OPRA, ORA, CIFR, and TIFR	

[39]		η-μ/inverse gamma	Ergodic CC	
[40]	Bivariate Fox-H function	α-η-μ	OPRA, ORA, CIFR, and TIFR	Provides more precise analysis but at the cost of implementation complexity.
[41]	Fox-H function	α-η-κ-μ	ACC	The expressions are simple and easy to implement.
[42]	Hypergeometric function	η−μ/Gamma	OPRA, ORA	This function provides an approximation of the analysis and can easily be implemented in the available software packages.
[43]		Generalized-K	OPRA, ORA, CIFR, and TIFR	
[44]		κ−μ/Inverse Gamma and η−μ/inverse Gamma	ORA	

Diversity: Diversity has been one of the techniques to reduce the effect of fading on the communication system performance. The study of fading channel with different diversity

techniques are present in the literature. The capacity analysis of Rayleigh fading is reported in [45] by using the MRC reception technique. Further, the ABER performance analysis for the TWDP fading channel is provided in [46] with the pre-detection MRC technique. The outage and ABER performance of the κ–μ fading channel with MRC diversity is studied in [47]. The capacity analysis of TWDP fading using MRC detection is provided in [48]. Table 2.2 presents the summary of diversity combining works over different fading channels.

Table 2.2 Performance analysis based on diversity combining techniques

Reference	Year	Fading Channel	Diversity Combining
[49]	2020	B-X	MRC
[12]	2017	Hoyt/Gamma	MRC
[50]	2018	Hoyt/Lognormal	MRC
[51]	2019	Generic and composite	MRC
[52]	2008	Co-related Weibull	SC
[26]	2019	Inverse gamma shadowed	SC
[30]	2016	$\kappa\text{-}\mu$ Shadowed	SC
[53]	2007	Generalized-K	MRC, EGC, SC
[54]	2015	$\eta - \mu$	MRC

CSI: The signal propagation information between the Tx and the Rx can be estimated if CSI is known in advance. Regarding this knowledge, three different scenarios, are

considered to estimate the CC of the wireless channel. A summary of the classification of

CC works based on the CSI is provided in Table 2.3.

Table 2.3 CC based on CSI condition

Reference	Year	CSI condition	Main Contribution
[55]	2001	No CSI	Proved that capacity accomplishing distribution for i.i.d. Rayleigh fading channel is discrete with a limited number of points.
[56]	2016	No CSI	Presented investigations over block fading Rayleigh channel. Concluded that the pilot-based demodulations are imperfect and channel estimation is certainly performed by a capacity-optimal decoder
[57]	1999	No CSI	Analyzed the capacity of block fading MIMO channel.
[58]	2019	No CSI	Used the first-order Gaussian Markov process for CC analysis for the system. Concluded that the channel rate information is a non-increasing function of the coherence channel co-efficient.
[37], [45]	1999, 2003	CSI known to Rx and Tx	ORA, OPRA and CIFR analysis for Rayleigh and Nakagami-q fading channel is performed.
[59]	1997	CSI known	For various fading channels expression for ergodic

		to Rx only	CC is derived
[33], [32]	2005, 2007	CSI known to Rx only	Expression for the ergodic CC for α-μ, κ-μ and η-μ fading channel is derived
[60], [61]	2010, 1997	CSI known to Rx only	P_{out} of Hoyt under Rayleigh interference and Lognormal shadowed Rician fading channel is studied

2.3   Works on 5G Fading Channels

For addressing the different propagation phenomenon of multiple LOS components along with the diffused power components, a new fading model for indoor propagation is proposed in [3] which is most suited for 5G scenarios where femtocells are used. The PDF of the envelope of the received signal over the BX fading channel is proposed in [3] and its performance in terms of symbol error rate is demonstrated. The BX fading model unifies the non-central chi, generalized Rician and κ–μ distributions for the modeling of fading channels and can be easily transformed to these distributions [3]. The second-order statistics, like average fade duration and level crossing rate of the channel is studied in [62]. The secrecy capacity performance over the BX fading channel has been well explored in [63]. The asymptotic expressions for the P_{out} and the error rate for the correlated BX fading channel with EGC and SC diversity have been presented in [64], [65]. MGF-based approach is used in [66] to study the comprehensive performance evaluation of the communication system. Along with the digital performance measures, the study in [66] is extended to evaluate the energy detection performance over the BX

fading channel. In [67], the EC expressions for the BX fading channel has been derived and presented. Recently in [68], the error probability performance over the STBC-OFDM system with imperfect channel state information over the BX fading model has been investigated.

Using the incomplete generalized MGF, closed-form expressions for the P_{out} of the MRC scheme are obtained over the κ-μ shadowed fading channels in [30]. Similarly, for α-κ-μ shadowed channel ACC is analyzed in [31], using mixture gamma distribution. Recently, the EC analysis over gamma shadowed α–η–μ and α–κ–μ fading channel has been carried out in [69] and [70] using mixture gamma distribution.

In [71], the practical channel measurements for D2D communication are taken and based on the empirical model it was concluded that the FSF fading channel provides the accurate modeling of the scenario. It was also shown that FSF distribution provide a better fit to the experimental data in comparison to the generalized-*K* channel. Recently the closed-form expressions for different power adaptation CC over FSF fading channel have been derived in [72]. Diversity as a method to overcome the effect of fading, the MRC diversity over FSF fading channel has been discussed in [73] .

2.4   Reviews of Effective Capacity Works

Now with the emergence of real-time applications like cellular communication, D2D communications, peer-to-peer video streaming, visible light communication, full-duplex communications, URLL communications, RIS-assisted communication system, video conferencing, smart grid network and online interactive gaming etc., not only the throughput but the delay sensitivity of the communication system has gain importance for

the system designer [74]. Shannon capacity is not able to characterize the effective rate of a system, when delay constraint is considered as a QoS parameter [75]. The EC performance over the α–η–µ/Lognormal and α–κ–µ/Lognormal distribution has been studied in [76]. Recently, the EC analysis over gamma shadowedα–η–µ and α–κ–µ fading channel has been carried out in [69] and [70] using mixture gamma distribution. The EC work on generalized and composite fading channels for low SNR analysis are found in [77], [78], [79].

In [80], authors have obtained EC over multiple antenna systems which indicate a significant capacity gain using multiple antennas. In [81], a general PDF-based approach over the multipath and composite MISO fading channels has been utilized for analyzing the EC performance. MGF-based framework is proposed in [82] to study the effect of delay QoS parameter over the generalized fading channel. Further to get more inside of the system performance the low and high SNR approximations are also presented. The variation of EC performance over correlated MISO Nakagami-*m* channel has been proposed in [83]. In [84] , the flexible and tractable effective rate expression is provided for outdoor and indoor urban scenario with MISO Weibull distribution. There are some instances where MGF-based approach seems practical where PDF-based approach seems impractical [85], [86]. In [87], the EC model over Rayleigh fading channel is used for optimal channel allocation in CRN, and in [88], this model is applied for the performance evaluation of voice applications over Ricean fading channel. The achievable capacity of the CRN in a delay-sensitive asymmetric fading channel is studied in [89], while a comprehensive survey of EC over the CRN for various multimedia applications is

presented in [90]. Taking into consideration, the multicast receiver cross-layer, EC analysis for the Nakagami-*m* fading channel is provided in [91].

EC model proposed in [7], bridges the gap between statistical QoS guarantees and the maximum achievable transmission rate. Since then, it has been widely used as a powerful analytical tool and QoS provisioning metric in different scenarios. In [92], the resource allocation and flow selection algorithms for video distribution over wireless networks have been studied based on the effective rate theory, where energy efficiency and statistical delay bound have been considered. In [93] and [94] , scheduling algorithms have been studied for the multi-user time division downlink systems, exploiting the effective rate as the key to characterize the QoS constraints. In [95], the effective rate of two-hop wireless communication systems has been studied, where the impact of nodes' buffer constraints on the throughput has been considered.

In [96], EC model over the VoIP applications for the end-to-end routing and link scheduling scheme for multi-hop WSN is explored. In [97], authors have examined the attainable rate of multi-hop mobile networks with different delay-bounds over VOIP application. Video applications are also challenging to analyse due to strict delay bound and burst flow of the networks. Regarding this, some excellent work using the concept of EC is performed for the video streaming application over different fading channels. To enable high and low-speed video transmission the authors in [98], have provided a QoS-driven resource allocation scheme to upper-bound the overall delay for the two-hop DF relay networks over Rayleigh fading channel. The probability distribution of a delay process with video streaming support over the Ricean fading channels is investigated in [99]. EC concept is utilized in [100],to support the real-time video streaming in a

heterogeneous network and the results are utilisedfor cooperative spectrum sensing to observe the QoS guarantee in CRNs. Similarly, in [101], QoS-driven power allocation scheme in the CRN is proposed and the EC performance for different sensing scenarios in the Nakagami-*m* fading environment is studied. Due to the requirement of critical delay constraints in the wireless tele-ultrasonography medical systems, the end-to-end EC-based delay distribution is studied in [102]. In another application, EC model is used to evaluate the support level of communication network for the smart grids irrespective of the network technologies [103].

2.5   Performance Analysis over different wireless systems

The study of the wireless systems in terms of design and network architectures are important and the performance analysis over the CRN, Cooperative network, WSN and the VANET has been well explored. We review the works on different networks and for different propagation scenarios in this section.

2.5.1   VANET

With the emergence of VANET, the concept of ad-hoc network for smart vehicles has been realized [104]. The V2V network performance of the communication channel is analyzed by the authors in [105]. In [106], the authors have provided ergodic capacity expression for V2V network established at 28 GHz and then performed a diversity analysis using this expression experiencing α-η-κ-μ fading. In [107], P_{out} is analyzed for a BS to vehicle communication at 60 GHz considering Rician fading channel. In [108], authors have analyzed the transmission capacity over the VANET model undergoing Rayleigh fading. Nakagami-*m* fading model is an excellent model to represent the V2V

communication environment. So, in [109], the authors have analyzed the performance of full-duplex V2V communication under this environment. The expressions for the P_{out} under different scenarios are derived to analyze the performance.

2.5.2 WSN

Due to the increasing demand of IoT, the implementation of WSN is rapidly increasing, both in urban as well as rural areas. Several sensors that can collect information about the parameters of the field are deployed there. The deployment of WSN and its components in an agricultural field is shown in figure 2.1.
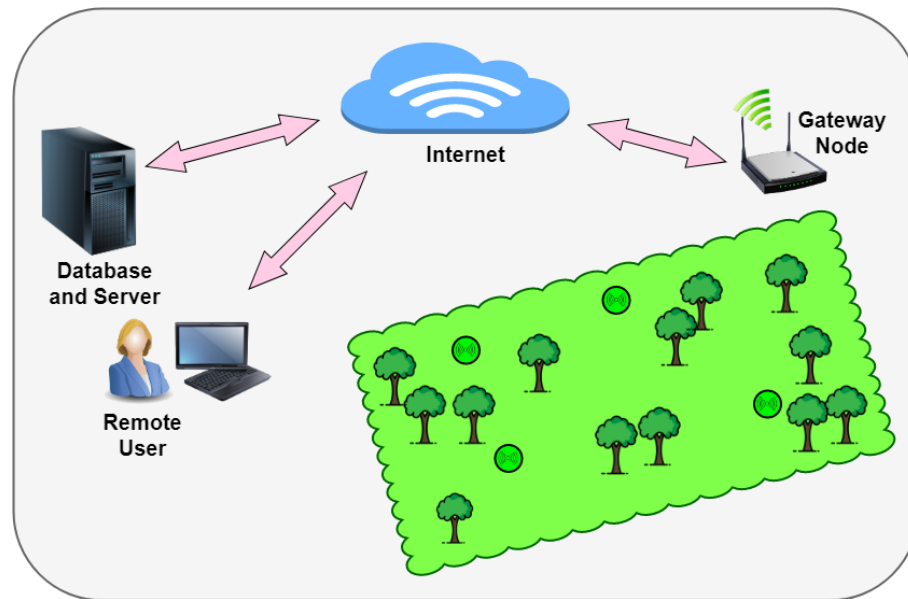
Figure 2.1 WSN deployment in agriculture application

In **[110]**, **[111]**, the study of WSN in terms of system performance over different fading channels are performed. In **[112]** and **[113]**, the study of STBC over the WSN system is presented. The study of WSN system over the Rayleigh and Ricean fading is demonstrated in **[114]**.

The performance of a WSN system for a railway scenario over Nakagami-m channel is studied **[115]**.

2.5.3 Cooperative network

Due to the ability of providing reliable data transmission, the communication over the cooperative network is gaining popularity among system designers. Authors in [116],have analyzed the capacity of Rayleigh faded cooperative network under various adaptive transmission schemes. Along with this, MRC and SC diversity combining techniques is also investigated. In [117] and [118] P_{out} and BER respectively, for decode and forward relaying is investigated over Rayleigh fading channel. For the same relaying technique capacity and outage performance of the underground tunnel system are studied in [119]. In [120], the performance of the amplify and forward (AF) technique implemented in a multi-relay system connecting multiple users via several relays to the destination is studied. The throughput performance of the full multi-packet reception model is explored in [121] over a slotted-time relay-assisted cooperative network. Some more existing work on the performance of the multi-hop cooperative network can be found in the literature [122] [123].

2.5.4 Cognitive Radio Networks

CRN is a promising technology for efficient utilization of the available spectrum and increases network capacity. It intelligently utilizes available side information about channel conditions, encoding strategies or transmitted data sequences of primary users with which it shares the spectrum. In recent years, a huge amount of work has been done to analyze the performance under the three paradigms of CRN, underlay, overlay, and

interweave [124]. In [125]authors have analyzed the capacity of CRN undergoing multipath effect by estimating CC and BER.
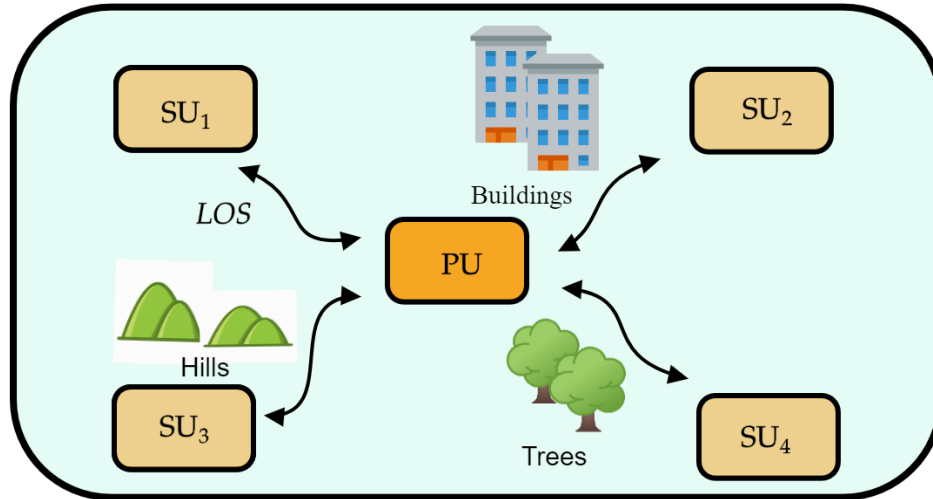
Figure 2.2 Cognitive Radio Network

For the underlay CRN, closed-form expressions for ergodic capacity and outage capacity of SU are determined in [126]. Here, authors have considered a composite fading channel and shown that on increasing shadowing the outage performance degrades. The schematic of the CRN is shown in figure 2.2. Authors have analyzed the performance of the energy detector method for spectrum sensing model in CRN over different fading channels [127], [128] [129] [130] [131] [75] [132].

2.5.5 Unmanned Aerial Communication

UAV-assisted wireless communication has stroked a great interest by both the industrial as well as academic community due to its diverse application in entertainment, wildlife monitoring, military and surveillance fields. In [133], the authors have derived the closed-form P_{out} expression in air-to-ground and ground-to-air transmission links. In [134], the authors have focused on the analysis of channel characteristics of the air-to-air

UAV communication considering Ricean model. Using three dimensional geometrically based single bounce cylinder model channel for the UAV-MIMO system, the influence of the UAV altitude parameters over the CC of the system is analyzed in [135]. The improvement in the performance of the high-altitude long-endurance UAV using the MIMO cooperative relay is analyzed in [136] considering the Rayleigh fading channel.

2.5.6 Hybrid free-space optics (FSO) and Radio-frequency (RF) links

The hybrid FSO and RF links as shown in figure 2.3 is an effective solution to meet the challenge of high data rates in urban scenarios. The communication system performance in terms of P_{out}, BER and CC for hybrid FSO-RF link over GG and Rayleigh fading respectively are studied in [137]. The effect of diversity combining techniques over the hybrid FSO-RF link is presented in [138], [139].
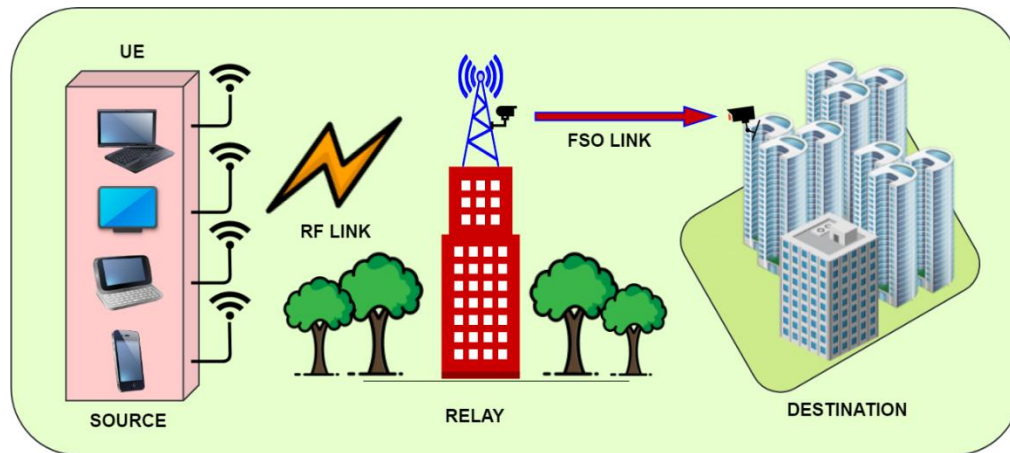
Figure 2.3 Hybrid RF and FSO link

A dual-hop relay-assisted hybrid parallel FSO/RF system is investigated in [140], to analyze the performance closed-form expressions for BER and the P_{out} is derived. In Gamma-Gamma atmospheric turbulence FSO link is considered with the impact of pointing error and the RF link is considered in Rayleigh fading.

2.5.7 Wireless body-area-network (WBAN)

This network typically consists of several body parameter monitoring sensors and actuators that are put at the different explicit locations inside and on the body and are connected through the wireless channel. The performance of the WBAN is strongly influenced by human movements and needs to be analyzed for the effective deployment of the on-body sensors. Numerical analysis of the P_{out}, as well as asymptotic analysis, is provided to obtain the behavior of the network. With the recent advances IoT technologies have been integrated with the WBANs. In [141], the P_{out} for three different protocols with energy harvesting is derived and formulated for the IoT-based health care system.

2.5.8 Hybrid Satellite Terrestrial Links

A hybrid satellite-terrestrial network takes the advantage of both the terrestrial and satellite communication network to provide an effective solution for the realization of the foreseen heterogeneous global network system [142]. In [143], the authors have derived an exact expression of ergodic CC for hybrid satellite-terrestrial single frequency network consisting of satellite as the source node, mobile as destination node and several gap filters as relay nodes on the ground. The performance of the various diversity combining techniques over the hybrid satellite-terrestrial link is studied in [144]. In this with the knowledge of CSI at the relay-destination link expression for the P_{out} is derived over SC and MRC combining techniques. Some other work on hybrid satellite-terrestrial link can be found in [145] [146] [147]. The deployment diagram of hybrid satellite-terrestrial link is given in figure 2.4.
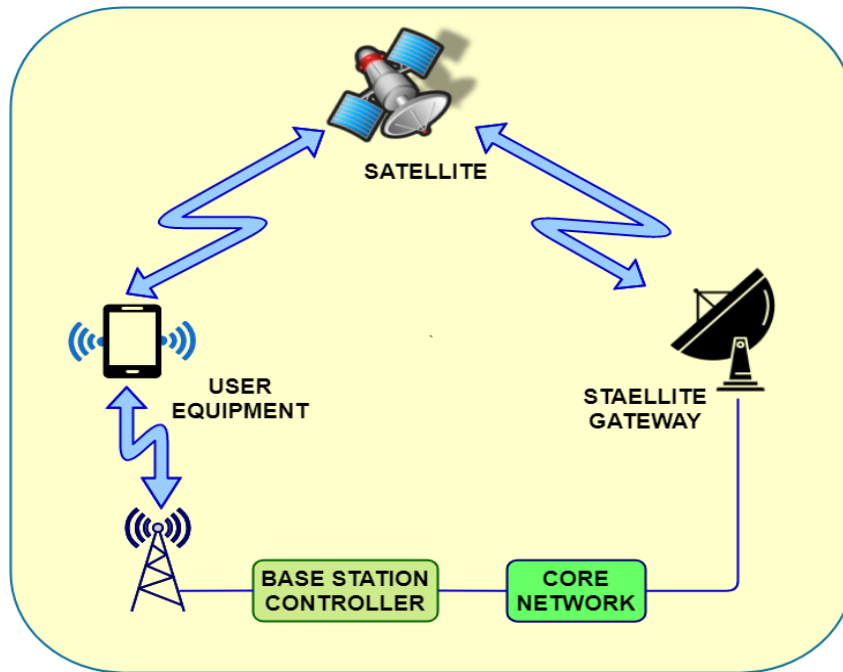
Figure 2.4 Hybrid satellite-terrestrial link

2.5.9   Other networks

There are many other emerging applications where the CC is considered as an important design parameter and is well studied.
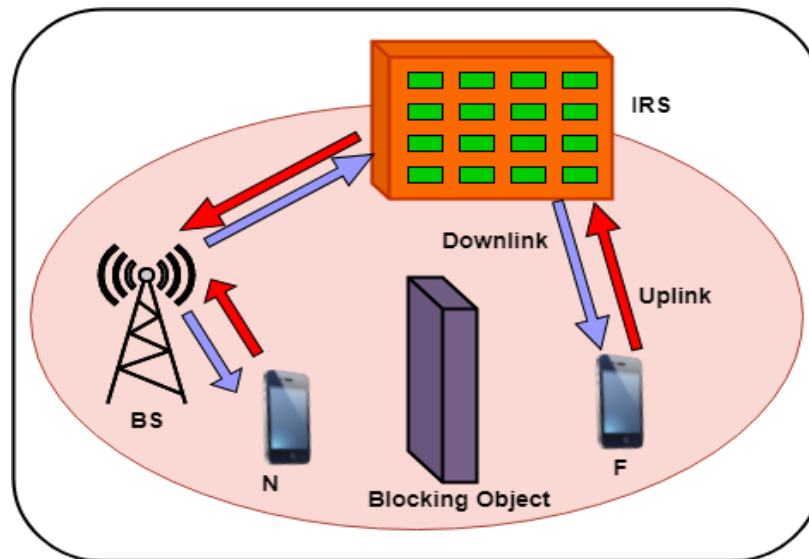
Figure 2.5 IRS assisted wireless network

For example, the IRS provides the promising solution to enhance the spectral efficiency by smartly tuning the reflection of the signal through its passive reflecting elements as shown in figure 2.5.
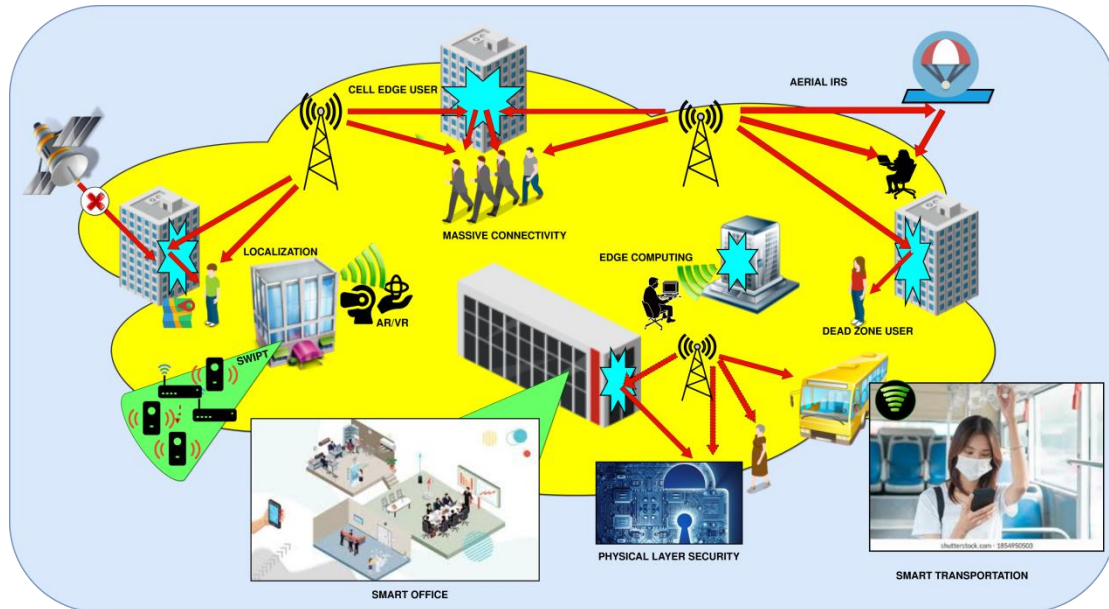
Figure 2.6 Application of IRS

In this regards, IRS-assisted relay networks are being studied to improve the system performances. Similarly, the MIMO-OFDM network is being studied over various fading channels in terms of its throughput performance. The applications of IRS can be found in many applications as shown in figure 2.6.

2.6   Research Gaps and Motivation

The size of the mobile cells in 3G/4G wireless technologies was relatively large, thus the signal propagation scenario was thought to be outdoor propagation. Due to the small areas of the cells in 5G, the signal propagation inside a femtocell is very difficult to model in the form of outdoor fading channels. For addressing the propagation

phenomenon in 5G and beyond technology, BX fading channel and FSF fading channel are introduced.

The LOS and the diffused power components inside the femtocells are modeled in the form of BX fading channel and it has found application in the signal propagation in small buildings and fast-moving trains. Although there are various works in literature related to the performance analysis over BX fading channel, but the MRC diversity analysis over the said channel has not received enough attention.

With the emergence of real-time applications in 5G and beyond networks, the effective rate analysis of the system is need of the hour and the EC performance over BX fading channel for multi-antenna system has not been investigated yet.

FSF fading channel is a composite fading model that is used to model the signal propagation for D2D and wearable communication links and the effective rate performance over FSF fading channel for multi-antenna system has not been explored in literature.

Moreover, the usefulness of the results for RIS-aided application for both the fading channels has not been studied earlier. Motived by these gaps, this thesis studies the performance evaluation of BX fading channel and FSF fading channel for multi-antenna system.

2.7   Problems Formulation

Based on the discussion presented in the previous section, we consider the following problems for analysis in this report. Analysis of diversity receivers over BX fading channel can be a potential area of research. The EC performance of BX fading channel

and FSF fading channel for multi-antenna system and their application in IRS-assisted communication can be of interest to the research community.

2.8   Aim and Objectives

The main aim and objectives of this thesis are highlighted in the following points:

- To study and analyze the performance metrics like AF, P_{out}, CC and ASEP for the sum of BX random variables.

- To study the EC analysis for the multi-antenna system over the BX fading channel.

- To analyze the EC performance over FSF fading channel for multi-antenna system.

- To study the application of the proposed results for RIS-aided system for both FSF fading channel and BX fading channel.

To fulfil the above-stated aims and objectives, we focus on the mathematical analysis of the performance measures of the receivers in the best possible compact form.

CHAPTER 3

PERFORMANCE ANALYSIS OF BEAULIEU-XIE FADING

CHANNEL WITH MRC COMBINING

This chapter presents the performance analysis of BX fading channel with combining. In this work, the performance of communication system inside a densely packed small cells or femtocells with MRC diversity is studied. The LOS and the diffused power components inside the femtocells are modeled in the form of BX fading channel and the performance metrics are derived. The closed-form expressions for P_{out}, AF and ASEP for coherent and non-coherent modulation schemes are derived for the said channel. Further, the CC analysis over different transmission policies is performed and the corresponding results are plotted. The effect of diversity and the other fading parameters on the performance measures are demonstrated. Analytical results are supplemented with Monte-Carlo simulations for validating the results of our study.

3.1   Channel Model

The PDF of γ for *l*th branch BX fading channel can be written with the help of equation (1.6) as

$$f_{\gamma_l}\left(\gamma_l\right) = \frac{\eta_l^{\frac{m_l+1}{2}}\gamma_l^{\frac{m_l-1}{2}}}{(m_lk_l)^{\frac{m_l-1}{2}}}\exp\left(-m_lk_l\right)\exp\left(-\eta_l\gamma_l\right)I_{m_l-1}\left(2\sqrt{m_lk_l\eta_l\gamma_l}\right) \qquad (3.1)$$

where $\eta_l = L_1^{m_l-1}(-m_l k_l)/\overline{\gamma}_l$. The variables m_l and $\overline{\gamma}_l$ are severity fading parameter, and average received SNR of the lth branch, respectively. k_l is the ratio of specular power to the diffuse power components. The sum distribution of received SNR plays a predominant role in the analysis of diversity systems. The distribution of the sum of received SNR at the output of an L-branch combiner can be defined using [12] as

$\gamma = \sum_{l=1}^{L} \gamma_l$. In terms of PDF, it can be written as

$$f_\gamma\left(\gamma\right) = \sum_{l=1}^{L} f_{\gamma_l}\left(\gamma_l\right) \tag{3.2}$$

The characteristic function of equation (3.1) can be easily evaluated using the relationship $\phi_\gamma\left(j\omega\right) = \int_0^\infty f_\gamma\left(\gamma\right) e^{-j\omega\gamma} d\gamma$ as

$$\phi_{\gamma_l}\left(j\omega_l\right) = \frac{\eta_l^{\frac{m_l+1}{2}} \exp\left(-m_l k_l\right)}{(m_l k_l)^{\frac{m_l-1}{2}}} \int_0^\infty \gamma_l^{\frac{m_l-1}{2}} \exp\left(-\gamma_l\left(\eta_l + j\omega_l\right)\right) I_{m_l-1}\left(\sqrt{2m_l k_l \eta_l \gamma_l}\right) d\gamma_l \tag{3.3}$$

Comparing with equation (6.643.2) of [148] we have

$\mu = \dfrac{m_l}{2}, \alpha = \eta_l + j\omega_l, v = \dfrac{m_l-1}{2}, b = \sqrt{m_l k_l \eta_l}$. Further simplifying we get

$$\phi_{\gamma_l}\left(j\omega_l\right) = \frac{\eta_l^{\frac{m_l+1}{2}} \exp\left(-m_l k_l\right)}{(m_l k_l)^{\frac{m_l-1}{2}}} (m_l k_l \eta_l)^{\frac{-1}{2}} e^{\frac{m_l k_l \eta_l}{2(\eta_l + j\omega_l)}} \left(\eta_l + j\omega_l\right)^{\frac{-m_l}{2}} M_{\frac{-m_l}{2},\frac{m_l-1}{2}}\left(\frac{m_l k_l \eta_l}{\eta_l + j\omega_l}\right) \tag{3.4}$$

Solving equation (3.4), we get

$$\phi_{\gamma_l}\left(j\omega_l\right) = \frac{\eta_l^{\frac{m_l+1}{2}-\frac{1}{2}}\exp\left(-m_l k_l\right)}{(m_l k_l)^{\frac{m_l}{2}-\frac{1}{2}+\frac{1}{2}}}\frac{e^{\frac{m_l k_l \eta_l}{2(\eta_l+j\omega_l)}}}{\left(\eta_l+j\omega_l\right)^{\frac{m_l}{2}}}M_{-\frac{m_l}{2},\frac{m_l-1}{2}}\left(\frac{m_l k_l \eta_l}{\eta_l+j\omega_l}\right) \quad (3.5)$$

Which is further reduced to

$$\phi_{\gamma_l}\left(j\omega_l\right) = \frac{\eta_l^{\frac{m_l}{2}}\exp\left(-m_l k_l\right)}{(m_l k_l)^{\frac{m_l}{2}}}\frac{e^{\frac{m_l k_l \eta_l}{2(\eta_l+j\omega_l)}}}{\left(\eta_l+j\omega_l\right)^{\frac{m_l}{2}}}M_{-\frac{m_l}{2},\frac{m_l-1}{2}}\left(\frac{m_l k_l \eta_l}{\eta_l+j\omega_l}\right) \quad (3.6)$$

Here $M_{a,b}\left(.\right)$ can be written in the form of Kummer's confluent hypergeometric function using equation (13.1.32) of [149]. Comparing with equation (13.1.32) of [149], we get

$$M_{-\frac{m_l}{2},\frac{m_l-1}{2}}\left(\frac{m_l k_l \eta_l}{\eta_l+j\omega_l}\right) = e^{-\frac{m_l k_l \eta_l}{2(\eta_l+j\omega_l)}}\left(\frac{m_l k_l \eta_l}{\eta_l+j\omega_l}\right)^{\frac{1}{2}+\frac{m_l}{2}-\frac{1}{2}}M\left(\frac{1}{2}+\frac{m_l}{2}-\frac{1}{2}+\frac{m_l}{2},1+m_l-1,\frac{m_l k_l \eta_l}{\eta_l+j\omega_l}\right) \quad (3.7)$$

Apply equation (3.7) in equation (3.6), we have

$$\phi_{\gamma_l}\left(j\omega_l\right) = \frac{\eta_l^{\frac{m_l}{2}}\exp\left(-m_l k_l\right)}{(m_l k_l)^{\frac{m_l}{2}}}e^{\frac{m_l k_l \eta_l}{2(\eta_l+j\omega_l)}-\frac{m_l k_l \eta_l}{2(\eta_l+j\omega_l)}}\frac{\left(m_l k_l \eta_l\right)^{\frac{m_l}{2}}}{\left(\eta_l+j\omega_l\right)^{m_l}}M\left(m_l,m_l,\frac{m_l k_l \eta_l}{\eta_l+j\omega_l}\right) \quad (3.8)$$

Further simplifying using equation (13.6.12) of **[149]**, we get

$$\phi_{\gamma_l}\left(j\omega_l\right) = \frac{\eta_l^{m_l}\exp\left(-m_l k_l\right)}{\left(\eta_l+j\omega_l\right)^{m_l}}\exp\left(\frac{m_l k_l \eta_l}{\eta_l+j\omega_l}\right) \quad (3.9)$$

The complementary function at the output of L branch MRC combiner can be defined as

$$\phi_\gamma = \prod_{l=1}^{L}\phi_{\gamma_l} \quad (3.10)$$

Putting equation (3.9) in equation (3.10) and assuming $\omega_1 = \omega_2 ... = \omega_L = \omega$

$$\phi_\gamma = \prod_{l=1}^{L} \frac{\eta_l^{m_l}}{\left(\eta_l + j\omega\right)^{m_l}} \exp\left(-m_l k_l\right) \exp\left(\frac{m_l k_l \eta_l}{\eta_l + j\omega}\right) \tag{3.11}$$

Applying the series expansion of exp(.) using equation (1.211) of [148] in equation (3.11)

$$\phi_\gamma = \prod_{l=1}^{L} \frac{\eta_l^{m_l}}{\left(\eta_l + j\omega\right)^{m_l}} \exp\left(-m_l k_l\right) \sum_{z=0}^{\infty} \frac{\left(\frac{m_l k_l \eta_l}{\eta_l + j\omega}\right)^z}{z!} \tag{3.12}$$

Further equation (3.12) can be simplified as

$$\phi_\gamma = \prod_{l=1}^{L} \eta_l^{ml} \exp\left(-m_l k_l\right) \sum_{z=0}^{\infty} \frac{\left(m_l k_l \eta_l\right)^z}{z!} \left(\frac{1}{\eta_l + j\omega}\right)^{z+m_l} \tag{3.13}$$

Rearranging equation (3.13), the complimentary function of the sum distribution is given by

$$\phi_\gamma = \prod_{l=1}^{L} \eta_l^{ml} \exp\left(-m_l k_l\right) \sum_{z=0}^{\infty} \frac{\left(m_l k_l n_l\right)^z}{z!\left(j\omega\right)^{(z+m_l)}} \left(1 + \frac{\eta_l}{j\omega}\right)^{-(z+m_l)} \tag{3.14}$$

Replacing $s = j\omega$ in the above equation

$$\phi_\gamma = \prod_{l=1}^{L} \eta_l^{m_l} \exp\left(-m_l k_l\right) \sum_{z=0}^{\infty} \frac{\left(m_l k_l n_l\right)^z}{z!\left(s\right)^{(z+ml)}} \left(1 + \frac{\eta_l}{s}\right)^{-(z+m_l)} \tag{3.15}$$

The PDF expression of the sum of i.n.i.d. branches SNR can be evaluated by applying equation (9.4.55) of [148] in equation (3.15)

$$f_\gamma\left(\gamma\right)=\prod_{l=1}^{L}\eta_l^{m_l}\exp\left(-m_l k_l\right)\sum_{z=0}^{\infty}\frac{\left(m_l k_l n_l\right)^z}{\Gamma\left(z+m_l\right)z!}\sum_{z=0}^{\infty}\gamma^{\sum_{l=1}^{L}z+m_l-1}$$

$$\times\phi_2^{(L)}\left(m_1+z,m_2+z.......m_L+z;\sum_{l=1}^{L}m_l+z;-\eta_l\gamma,-\eta_2\gamma,......-\eta_L\gamma\right)$$

(3.16)

where $\phi_2^{(L)}(.;.;.)$ is defined in equation (1.4.8) of [148]. Using equation (3.16) and following the similar approach as used to calculate equation (8) of [150], the CDF expression of the sum of i.n.i.d. branches SNR can be given as

$$F_\gamma\left(\gamma\right)=\prod_{l=1}^{L}\eta_l^{m_l}\exp\left(-m_l k_l\right)\sum_{z=0}^{\infty}\frac{\left(m_l k_l n_l\right)^z}{z!\,\Gamma\left(z+m_l+1\right)}\sum_{z=0}^{\infty}\gamma^{\sum_{l=1}^{L}m_l+z}$$

$$\times\phi_2^{(L)}\left(m_1+z,m_2+z.......m_L+z;1+\sum_{l=1}^{L}m_l+z;-\eta_l\gamma,-\eta_2\gamma,......-\eta_L\gamma\right)$$

(3.17)

For i.i.d. branches, the PDF expression at the output of MRC combiner can be easily evaluated using equation (9) of [150] in equation (3.16)

$$f_\gamma\left(\gamma\right)=\eta^{mL}\exp\left(-m\,k\,L\right)\prod_{l=1}^{L}\left(\sum_{z=0}^{\infty}\frac{\left(m\,k\,\eta\right)^z}{\Gamma\left(z+m\right)z!}\right)\sum_{z=0}^{\infty}\gamma^{z+mL-1}\phi_2\left[mL+zL;mL+zL;\eta\gamma\right]$$

$$=\frac{\eta^{mL}\exp\left(-m\,k\,L\right)}{\Gamma\left(zL+mL\right)}\sum_{z=0}^{\infty}\frac{\left(m\,k\,\eta L\right)^z}{z!}\gamma^{zL+mL-1}\sum_{z=0}^{\infty}\phi_2\left[mL+zL;mL+zL;\eta\gamma\right]$$

(3.18)

Then applying the series expansion of $\phi_2(.;.;.)$ using equation (1.3.17) of [148], we get

$$f_\gamma\left(\gamma\right)=\frac{\eta^{mL}}{\Gamma\left(mL\right)}\exp\left[\left(-m\,k\,L+\eta\gamma\right)\right]\gamma^{(mL-1)}\sum_{z=0}^{\infty}\frac{\left(m\,k\,\eta L\gamma\right)^z\Gamma\left(mL\right)}{z!\,\Gamma\left(mL+zL\right)}$$

(3.19)

Using the series expansion of $_0F_1(;.;.)$, the final expression of SNR PDF of sum of L-branch comes out as

$$f_\gamma(\gamma) = \frac{\eta^{mL}}{\Gamma(mL)} \exp\left[\left(-m\,k\,L + \eta\gamma\right)\right] \gamma^{(mL-1)} {}_0F_1(;mL;mKL\eta\gamma) \tag{3.20}$$

3.2 Performance Analysis

3.2.1 Outage Probability

The P_{out} can be derived by putting equation (3.20) in equation (1.8) as

$$P_{out} = \frac{\eta^{mL}\exp(-mkL)}{\Gamma(mL)} \int_0^{\gamma_{th}} \gamma^{(mL-1)} \exp(-\eta\gamma)\,{}_0F_1(;mL;mKL\eta\gamma)d\gamma \tag{3.21}$$

Using the infinite series expansion of $_0F_1(;.;.)$ in equation (3.21)

$$P_{out} = \frac{\eta^{mL}\exp(-mkL)}{\Gamma(mL)} \sum_{z=0}^{\infty} \frac{\Gamma(mL)}{\Gamma(mL+z)z!} (m\,k\,\eta L)^z \int_0^{\gamma_{th}} \gamma^{(mL-1)+z} \exp\left[-\gamma(\eta)\right]d\gamma \tag{3.22}$$

Comparing $\int_0^{\gamma_{th}} \gamma^{(mL-1)+z} \exp\left[-\gamma(\eta)\right]d\gamma$ with equation (3.381.1) of [148] we get

$$\int_0^{\gamma_{th}} \gamma^{(mL-1)+z} \exp\left[-\gamma(\eta)\right]d\gamma = \frac{Y(mL+z,\eta\gamma_{th})}{\eta^{(mL+z)}} \tag{3.23}$$

Putting equation (3.23) in equation (3.22), we get the final expression of P_{out}

$$P_{out} = \exp(-mkL) \sum_{z=0}^{\infty} \frac{(mkL)^z}{\Gamma(mL+z)z!} Y(mL+z,\eta\gamma_{th}) \tag{3.24}$$

It is noted that the above equation is in the form of an infinite series. The upper bound on the truncation error in the expression of P_{out} by z number of terms can be evaluated as:

$$E_z = \exp(-mkL) \sum_{z=Z}^{\infty} \frac{(mkL)^z}{z! \Gamma(mL+z)} Y(mL+z, \eta\gamma_{th}) \tag{3.25}$$

Put z-Z=g in the above equation

$$E_z = \exp(-mkL) \sum_{g=0}^{\infty} \frac{(mkL)^{Z+g}}{(Z+g!)\Gamma(mL+Z+g)} Y(mL+Z+g, \eta\gamma_{th}) \tag{3.26}$$

Using equation (8.351.2) of [148]

$$Y(mL+Z+g, \eta\gamma_{th}) = \frac{(\eta\gamma_{th})^{mL+Z+g}}{(mL+Z+g)} \, {}_1F_1(mL+Z+g; mL+Z+g+1; -\eta\gamma_{th}) \tag{3.27}$$

Put equation (3.27) in equation (3.26), we get

$$E_z = (\eta\gamma_{th})^{mL} \exp(-mkL) \sum_{g=0}^{\infty} \frac{(mkL\eta\gamma_{th})^{Z+g}}{(Z+g!)(mL+Z+g)!} \, {}_1F_1(mL+Z+g; mL+Z+g+1; -\eta\gamma_{th})$$

$$\tag{3.28}$$

The $_1F_1(.,.,.)$ in equation (3.28) is monotonically decreasing function with respect to g, hence it can be upper bounded as

$$E_z \le (\eta\gamma_{th})^{mL} (mkL\eta\gamma_{th})^Z \exp(-mkL) \, {}_1F_1(mL+Z; mL+Z+1; -\eta\gamma_{th}) \sum_{g=0}^{\infty} \frac{(mkL\eta\gamma_{th})^g}{(S+g!)(mL+S+g)!}$$

$$\tag{3.29}$$

Using the result,

$$\sum_{g=0}^{\infty} \frac{(mkL\eta\gamma_{th})^g}{(S+g!)(mL+S+g)!} = \frac{(1)_g}{(g!)(S+1)_g(S+mL+1)_g\Gamma(S+1)\Gamma(S+mL+1)} \quad \text{and} \quad \text{putting}$$

$$\frac{(1)_g}{(g!)(S+1)_g(S+mL+1)_g} = {}_1F_2(1;S+1,S+mL+1;mkL\eta\gamma_{th}) \quad \text{in above equation, we get}$$

$$\sum_{g=0}^{\infty} \frac{(mkL\eta\gamma_{th})^g}{(S+g!)(mL+S+g)!} = \frac{{}_1F_2(1;S+1,S+mL+1;mkL\eta\gamma_{th})}{\Gamma(S+1)\Gamma(S+mL+1)} \quad (3.30)$$

Put equation (3.30) in equation (3.29), we get

$$E_z \le (\eta\gamma_{th})^{mL}(mkL\eta\gamma_{th})^Z \exp(-mkL){}_1F_1(mL+S;mL+S+1;-\eta\gamma_{th})$$
$$\times \frac{{}_1F_2(1;S+1,S+mL+1;mkL\eta\gamma_{th})}{\Gamma(S+1)\Gamma(S+mL+1)} \quad (3.31)$$

3.2.2   Amount of Fading

The i_{th} moment of γ can be defined as $E[i] = \int_0^{\infty} \gamma^i f_\gamma(\gamma) d\gamma$ and using equation (3.20) can

be written in the form of series expansion as

$$E[\gamma^i] = \frac{\eta^{mL}}{\Gamma(mL)} \exp(-mkL) \int_0^{\infty} \gamma^{mL+i-1} \exp(-\eta\gamma){}_0F_1(;mL;mKL\eta\gamma) d\gamma \quad (3.32)$$

Using series expansion ${}_0F_1(;.;.)$, we have

$$E[\gamma^i] = \frac{\eta^{mL}}{\Gamma(mL)} \exp(-mkL) \sum_{s=0}^{\infty} \frac{\Gamma(mL)}{(s!)\Gamma(mL+s)}(mkL\eta)^s \int_0^{\infty} \gamma^{mL+i+s-1} \exp(-\eta\gamma) d\gamma \quad (3.33)$$

The integral term in the above equation can be simplified using equation (3.381.4) of

[148], $\int_0^{\infty} \gamma^{mL+i+s-1} \exp(-\eta\gamma) d\gamma = \frac{\Gamma(mL+s+i)}{\eta^{(mL+s+i)}}$ as

43

$$E[\gamma^i] = \frac{\eta^{mL}}{\Gamma(mL)} \exp(-mkL) \sum_{s=0}^{\infty} \frac{\Gamma(mL)}{(s!)\Gamma(mL+s)} (mkL\eta)^s \frac{\Gamma(mL+s+i)}{\eta^{(mL+s+i)}} \qquad (3.34)$$

The above equation can be simplified as

$$E[\gamma^i] = \frac{\eta^{mL}}{\Gamma(mL)} \eta^{(-mL-i)} \exp(-mkL) \sum_{s=0}^{\infty} \frac{\Gamma(mL)}{(s!)\Gamma(mL+s)} \frac{\Gamma(mL+s+i)}{\Gamma(mL+i)} \Gamma(mL+i)(mkL)^s$$

$$(3.35)$$

Further simplifying equation (3.35), we get

$$E[\gamma^i] = \eta^{-i} \exp(-mkL) \frac{\Gamma(mL+i)}{\Gamma(mL)} \sum_{s=0}^{\infty} \frac{(mL+i)_s}{(s!)(mL)_s} (mkL)^s \qquad (3.36)$$

Doing further manipulation, the simplified closed-form expression of the *i*th moment comes out as

$$E[\gamma^i] = \frac{(mL)_i}{\eta^i \exp(mkL)} {}_1F_1[(mL+i;mL;mkL)] \qquad (3.37)$$

AF is a measure of the severity of the channel and is defined as $AF = E\left[\gamma^2\right]\big/\left(E\left[\gamma\right]^2 - 1\right)$. The final expression of AF can be easily evaluated using equation (3.37).

3.2.3 Channel Capacity

The CC is gaining high importance with tremendous growth in the field of wireless communication. It gives the capacity limits i.e., the maximum data rates that can be sustained by a channel. Without putting a limit on the complexity or delay of the encoder and decoder, CC is having different transmission policies for fixed transmission power

like ORA, OPRA, CIFR and TIFR. In this section, the CC of the BX fading model is studied by deriving the closed-form expressions for different adaptive transmission techniques.

3.2.3.1 *ORA*

In this transmission policy, the transmitting power remains constant and the CSI is present only at the Rx. The mathematical expression of ORA CC is given by [50] as

$$\frac{C_{ORA}}{B} = \int_0^{\infty} \log_2(1+\gamma) f_{\gamma}(\gamma) d\gamma \tag{3.38}$$

here B denotes the bandwidth of the fading channel. Putting equation (3.20) in the above equation and using the infinite series expansion of $_0F_1(;.;.)$, equation (07.34.03.0228.01) of [151] and equation (07.34.03.0456.01) of [151] we get

$$\frac{C_{ORA}}{B} = \frac{\eta^{mL}}{\Gamma(mL)} \frac{\exp(-mkL)}{\ln(2)} \sum_{s=0}^{\infty} \frac{\Gamma(mL)(mkL\eta)^s}{(s!)\Gamma(mL+s)} \int_0^{\infty} \gamma^{mL+s-1} \log_2(1+\gamma) \exp(-\eta\gamma) d\gamma \tag{3.39}$$

Using $\log(1+\gamma) = G_{2,2}^{1,2}\left(\gamma \left| \begin{matrix} 1 & 1 \\ 1 & 0 \end{matrix}\right.\right)$ and $\exp(-\eta\gamma) = G_{0,1}^{1,0}\left(\eta\gamma \left| 0 \right.\right)$ in above equation, we get

$$\frac{C_{ORA}}{B} = \frac{\eta^{mL}}{\ln(2)} \exp(-mkL) \sum_{s=0}^{\infty} \frac{(mkL\eta)^s}{(s!)\Gamma(mL+s)} \int_0^{\infty} \gamma^{mL+s-1} G_{2,2}^{1,2}\left(\gamma \left| \begin{matrix} 1 & 1 \\ 1 & 0 \end{matrix}\right.\right) G_{0,1}^{1,0}\left(\eta\gamma \left| 0 \right.\right) d\gamma \tag{3.40}$$

Applying equation (07.34.21.0011.01) of [151], the integral term in the above equation can be simplified as

$$\int_0^{\infty} \gamma^{mL+s-1} G_{2,2}^{1,2}\left(\gamma \left| \begin{matrix} 1 & 1 \\ 1 & 0 & - \end{matrix}\right.\right) G_{0,1}^{1,0}\left(\eta\gamma \left| 0 \right.\right) d\gamma = (1)^{-(mL+s)} G_{2\ 3}^{2\ 1}\left(\eta \left| \begin{matrix} 1-(mL+s)-1 & & 1-(mL+s)-0 \\ 0 & 1-(mL+s)-1 & 1-(mL+s)-1 \end{matrix}\right.\right)$$

$$\tag{3.41A}$$

On further rearranging the above equation, we have

$$\int_0^\infty \gamma^{mL+s-1} G_{2,2}^{1,2}\left(\gamma \left|\begin{matrix} 1 & 1 \\ 1 & 0 & - \end{matrix}\right.\right) G_{0\,1}^{1,0}\left(\eta\gamma \left|\begin{matrix} \\ 0 \end{matrix}\right.\right) d\gamma = G_{2\,3}^{3\,1}\left(\eta \left|\begin{matrix} -(mL+s) & & (1-mL-s) \\ 0 & -(mL+s) & -(mL+s) \end{matrix}\right.\right)$$

(3.41B)

Put equation (3.41B) in equation (3.40), we get

$$\frac{C_{ORA}}{B} = \frac{\eta^{mL}}{\ln(2)}\exp(-mkL)\sum_{s=0}^\infty \frac{(mkL\eta)^s}{(s!)\Gamma(mL+s)} G_{2\,3}^{3\,1}\left(\eta \left|\begin{matrix} -(mL+s) & & (1-mL-s) \\ 0 & -(mL+s) & -(mL+s) \end{matrix}\right.\right)$$

(3.42)

3.2.3.2 *OPRA*

In this technique, CSI is available at both the Tx and the Rx. The main motivation of using this adaptation is to assign more power to the channel with higher SNR values and lesser power to the channel with lower SNR values. The OPRA CC is defined by [152] as

$$\frac{C_{OPRA}}{B} = \int_{\gamma_{th}}^\infty \log_2\left(\frac{\gamma}{\gamma_{th}}\right) f_\gamma(\gamma) d\gamma$$

(3.43)

where γ_{th} is the cutoff SNR level below which the transmission is suspended. The above equation is valid under the condition:

$$\int_{\gamma_{th}}^\infty \left(\frac{1}{\gamma_{th}} - \frac{1}{\gamma}\right) f_\gamma(\gamma) d\gamma = 1$$

(3.44)

The condition in equation (3.44) can be rewritten in simplified form as

$$\underbrace{\frac{1}{\gamma_{th}}(1-P_{out})}_{I_1} - \underbrace{\int_{\gamma_{th}}^\infty \frac{1}{\gamma} f_\gamma(\gamma) d\gamma}_{I_2} = 1$$

(3.45)

Using equation (3.24) we can write I_1 as

$$I_1 = \frac{1}{\gamma_{th}}\left[1 - \exp(-mkL)\sum_{z=0}^{\infty} \frac{(mkL)^z}{(z!)\Gamma(mL+z)} Y(mL+z, \eta\gamma_{th})\right] \qquad (3.46)$$

Using equation (3.20), and the infinite series expansion of ${}_0F_1(;.;.)$ I_2 can be written as

$$I_2 = \frac{\eta^{mL}}{\Gamma(mL)}\exp(-mkL)\sum_{s=0}^{\infty} \frac{(mkL\eta)^s \Gamma(mL)}{(s!)\Gamma(mL+s)}\int_{\gamma_{th}}^{\infty} \gamma^{(mL+s-1)-1}\exp(-\eta\gamma)d\gamma \qquad (3.47)$$

Applying equation (3.381.3) of [148] we get

$$I_2 = \frac{\eta^{mL}}{\Gamma(mL)}\exp(-mkL)\sum_{s=0}^{\infty} \frac{(mkL\eta)^s \Gamma(mL)}{(s!)\Gamma(mL+s)}\left[\frac{\Gamma(mL+s-1)}{\eta^{(mL+s-1)}} - \frac{Y(mL+s-1, \eta\gamma_{th})}{\eta^{(mL+s-1)}}\right] \qquad (3.48)$$

The above equation can be further simplified as

$$I_2 = \eta\exp(-mkL)\left[\sum_{s=0}^{\infty} \frac{(mkL)^s \Gamma(mL+s-1)}{(s!)\Gamma(mL+s)} - \sum_{s=0}^{\infty} \frac{(mkL)^s}{(s!)\Gamma(mL+s)} Y(mL+s-1, \eta\gamma_{th})\right] \qquad (3.49)$$

Further simplifying (3.49), we get

$$I_2 = \eta\exp(-mkL)\sum_{s=0}^{\infty}\left[\begin{array}{l} \dfrac{(mkL)^s}{(s!)} \dfrac{\Gamma(mL)}{\Gamma(mL+s)} \dfrac{\Gamma(mL+s-1)}{\Gamma(mL)} \dfrac{\Gamma(mL-1)}{\Gamma(mL-1)} \\[2mm] -\dfrac{(mkL)^s}{(s!)\Gamma(mL+s)} Y(mL+s-1, \eta\gamma_{th}) \end{array}\right] \qquad (3.50)$$

Rearranging the terms, we get

$$I_2 = \eta\exp(-mkL)\left[\sum_{s=0}^{\infty} \frac{(mkL)^s (mL-1)_s}{(s!)(mL)_s (mL-1)} - \sum_{s=0}^{\infty} \frac{(mkL)^s}{(s!)\Gamma(mL+s)} Y(mL+s-1, \eta\gamma_{th})\right] \qquad (3.51)$$

The final expression of I_2 comes out as

$$I_2 = \eta \exp(-mkL) \left[\frac{{}_1F_1(mL-1, mL; mkL)}{(mL-1)} - I_3 \right] \tag{3.52}$$

where

$$I_3 = \eta \sum_{s=0}^{\infty} \frac{(mkL)^s}{(s!)\Gamma(mL+s)} Y(mL+s-1, \eta\gamma_{th}) \exp(-mkL) \tag{3.53}$$

The upper bound on the truncation error in the expression of I_3 by S number of terms can be evaluated as

$$E_{I_3} = \eta \sum_{s=S}^{\infty} \frac{(mkL)^s}{(s!)\Gamma(mL+s)} Y(mL+s-1, \eta\gamma_{th}) \exp(-mkL) \tag{3.54}$$

Put g=s-S

$$E_{I_3} = \eta \sum_{g=0}^{\infty} \frac{(mkL)^{g+S}}{(g+s)!\Gamma(mL+g+S)} Y(mL+g+S-1, \eta\gamma_{th}) \exp(-mkL) \tag{3.55}$$

Using equation (8.351.2) of [148], we have

$$Y(mL+g+S-1, \eta\gamma_{th}) = \frac{(\eta\gamma_{th})^{mL+g+S-1}}{(mL+g+S-1)} {}_1F_1(mL+g+S-1, mL+g+S, -\eta\gamma_{th}) \tag{3.56}$$

Putting equation (3.56) in equation (3.55), and rearranging we get

$$E_{I_3} = \eta \sum_{g=0}^{\infty} \frac{(mkL)^{g+S}}{(g+S)!\Gamma(mL+g+S)} \frac{(\eta\gamma_{th})^{mL+g+S-1}}{(mL+g+S-1)} \exp(-mkL) {}_1F_1(mL+g+S-1, mL+g+S, -\eta\gamma_{th})$$

$$\tag{3.57}$$

Further simplifying equation (3.57), we have

$$E_{I_3} \leq (\eta\gamma_{th})^{mL-1}(mkL\eta\gamma_{th})^S {}_1F_1(mL+S-1, mL+S, -\eta\gamma_{th})\eta\exp(-mkL)$$

$$\times \sum_{g=0}^{\infty} \frac{(mkL\eta\gamma_{th})^g}{(g+S)!\Gamma(mL+g+S)} \frac{1}{(mL+g+S-1)} \tag{3.58}$$

In equation (3.58), $\displaystyle\sum_{g=0}^{\infty} \frac{(mkL\eta\gamma_{th})^g}{(g+S)!\Gamma(mL+g+S)} \frac{1}{(mL+g+S-1)}$ can be written as

$$\sum_{g=0}^{\infty} \frac{(mkL\eta\gamma_{th})^g}{(g+S)!\Gamma(mL+g+S)} \frac{1}{(mL+g+S-1)} = \sum_{g=0}^{\infty} \frac{(mkL\eta\gamma_{th})^g}{\Gamma(g+S+1)\Gamma(mL+g+S)} \frac{(mL+g+S-2)!}{(mL+g+S-1)!}$$

$$(3.59A)$$

On further simplification, we get

$$\sum_{g=0}^{\infty} \frac{(mkL\eta\gamma_{th})^g}{(g+S)!\Gamma(mL+g+S)} \frac{1}{(mL+g+S-1)} = \sum_{g=0}^{\infty} \frac{(mkL\eta\gamma_{th})^g}{\Gamma(g+S+1)\Gamma(mL+g+S)} \frac{\Gamma(mL+g+S-1)}{\Gamma(mL+g+S)}$$

$$(\,3.59\ B)$$

Which can be further solved as

$$\sum_{g=0}^{\infty} \frac{(mkL\eta\gamma_{th})^g}{(g+S)!\Gamma(mL+g+S)} \frac{1}{(mL+g+S-1)} =$$

$$\sum_{g=0}^{\infty} \frac{(mkL\eta\gamma_{th})^g}{g!} \frac{(1)_g}{(S+1)_g} \frac{(mL+S-1)_g}{(mL+S)_g(mL+S)_g} \frac{\Gamma(mL+S-1)}{\Gamma(S+1)\Gamma(mL+S)\Gamma(mL+S)} \tag{3.59 C}$$

Put equation (3.59C) in equation (3.58), we have

$$E_{I_3} \leq \frac{(\eta\gamma_{th})^{mL-1}(mkL\eta\gamma_{th})^S {}_1F_1(mL+S-1, mL+S; -\eta\gamma_{th})\Gamma(mL+S-1)\exp(-mkL)}{(S!)\Gamma(mL+S+1\Gamma(mL+S)}$$

$$\times {}_2F_3\left[\begin{matrix} 1 & (mL+S-1) \\ (S+1) & (mL+S) & (mL+S) \end{matrix}\middle| mkL\eta\gamma_{th}\right] \tag{3.60}$$

49

We know, $\dfrac{\Gamma(mL+S-1)}{\Gamma(mL+S)} = \dfrac{1}{(mL+S-1)}$. For solving the expression of   OPRA   CC,

put equation (3.20) in equation (3.43), we get

$$\frac{C_{OPRA}}{B} = \int_{\gamma_{th}}^{\infty} \log_2(\frac{\gamma}{\gamma_{th}}) \frac{\eta^{mL}}{\Gamma(mL)} \exp(-mkL) \exp(-\eta\gamma)\gamma^{(mL-1)} \sum_{s=0}^{\infty} \frac{\Gamma(mL)}{\Gamma(mL+s)} (mkL\eta\gamma)^s d\gamma \quad (3.61)$$

Further simplifying the above equation, we have

$$\frac{C_{OPRA}}{B} = \frac{\eta^{mL}\exp(-mkL)}{\ln(2)} \sum_{s=0}^{\infty} \frac{(mkL\eta)^s}{s!\,\Gamma(mL+s)} \int_{\gamma_{th}}^{\infty} \log(\frac{\gamma}{\gamma_{th}})\gamma^{(mL+s-1)} \exp(-\eta\gamma)d\gamma \quad (3.62)$$

Applying the change of variable $z=(\gamma/\gamma_{th})$ and $dz = \dfrac{1}{\gamma_{th}}d\gamma$

$$\frac{C_{OPRA}}{B} = \frac{\eta^{mL}\exp(-mkL)}{\ln(2)} \sum_{s=0}^{\infty} \frac{(mkL\eta)^s}{s!\,\Gamma(mL+s)} \int_{1}^{\infty} \log(z)(z\gamma_{th})^{(mL+s-1)} \exp(-\eta\gamma_{th})\gamma_{th}dz \quad (3.63)$$

On further simplifying we get

$$\frac{C_{OPRA}}{B} = \frac{\eta^{mL}\exp(-mkL)}{\ln(2)}(\gamma_{th})^{(mL+s)} \sum_{s=0}^{\infty} \frac{(mkL\eta)^s}{s!\,\Gamma(mL+s)} \int_{1}^{\infty} (z)^{(mL+s-1)} \log z\, e\,\mathrm{xp}(-\eta\gamma_{th}z)dz \quad (3.64)$$

Using   equation   (4.358.1)   of   [148],

$$\int_{1}^{\infty} (z)^{(mL+s-1)} \log z\, e\,\mathrm{xp}(-\eta\gamma_{th}z)dz = \frac{\partial}{\partial(mL+s)}(\eta\gamma_{th})^{-(mL+s)} \Gamma(mL+s,\eta\gamma_{th}) \text{ in } \text{ equation } (3.64),$$

we have

$$\frac{C_{OPRA}}{B} = \frac{\eta^{mL}\exp(-mkL)}{\ln(2)} \sum_{s=0}^{\infty} \frac{(mkL\eta\gamma_{th})^s}{s!\,\Gamma(mL+s)} \frac{\partial}{\partial(mL+s)}(\eta\gamma_{th})^{-(mL+s)} \Gamma(mL+s,\eta\gamma_{th}) \quad (3.65)$$

Solving the following term in the above equation

$$\frac{\partial}{\partial(mL+s)}\left(\eta\gamma_{th}\right)^{-(mL+s)}\Gamma(mL+s,\eta\gamma_{th}) \tag{3.66}$$

We have

$$\frac{\partial[\left(\eta\gamma_{th}\right)^{-(mL+s)}\Gamma(mL+s,\eta\gamma_{th})]}{\partial(mL+s)}=\left(\eta\gamma_{th}\right)^{-(mL+s)}\frac{\partial}{\partial(mL+s)}\Gamma(mL+s,\eta\gamma_{th})+\Gamma(mL+s,\eta\gamma_{th})\frac{\partial}{\partial(mL+s)}\left(\eta\gamma_{th}\right)^{-(mL+s)}$$

$$\tag{3.67}$$

Solving the term, $\Gamma(mL+s,\eta\gamma_{th})\dfrac{\partial}{\partial(mL+s)}\left(\eta\gamma_{th}\right)^{-(mL+s)}$, we get

$$\Gamma(mL+s,\eta\gamma_{th})\frac{\partial}{\partial(mL+s)}\left(\eta\gamma_{th}\right)^{-(mL+s)}=-\Gamma(mL+s,\eta\gamma_{th})\log(\eta\gamma_{th})\left(\eta\gamma_{th}\right)^{-(mL+s)} \tag{3.68}$$

As per [24], we have

$$\left(\eta\gamma_{th}\right)^{-(mL+s)}\frac{\partial}{\partial(mL+s)}\Gamma(mL+s,\eta\gamma_{th})=\left(\eta\gamma_{th}\right)^{-(mL+s)}\left[\Gamma(mL+s,\eta\gamma_{th})\log\left(\eta\gamma_{th}\right)+G_{2,3}^{3,0}\left(\eta\gamma_{th}\left|\begin{matrix}1 & 1 \\ 0 & 0 & mL+s\end{matrix}\right.\right)\right] \tag{3.69}$$

Using equation (3.68) and equation (3.69) in equation (3.67), we get

$$\frac{\partial[\left(\eta\gamma_{th}\right)^{-(mL+s)}\Gamma(mL+s,\eta\gamma_{th})]}{\partial(mL+s)}=\left(\eta\gamma_{th}\right)^{-(mL+s)}[\Gamma(mL+s,\eta\gamma_{th})\log\left(\eta\gamma_{th}\right)$$
$$+G_{2,3}^{3,0}\left(\eta\gamma_{th}\left|\begin{matrix}1 & 1 \\ 0 & 0 & mL+s\end{matrix}\right.\right)]-\Gamma(mL+s,\eta\gamma_{th})\log(\eta\gamma_{th})\left(\eta\gamma_{th}\right)^{-(mL+s)}$$

$$\tag{3.70}$$

Further simplifying equation (3.70), we have

$$\frac{\partial[\left(\eta\gamma_{th}\right)^{-(mL+s)}\Gamma(mL+s,\eta\gamma_{th})]}{\partial(mL+s)}=\left(\eta\gamma_{th}\right)^{-(mL+s)}G_{2,3}^{3,0}\left(\eta\gamma_{th}\left|\begin{matrix}1 & 1 \\ 0 & 0 & mL+s\end{matrix}\right.\right) \tag{3.71}$$

Put equation (3.71) in equation (3.65), we get the final expression of OPRA CC as

$$\frac{C_{OPRA}}{B} = \frac{\eta^{(mL-mL+s-s)} \exp(-mkL)}{\ln(2)} \sum_{s=0}^{\infty} \frac{(mkL)^s}{s!\,\Gamma(mL+s)} G_{2,3}^{3,0}\left(\eta\gamma_{th} \left| \begin{array}{ccc} 1 & 1 & \\ 0 & 0 & mL+s \end{array} \right. \right)$$

(3.72)

3.2.3.3 CIFR

CIFR policy is also known as zero-outage capacity due to the reason that it maintains a fixed data rate regardless of the channel conditions. Under this policy, the transmitter allocates higher power to the channel with low SNR and lower power to the channel with high SNR so that the non-fluctuating received power is maintained. The CC under this scheme is defined by [50] as

$$C_{CIFR} = B \log_2 \left(1 + \frac{1}{\int_0^{\infty} (\frac{f_{\gamma}(\gamma)}{\gamma}) d\gamma} \right)$$

(3.73)

$$\text{Let } I_4 = \int_0^{\infty} \left(\frac{f_{\gamma}(\gamma)}{\gamma} \right) d\gamma$$

(3.74)

Taking into consideration I_4, it is nothing but the $E[1/\gamma]$, which can be directly evaluated by putting $i = -1$ in equation (3.37) as

$$I_4 = \frac{(mL)_{-1}}{\eta^{-1} \exp(mkL)} \,_1F_1(mL-1;mL;mkL)$$

(3.75)

Put equation (3.75) in equation (3.73), we get

$$C_{CIFR} = B \log_2 \left(1 + \frac{1}{\frac{\eta(mL)_{-1}}{\exp(mkL)} \,_1F_1(mL-1;mL;mkL)} \right)$$

(3.76)

3.2.3.4 *TIFR*

CIFR transmission policy is suffered from an efficiency drawback as it needs to invest more power to compensate the deep fades. An efficient way to compensate for this loss is to assign the power only if the received SNR is above the fixed threshold SNR. This policy is known as truncated CIFR (TIFR) CC and its expression over a fading channel can be obtained by [50] as

$$C_{TIFR} = B \log_2 \left(1 + \frac{1}{\int_{\gamma_{th}}^{\infty} \frac{f_\gamma(\gamma)}{\gamma}} \right) (1 - P_{out})$$

(3.77)

Let $I_2 = \int_{\gamma_{th}}^{\infty} \frac{f_\gamma(\gamma)}{\gamma}$. I_2 has already been evaluated and given in equation (3.52) and P_{out} is given by equation (3.24). The value of γ_{th} can be chosen to achieve a predetermined P_{out} or to maximize equation (3.77). P_{out} is achieved at the cutoff value γ_{th} which can be directly evaluated using equation (3.24). The final expression of C_{TIFR} can be given as

$$C_{TIFR} = \max \left[B \log_2 \left(1 + \frac{1}{I_2} \right) (1 - P_{out}) \right]$$

(3.78)

3.2.4 ASEP/ABEP

In case of fading channels, ASEP can be mathematically calculated out by averaging the instantaneous error probability and is given by [12] as

$$\overline{P} = E[P(\gamma)] = \int_0^\infty P(\gamma) f_\gamma(\gamma) d\gamma \qquad (3.79)$$

where $P(\gamma)$ is the instantaneous symbol error probability, which depends upon the modulation techniques used in the communication system.

3.2.4.1 *Coherent Modulation Scheme*

The generalized symbol error probability expression for the coherent modulation scheme is given by [12] as

$$P_{Coherent}(\gamma) = \sum_{d=1}^{D} \alpha_d [Q(\sqrt{C_0 \gamma})]^d \qquad (3.80)$$

The values of D, α_d and C_0 for different coherent modulation schemes are defined in [153]

$$Q(\sqrt{C_0 \gamma}) = (\frac{a_1}{2} e^{-\frac{C_0 f \gamma}{2}} + \frac{a_2}{2} e^{-C_0 f \gamma})^d \qquad (3.81)$$

Putting equation (3.81) in equation (3.80), we get

$$P_{Coherent}(\gamma) = \sum_{d=1}^{D} \alpha_d (\frac{a_1}{2} e^{-\frac{C_0 f \gamma}{2}} + \frac{a_2}{2} e^{-C_0 f \gamma})^d \qquad (3.82)$$

Putting equation (3.82) and equation (3.20) in equation (3.79) and using the approximation of Marcum Q-function as defined in [153] we can write the ASEP for the fading channels as

$$\overline{P}_{Coh} \approx \frac{\eta^{mL}}{\Gamma(mL)} \exp(-mkL) \sum_{s=0}^{\infty} \frac{(mk\eta L)^s \Gamma(mL)}{s! \Gamma(mL+s)} \int_0^\infty \gamma^{(mL+s-1)} \exp(-\eta \gamma) \sum_{d=1}^{D} \alpha_d (\frac{a_1}{2} e^{-\frac{C_0 f \gamma}{2}} + \frac{a_2}{2} e^{-C_0 f \gamma})^d d\gamma$$

$$(3.83)$$

54

The parameters a_1, a_2 and b have their usual meaning as defined in [12], and using the

Binomial expansion in the above equation as

$$\sum_{\alpha=1}^{D} \alpha_d \left(\frac{a_1}{2} e^{-\frac{C_0 f \gamma}{2}} + \frac{a_2}{2} e^{-C_0 f \gamma}\right)^d = \sum_{d=1}^{D} \alpha_d \sum_{r=0}^{\alpha} C(d,r)\left(\frac{a_1}{2} e^{-\frac{C_0 f \gamma}{2}}\right)^{d-r} \left(\frac{a_2}{2} e^{-C_0 f \gamma}\right)^r \qquad (3.84)$$

Putting equation (3.84) in equation (3.83), we get

$$\bar{P}_{Coh} = \eta^{mL} \exp(-mkL) \sum_{s=0}^{\infty} \frac{(mk\eta L)^s}{s!\,\Gamma(mL+s)} \sum_{d=1}^{D} \alpha_d \sum_{r=0}^{\alpha} C(d,r)\left(\frac{a_1}{2}\right)^{d-r} \left(\frac{a_2}{2}\right)^r \int_0^{\infty} \gamma^{(mL+s-1)} e^{-\left(\frac{C_0 f \gamma}{2}(d-r)-C_0 f \gamma(r)\right)} \exp(-\eta\gamma)d\gamma$$

$$(3.85)$$

Solving the above integral terms using

$$\int_0^{\infty} \gamma^{(mL+s-1)} e^{-\left(\frac{C_0 f \gamma}{2}(d-r)-C_0 f \gamma(r)\right)} \exp(-\eta\gamma)d\gamma = \int_0^{\infty} \gamma^{(mL+s-1)} e^{-C_0 f \gamma\left(\frac{d}{2}-\frac{r}{2}+r\right)} \exp(-\eta\gamma)d\gamma \qquad (3.86)$$

We get

$$\int_0^{\infty} \gamma^{(mL+s-1)} e^{-\left(\frac{C_0 f \gamma}{2}(d-r)-C_0 f \gamma(r)\right)} \exp(-\eta\gamma)d\gamma = \int_0^{\infty} \gamma^{(mL+s-1)} \exp\left(-\gamma\left(\eta + \frac{C_0 f(d+r)}{2}\right)\right)d\gamma$$

$$(3.87)$$

Using equation (3.381.4) of [148], in the above equation as

$$\int_0^{\infty} \gamma^{(mL+s-1)} \exp\left(-\gamma\left(\eta + \frac{C_0 f(d+r)}{2}\right)\right)d\gamma = \frac{\Gamma(mL+s)}{\left(\eta + \frac{C_0 f(d+r)}{2}\right)^{mL+s}} \qquad (3.88)$$

Putting equation (3.88) in equation (3.85)

$$\overline{P}_{Coh} \approx \eta^{mL} \exp(-mkL) \sum_{s=0}^{\infty} \frac{(mk\eta L)^s}{s!} \sum_{d=1}^{D} \alpha_d \sum_{r=0}^{\alpha} C(d,r)(\frac{a_1}{2})^{d-r}(\frac{a_2}{2})^r (\frac{2}{2\eta + C_0 f(d+r)})^{mL+s}$$

(3.89)

Solving $\displaystyle\sum_{s=0}^{\infty} \frac{(mk\eta L)^s}{s!}(\frac{2}{2\eta + C_0 f(d+r)})^s = \sum_{s=0}^{\infty} \frac{\left(\dfrac{mk\eta L2}{2\eta + C_0 f(d+r)}\right)^s}{s!}$ using equation (1.211.1)

of [148] we get

$$\overline{P}_{Coh} \approx (\frac{2\eta}{2\eta + C_0 f(d+r)})^{mL} \exp(\frac{2mkL\eta}{2\eta + C_0 f(d+r)}) \exp(-mkL) \sum_{d=1}^{D} \alpha_d \sum_{r=0}^{\alpha} C(d,r)(\frac{a_1}{2})^{d-r}(\frac{a_2}{2})^r$$

(3.90)

Rearranging equation (3.90), final closed-form expression for generalized expression ASEP of coherent modulation schemes comes out as

$$\overline{P}_{coh} \approx (\frac{2\eta}{2\eta + C_0 f(d+r)})^{mL} \sum_{d=1}^{D} \alpha_d \sum_{r=0}^{\alpha} C(d,r)(\frac{a_1}{2})^{d-r}(\frac{a_2}{2})^r \exp(mkL(\frac{2\eta}{2\eta + C_0 f(d+r)} - 1))$$

(3.91)

3.2.4.2 *Non-coherent Modulation Scheme*

The system performance of coherent modulation techniques outperforms that of non-coherent modulation in terms of ASEP, but the biggest challenge involved in coherent detection is the hardware complexity involved during carrier phase recovery information, which makes the practical implementation of such system very difficult. The advantage of the non-coherent detection scheme is that it does not require carrier phase information and utilizes methods like square law detection to recover the transmitted data. The

mathematical expression of instantaneous error probability for non-coherent detection schemes is expressed using [154] as

$$P_{Non-coherent}(\gamma) = A\exp(-\gamma B)$$ (3.92)

where the values of A and B for different non-coherent detection schemes are defined in [154]. The expression for ASEP for non-coherent detection can be evaluated by putting equation (3.91) in equation (3.79) as

$$\bar{P}_{Non-coherent} = A\eta^{mL}\exp(-mkL)\sum_{s=0}^{\infty}\frac{(mk\eta L)^s}{s!\Gamma(mL+s)}\int_0^{\infty}\gamma^{mL+s-1}\exp(-\gamma(\eta+B))d\gamma$$ (3.93)

Using equation (3.381.4) of [148], $\int_0^{\infty}\gamma^{mL+s-1}\exp(-\gamma(\eta+B))d\gamma = \dfrac{\Gamma(mL+s)}{(\eta+B)^{mL+s}}$, we get

$$\bar{P}_{Non-coherent} = A(\frac{\eta}{\eta+B})^{mL}\exp(-mkL)\sum_{s=0}^{\infty}\frac{\left(\dfrac{mk\eta L}{\eta+B}\right)^s}{s!}$$ (3.94)

$$= A(\frac{\eta}{\eta+B})^{mL}\exp(-mkL)\exp(\frac{mkL\eta}{\eta+B})$$ (3.95)

After simplifying equation (3.95), the final expression comes out as

$$= A(\frac{\eta}{\eta+B})^{mL}\exp(mkL(\frac{\eta}{\eta+B}-1))$$ (3.96)

It is noted that the generalized ASEP expression produced in equation (3.91) for coherent detection and equation (3.96) for non-coherent detection is direct and easily implementable. The advantage of getting these straight forward expressions is that high

power and low power analysis of ASEP is not required to be performed as the original results are already very simplified and provide insights into the system performance.

3.3   Numerical Results and Discussions

This section provides the numerical results for the analytical expressions obtained in previous sections. For validating the correctness of the derived expressions, the corresponding Monte-Carlo simulations are also included in plots. In the Monte-Carlo simulations 10^6 random samples are generated, which are sufficient for the desired accuracy of the proposed methodology. Figure 3.1 illustrates the analytical and simulated results for Pout as a function of normalized outage threshold for various values of m and L. It is observed from the plots that diversity reduces the chances that the received SNR falls below a fixed threshold by a huge margin.
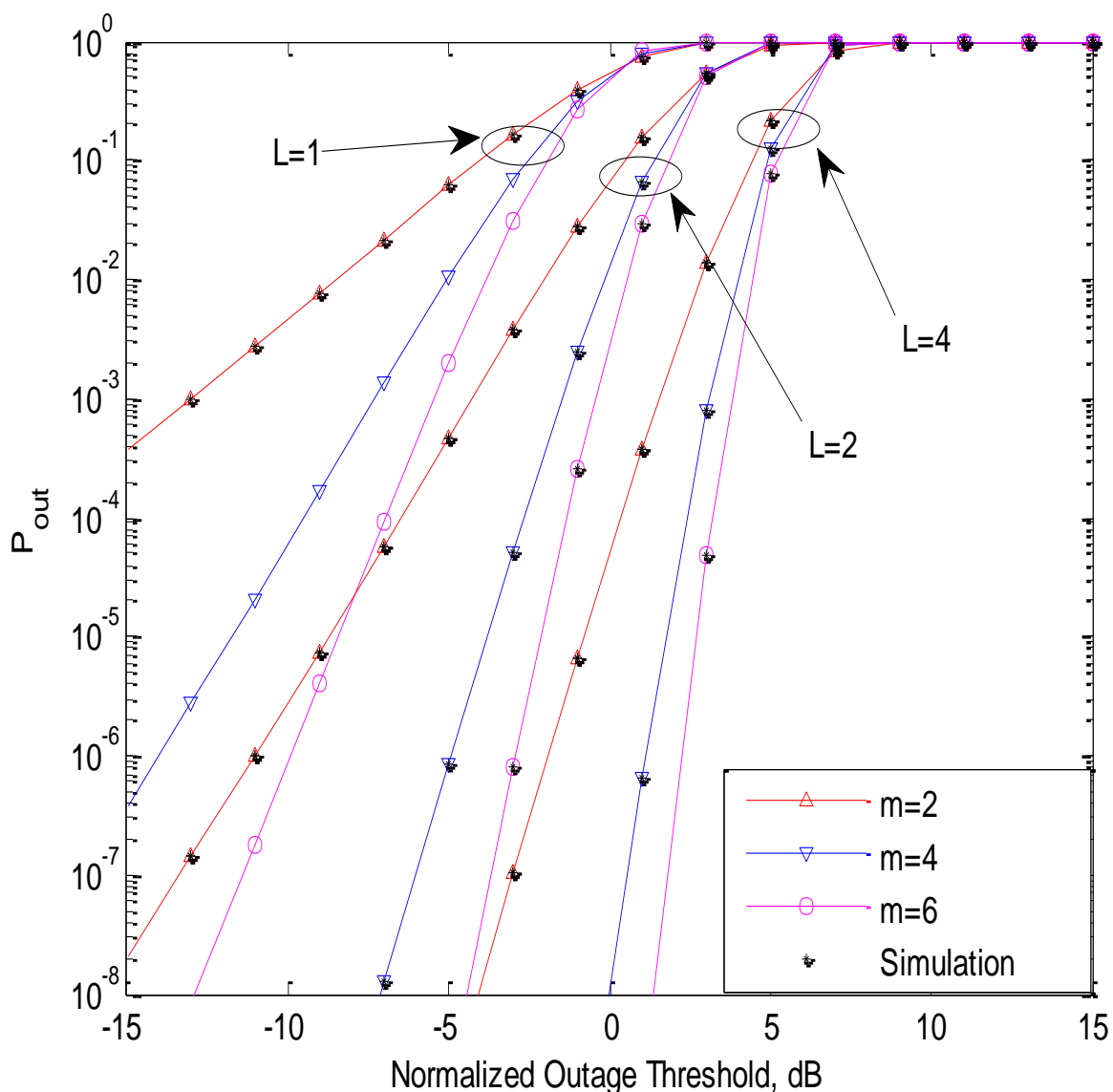
Figure 3.1 Pout versus normalized outage threshold for different values of m and diversity order

The number of terms required to get the desired accuracy in the closed-form analytical expression of P_{out} is shown in Figure 3.2. It is noted that the truncation error for a fixed value of *S* reduces with the decrease in average received SNR. The diversity has the advantage for lower values of *S* in terms of accuracy, but this behavior of the system gets reversed for higher values of *S*.
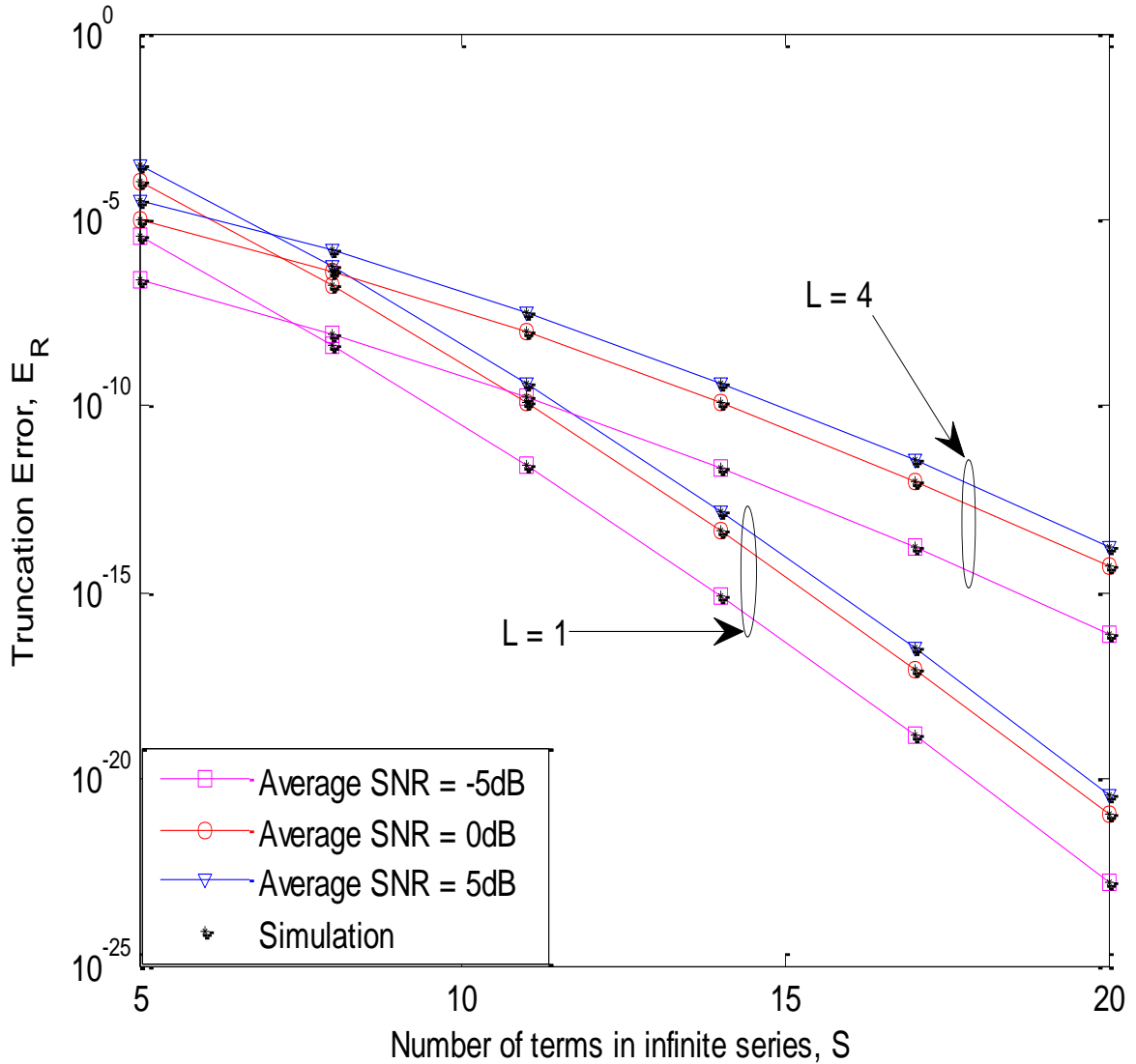
Figure 3.2 Truncation error versus the number of terms in the infinite series for different values of
average received SNR and diversity order

The variation of severity fading parameters versus the number of diversity branches is

shown in Figure 3.3. It is noted that the channel condition is improved with the increase

in L and k values. For the initial increase in L, the improvement in the system

performance is very predominating, which becomes saturated for further increase in L.
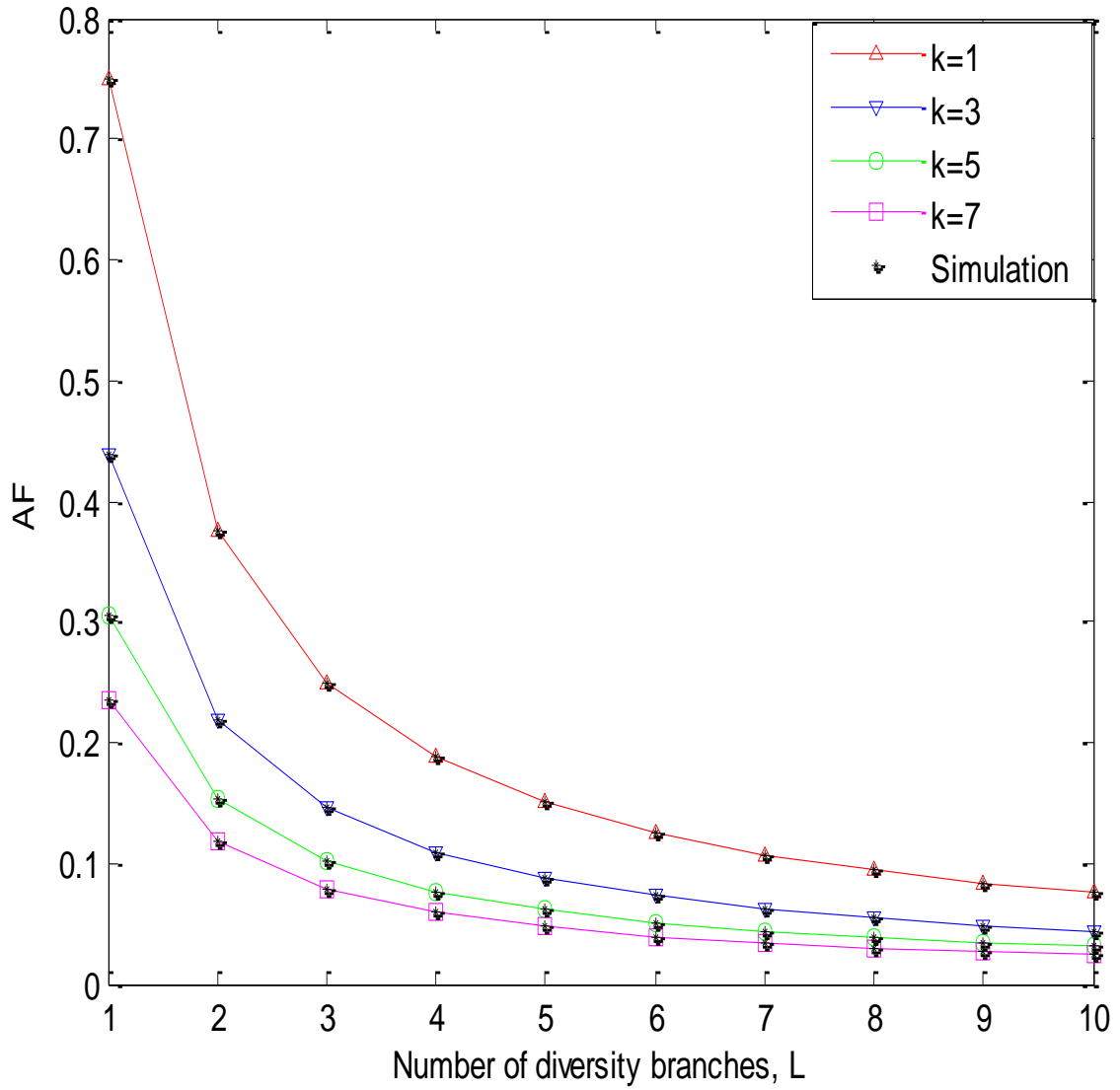
Figure 3.3 Amount of fading as a function of diversity branch for different values of k
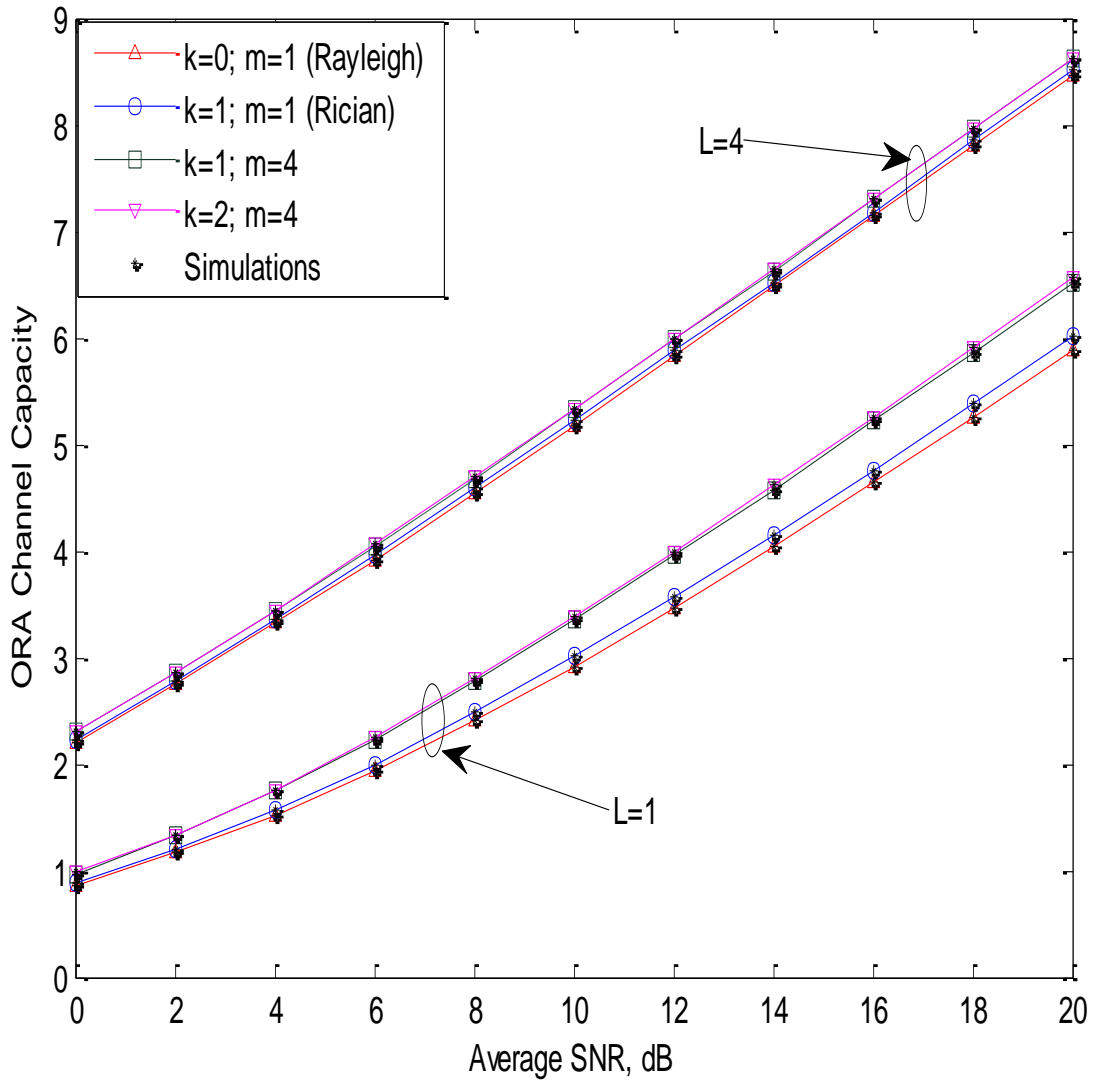
Figure 3.4 ORA CC versus average received SNR for various values of m, k and L

Figure 3.4 shows the ORA CC versus average received SNR for *L*-MRC BX fading channel. The effect of diversity order on the special cases of BX as Rayleigh (*k*=0, *m*=1) and Rician (*k*=1, *m*=1) fading are also shown here. It can be seen from this figure that the performance difference between *L=1* and *L=4* plots decrease with the increase in *L* values.
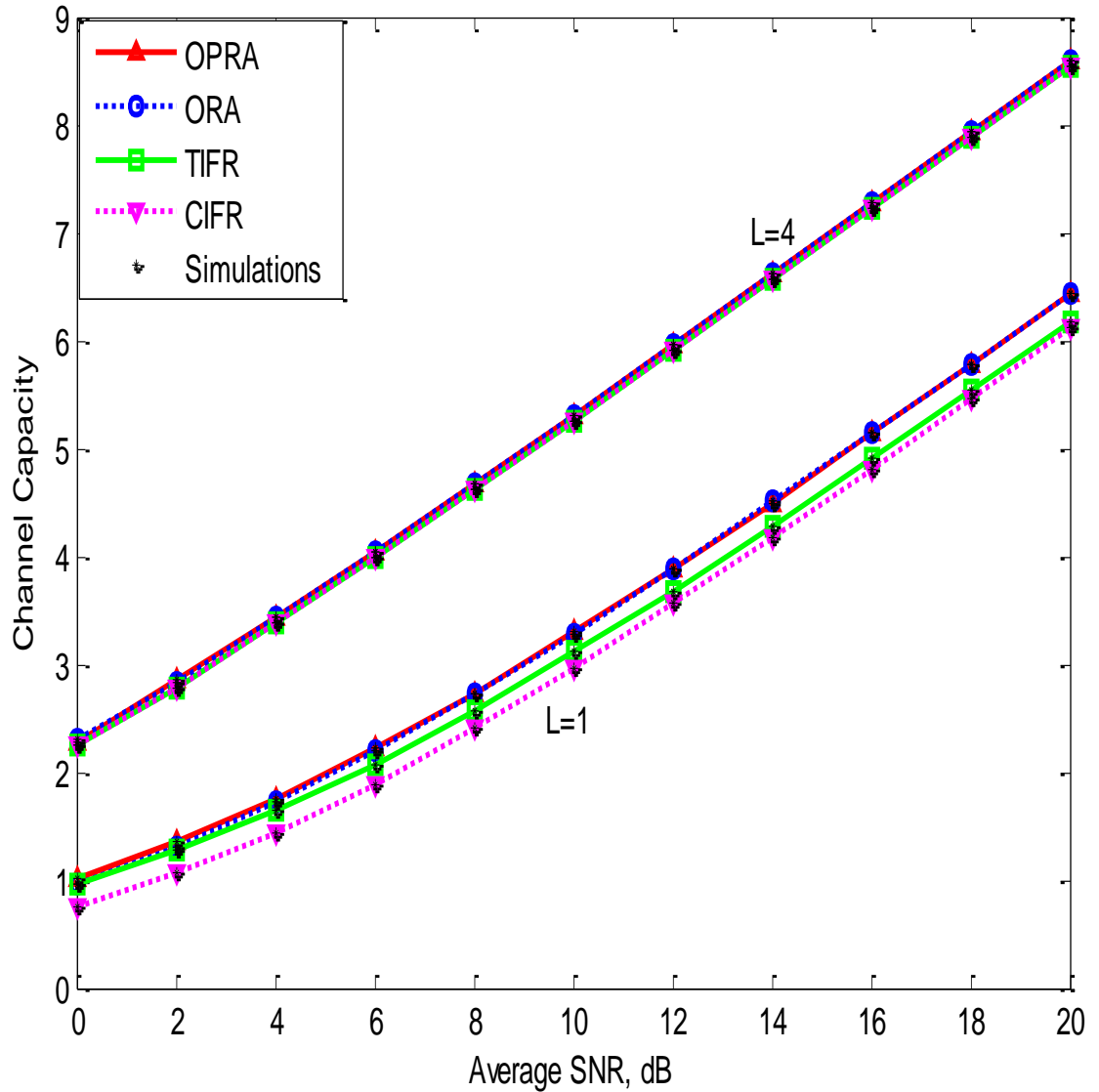
Figure 3.5 Variation of CC under different adaptive transmission schemes with average received SNR

Figure 3.5 illustrates the CC plots with two-branch and four-branch diversity for the different adaptive transmission techniques. It is clear from the figure that OPRA yields the maximum capacity among the available transmission schemes. It is also seen that increasing the number of branches tends to decrease the disparity in capacity between the different schemes. We also noticed that CIFR suffers a large capacity penalty than TIFR

scheme, because in TIFR truncated channel inversion is included in place of complete channel inversion. Figure 3.6 plots the ASEP against average received SNR for the coherent MPSK modulation scheme for various *m* values and also portray the impact of diversity order along with constellation size. The trend perceived here is that with the increment in the value of *L*, ASEP decreases while increment in the value of constellation size deteriorates the system performance by elevating error rate (upward shift of plot) and hence increases ASEP.
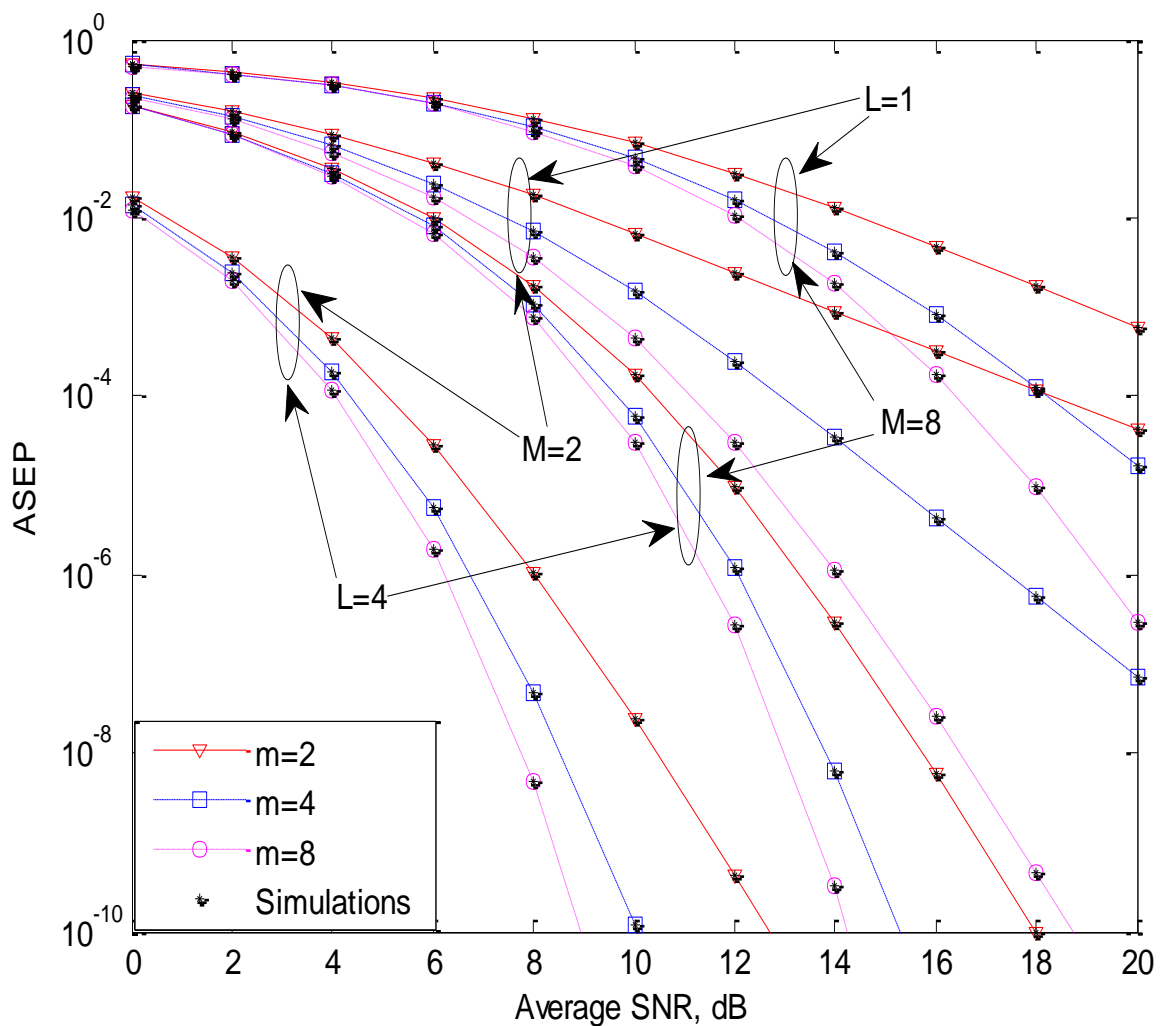
Figure 3.6 ASEP for M-PSK with several values of M, m and diversity order
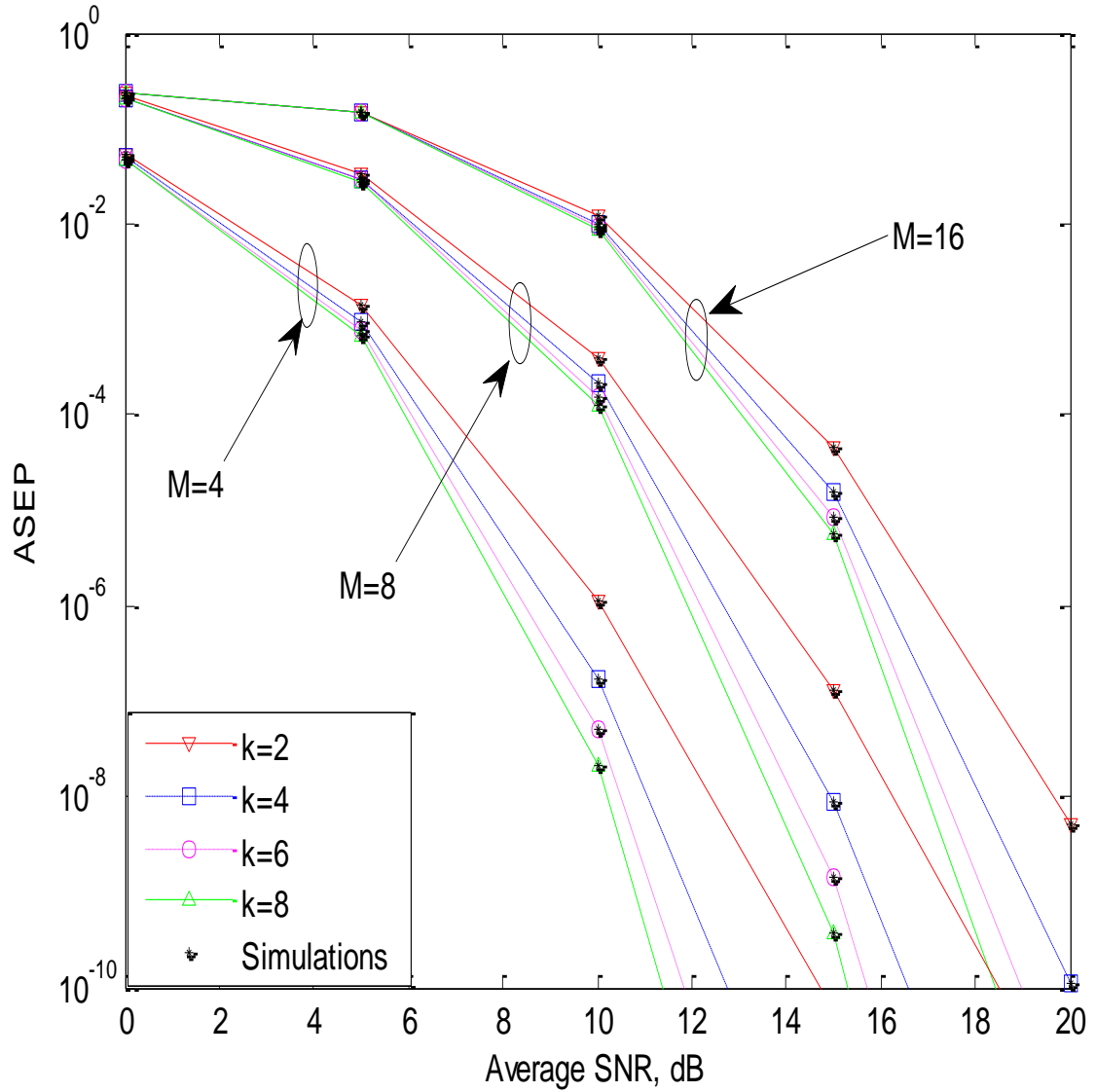
Figure 3.7 ASEP for M-QAM over different values of M and fading parameter k

Figure 3.7 exhibits the ASEP performance curves for *M*-QAM coherent modulation schemes for different values of *k* and *M*. It is clear from the figure that the increase in the parameter *k* makes the ASEP plot move downwards, which means error introduced by channel decreases and hence performance of the system improves.
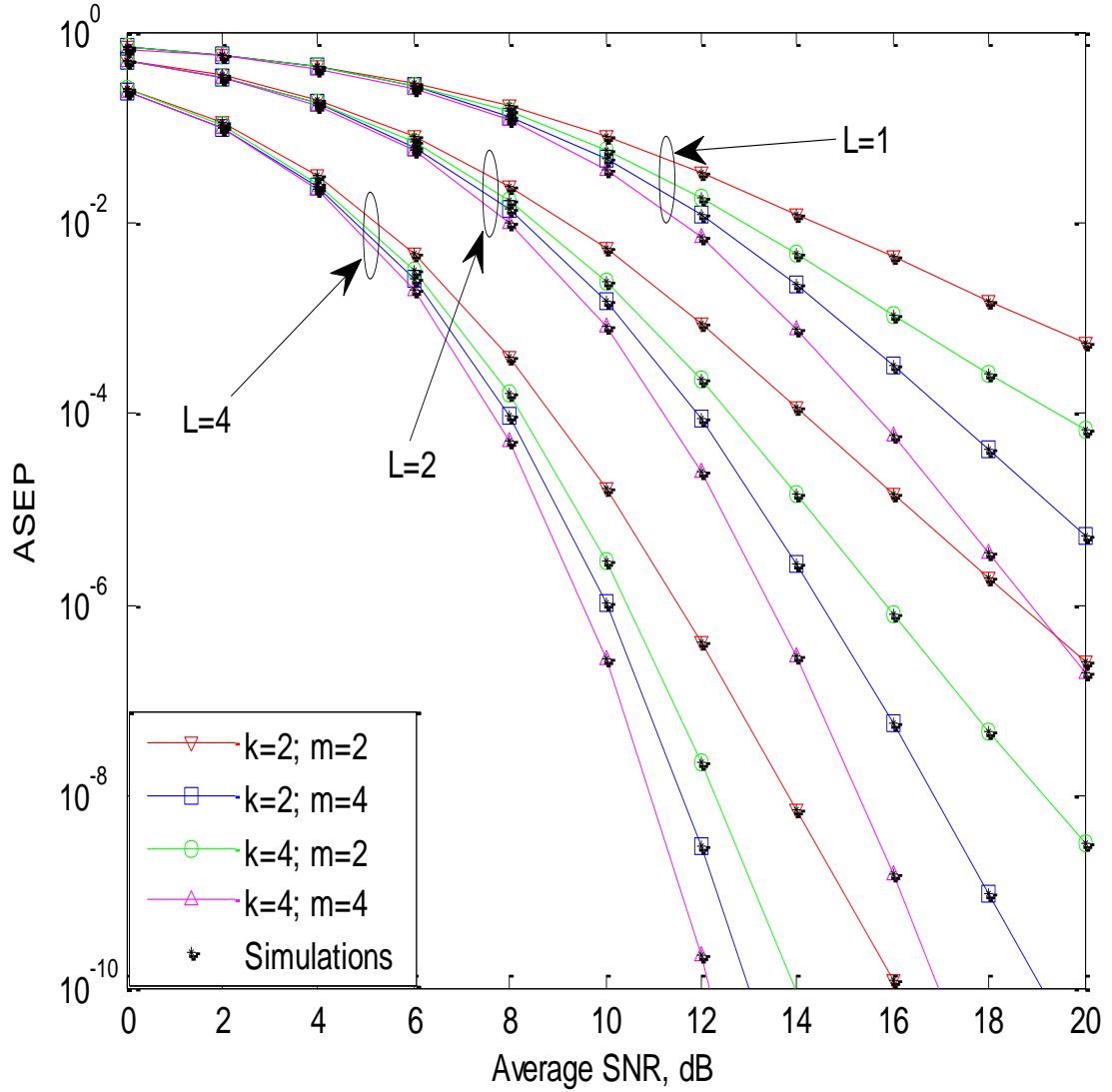
Figure 3.8 ASEP for non-coherent 8-FSK over various values of m, k and diversity order

ASEP performance of non-coherent M-FSK scheme for different values of *m, k* and *L* is illustrated in Figure 3.8 The effect of fading can be counter-attacked by applying the diversity scheme, as can be seen from the plot that increase in diversity order improves the channel conditions (as plot shifts downwards).

66

3.4   Significance Findings

This chapter presents the performance analysis over BX fading channel with MRC diversity. The closed-form expressions of the P_{out}, AF, CC and ASEP (coherent and non-coherent) are derived for the fading channel. The effect of diversity order and fading parameters on the system performance are analyzed. It is observed that with the increase in the number of diversity branches the deteriorating effect of fading is reduced. Along with ORA, OPRA, CIFR and TIFR CC policies, P_{out} analysis is also performed. The unified analytical expressions for various coherent and non-coherent modulation schemes with MRC diversity is also derived and demonstrated.

CHAPTER 4

PERFORMANCE ANALYSIS OF EC OVER BEAULIEU-XIE FADING CHANNEL WITH MULTI-ANTENNA SYSTEM

In this chapter, EC performance of the delay sensitive communication system over BX fading channel with multi-antenna system is studied. The closed-form mathematical expressions for the EC are derived and the effect of different fading parameters on the effective throughput of the system is demonstrated. The simplified asymptotic expression for high signal-to-noise ratio (SNR) and low SNR regimes are provided to gain more insight into the system.

4.1   System Model

To facilitate the efficient support of QoS in the next-generation wireless networks, it is essential to model a wireless channel in terms of connection-level QoS metrics such as data rate, delay and delay-violation probability. However, the existing wireless channel models, i.e., physical-layer channel models, do not explicitly characterize a wireless channel in terms of these QoS metrics. The reason is that, these complex QoS requirements need an analysis of the queueing behavior of the connection, which is hard to extract from physical layer models. To address this issue, a link-layer channel model termed the EC model is developed in [7]. In this approach, a wireless link is modeled by

two EC functions, namely, the probability of non-empty buffer, $\gamma^c(\mu)$ and the QoS

exponent, $\theta(\mu)$ of the connection. The QoS guarantees heavily rely on this queueing

model as shown in Figure 4.1. This figure shows that the source traffic and the network

service are matched using a FIFO buffer (queue).
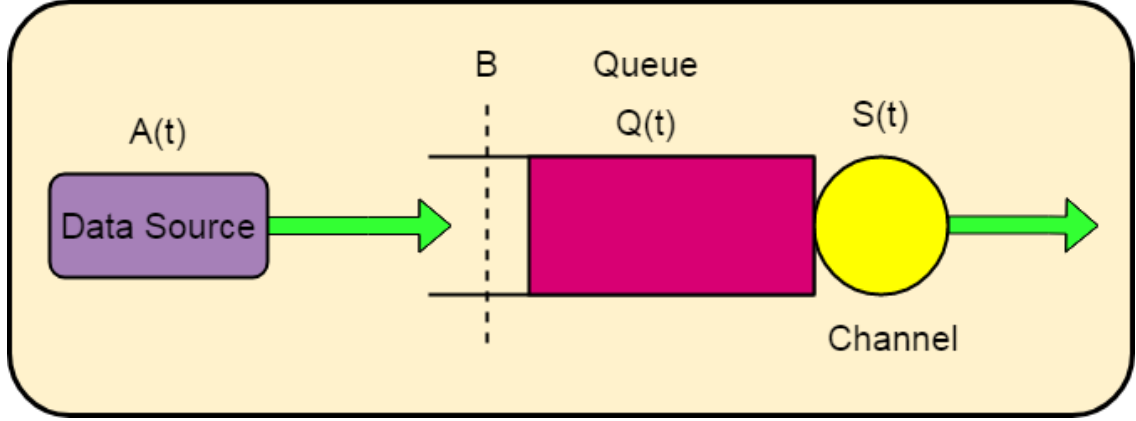
Figure 4.1 A Queueing system model

Considering a queue of infinite buffer size, *Q(t)* having a constant data rate with variable

CC. If the delay, *D(t)* is experienced by a source packet arriving at time *t*, then

probability of the *D(t)* exceeding a delay bound, *D_{max}* must satisfy the below condition

[7]

$$P_r\left(D(t) \geq D_{\max}\right) \approx \gamma^c\left(\mu\right)\exp\left(-\theta\left(\mu\right)D_{\max}\right) \tag{4.1}$$

where $\left\{\gamma^c\left(\mu\right), \theta\left(\mu\right)\right\}$ are the functions of the source rate $\left(\mu\right)$. For a given source rate,

$\gamma^c\left(\mu\right)$ and $\theta\left(\mu\right)$ at a time *t* are defined in [7] as

$$\gamma^c\left(\mu\right) = P_r\left(Q(t) \geq 0\right) \tag{4.2}$$

$$\theta\left(\mu\right) = -\lim_{B \to \infty} \frac{\log(P_r\left(Q(t) \geq B\right)}{B} \tag{4.3}$$

where B is the buffer size.

4.2   Channel Model

The PDF of the sum of L-branch SNR is given in equation (3.20). The MGF of a distribution function can be defined as

$$M_\gamma(s) = E\left[\exp(-s\gamma)\right] = \int_0^\infty \exp(-s\gamma)f_\gamma(\gamma)d\gamma \qquad (4.4)$$

Putting equation (3.20) into equation (4.4) and using the expansion of confluent hypergeometric function, we obtain

$$M_\gamma(s) = \frac{\eta^{mL}}{\exp(mkL)}\sum_{d=0}^\infty \frac{(mkL\eta)^d}{\Gamma(mL+d)(d!)}\int_0^\infty \gamma^{mL+d-1}\exp\left[(-\eta-s)^\gamma\right]d\gamma \quad (4.5)$$

Solving equation (4.5) using equation (3.478.1) of [148] and performing some mathematical simplifications, we get

$$M_\gamma(s) = \frac{1}{\exp(mkL)}\sum_{d=0}^\infty \frac{(mkL)^d}{d!}\left(1+\frac{s}{\eta}\right)^{-(mL+d)} \qquad (4.6)$$

To simplify the analysis, equation (4.6) can be further reduced using equation (8.4.2.5) of [155] as

$$M_\gamma(s) = \frac{1}{\exp(mkL)}\sum_{d=0}^\infty \frac{(mkL)^d}{(d!)\Gamma(mL+d)}G_{11}^{11}\left(\frac{s}{\eta}\Big|_0^{1-(mL+d)}\right) \qquad (4.7)$$

4.3   Performance Analysis

Consider a multi-antenna system model with L transmitting antennas and only one receiving antenna. The channels between different transmit and receive antennas are

assumed to be flat-fading channels. The channel's input-output relation can be given by

$y_d = h_{MISO} x + n$, where $h_{MISO} \in C^{1 \times L}$ denotes the MISO channel vector, x is the transmit

signal vector, and n represents the complex AWGN.

4.3.1 PDF-based Approach

4.3.1.1 Exact Analysis

For a $L \times 1$ MISO fading channel, the maximal arrival rate that can be supported under a

statistical QoS constraint can be expressed by [81] as

$$R(\rho,\theta) = -\frac{1}{A} \log_2 \left[E \left\{ \left(1 + \frac{\rho}{L} \gamma \right)^{-A} \right\} \right] = -\frac{1}{A} \log_2 \left[\int_o^\infty \left(1 + \frac{\rho}{L} \gamma \right)^{-A} f_\gamma(\gamma) d\gamma \right] \quad (4.8)$$

The average transmit SNR is defined as, $\rho = P_s / N_0$, where P_s is the average transmit

power of the system. Putting equation (3.20) in equation (4.8) and using the infinite series

expansion of $_0F_1(;.;.)$, we get

$$R(\rho,\theta) = -\frac{1}{A} \log_2 \left[\eta^{mL} \exp(-mkL) \sum_{d=0}^\infty \frac{(mkL\eta)^d}{d! \Gamma(mL+d)} \int_o^\infty \gamma^{(mL+d)-1} \exp(-\eta\gamma) \left(1 + \frac{\rho}{L} \gamma \right)^{-A} d\gamma \right]$$

$$(4.9)$$

The integration of equation (4.9) can be simplified using equation (39) of [156]. Using

equation (07.33.17.0007.01) of [151], the final expression of EC can be obtained as

$$R(\rho,\theta) = \frac{mkL}{A \ln(2)} - \log_2 \left(\frac{\eta L}{\rho} \right) - \frac{1}{A} \log_2 \left[\sum_{d=0}^\infty \frac{(mkL)^d}{d!} U \left(A; A - mL + 1 - d; \frac{\eta L}{\rho} \right) \right]$$

$$(4.10)$$

The above equation is in the form of infinite series summation. The error in equation (4.10) by truncating the series by D number of terms can be given by

$$E_D = \sum_{d=D}^{\infty} \frac{(mkL)^d}{d!} U\left(A; A - mL + 1 - d; \frac{\eta L}{\rho}\right) \quad (4.11)$$

Putting $g=d-D$ in the above equation and rearranging we get

$$E_D = (mkL)^D \sum_{g=0}^{\infty} \frac{(mkL)^g}{\Gamma(D+g+1)} U\left(A; A - mL + 1 - D - g; \frac{\eta L}{\rho}\right) \quad (4.12)$$

Since $U\left(A; A - mL + 1 - D - g; \frac{\eta L}{\rho}\right)$ is a monotonically decreasing function with respect to g. Therefore, E_D can be upper bounded as

$$E_D \le (mkL)^D \sum_{g=0}^{\infty} \frac{(mkL)^g}{\Gamma(D+g+1)} U\left(A; A - mL + 1 - D; \frac{\eta L}{\rho}\right) \quad (4.13)$$

Using equation (39) of [81], the above equation becomes as

$$E_D \le \left[1 - \frac{\Gamma(D, mkL)}{\Gamma(D)}\right] \exp(mkL) U\left(A; A - mL + 1 - D; \frac{\eta L}{\rho}\right) \quad (4.14)$$

4.3.1.2 Asymptotic Analysis

In general, the closed-form expression obtained in equation (4.10) is in the form of infinite series, thus the direct interpretation of the CC under QoS constraint becomes a bit difficult task. In this section, we derive closed-form approximations of the effective rate in both high-SNR and low-SNR regimes. These approximations reduce the computational

complexity and provide a straightforward way to understand the parameters' impact on

the system performance.

a) High SNR Approximation

High power analysis provides intuitive insight as how the system performance behaves

with respect to channel fading parameters at high SNR. The expression of EC at high

SNR ($\gamma \to \infty$) can be written using $\left(1+\rho\gamma/L\right)^{-A} \cong \left(\rho\gamma/L\right)^{-A}$ approximation in equation

(4.8) as

$$R\left(\rho \to \infty, \theta\right) \cong -\frac{1}{A}\log_2\left(I\right) \tag{4.15}$$

Putting equation (3.20) in equation (4.15) and using the series expansion of $_0F_1\left(;.;.\right)$, I

can be written as

$$I = \left(\frac{L}{\rho}\right)^A \eta^{mL} \exp(-mkL) \sum_{d=0}^{\infty} \frac{\left(mkL\eta\right)^d}{d\,!\Gamma\left(mL+d\right)} \int_0^{\infty} \gamma^{(mL+d-A)-1} \exp\left(-\eta\gamma\right) d\gamma \tag{4.16}$$

Applying equation (3.381.4) of [148] in the above expression, we get

$$I = \left(\frac{\eta L}{\rho}\right)^A \frac{\left(mL\right)_{-A}}{\exp(mkL)} {}_1F_1\left(mL-A;mL;mkL\right) \tag{4.17}$$

The expression of the EC for high-SNR regime can be obtained by putting equation

(4.17) in equation (4.15) as

$$R\left(\rho \to \infty, \theta\right) \cong -\frac{1}{A}\log_2\left(\left(\frac{\eta L}{\rho}\right)^A \frac{\left(mL\right)_{-A}}{\exp(mkL)} {}_1F_1\left(mL-A;mL;mkL\right)\right) \tag{4.18}$$

b) Low SNR Approximation

In many communication networks, such as cellular networks, systems often operate in low-SNR situations. Hence it is beneficial to derive an approximation of (4.10) in the low-SNR regime. Note that in the low-SNR regime, analysis based on SNR would lead to misleading conclusions. The capacity analysis should be better conducted using the transmitted normalized energy per information bit E_b/N_0 rather than the average SNR ρ. Following the same method as in [84], the effective rate in the low-SNR regime can be approximated by

$$R\left(\frac{E_b}{N_0}\right) \approx S_0 \log_2\left(\frac{E_b/N_0}{E_b/N_{0\,min}}\right) \tag{4.19}$$

where

$$S_0 = \frac{-2\left(R'(0,\theta)\right)^2 \ln(2)}{R''(0,\theta)} \quad \text{and} \quad \left(\frac{E_b}{N_{0\,min}}\right) = \frac{1}{R'(0,\theta)} \tag{4.20}$$

$R'(0,\theta)$ and $R''(0,\theta)$ are the first and second-order derivatives of $R(0,\theta)$, which are defined in terms of first and second moments of γ as

$$R'(0,\theta) = \frac{E[\gamma]}{L\ln(2)} \quad \text{and} \quad R''(0,\theta) = \frac{1}{L^2\ln(2)}\left[A\left(E[\gamma]\right)^2 - (A+1)E[\gamma^2]\right] \tag{4.21}$$

Putting equation (3.20) in the definition of $E[\gamma]$, $E[\gamma^2]$ and using equation (3.381.4) of [148], we get

$$E[\gamma] = \frac{(mL)_1}{\eta} \exp(-mkL) {}_1F_1(mL+1;mL;mkL) \qquad (4.22)$$

$$E[\gamma^2] = \frac{(mL)_2}{\eta^2} \exp(-mkL) {}_1F_1(mL+2;mL;mkL) \qquad (4.23)$$

Putting equation (4.22) and (4.23) into equation (4.21), we get the expressions of $R'(0,\theta)$ and $R''(0,\theta)$, which are further used to get the value of S_0 and $E_b/N_{0\,min}$ as in equation (4.20). Further substituting S_0 and $E_b/N_{0\,min}$ in equation (4.19), we get the final expression for the EC at low SNR as

$$R\left(\frac{E_b}{N_0}\right) = \frac{2\log_2\left\{\dfrac{E_b}{N_0} \dfrac{(mL)_1 \exp(-mkL) {}_1F_1(mL+1;mL;mkL)}{\eta L \ln(2)}\right\}}{\left\{\dfrac{(A+1)(mL)_2 \exp(mkL) {}_1F_1(mL+2;mL;mkL)}{(mL)_1^2 \left[{}_1F_1(mL+1;mL;mkL)\right]^2} - A\right\}} \qquad (4.24)$$

To further simplify this using the expansion of ${}_1F_1(\ )$ function, we get

$$R\left(\frac{E_b}{N_0}\right) = \frac{2\log_2\left\{\dfrac{E_b}{N_0} \dfrac{\exp(-mkL)}{\eta L \ln(2)} \displaystyle\sum_{n=0}^{\infty} \dfrac{(mL+n)(mkL)^n}{n!}\right\}}{\left\{(A+1)\exp(mkL)\displaystyle\sum_{n=0}^{\infty} \dfrac{(mL+1+n)n!}{(mL+n)(mkL)^n} - A\right\}} \qquad (4.25)$$

4.3.2 MGF-based Approach

4.3.2.1 Exact Analysis

Compared to the PDF-based approach, the MGF-based approach has many advantages. First, the PDF-based approach can be viewed as a special case of the MGF-based approach. This is due to the fact that in the PDF-based approach, the joint PDF has to be

obtained in advance of further analysis. Rewriting equation (4.8) in terms of MGF as given in [157], we get the expression of EC as

$$R(\rho,\theta) = -\frac{1}{A}\log_2\left[\frac{1}{\Gamma(A)}\int_0^\infty s^{A-1}\exp(-s)M_\gamma\left(\frac{\rho s}{L}\right)ds\right] \qquad (4.26)$$

Substituting equation (4.7) into equation (4.26), using variable transformation and using equation (07.34.03.0228.01) of [151], we get

$$R(\rho,\theta) = -\frac{1}{A}\log_2\left[\begin{array}{c}\dfrac{1}{\Gamma(A)\exp(mkL)}\\ \times\displaystyle\sum_{d=0}^\infty \dfrac{(mkL)^d}{(d!)\Gamma(mL+d)}\int_0^\infty s^{A-1}G_{01}^{10}\left(s\,\big|_0^{-}\right)G_{11}^{11}\left(\dfrac{\rho s}{\eta L}\,\big|_0^{1-(mL+d)}\right)ds\end{array}\right] \qquad (4.27)$$

Furthermore, applying (07.34.21.0011.01) of [151] in the above equation, we get

$$R(\rho,\theta) = -\frac{1}{A}\log_2\left[\frac{1}{\Gamma(A)\exp(mkL)}\sum_{d=0}^\infty \frac{(mkL)^d}{(d!)\Gamma(mL+d)}G_{21}^{12}\left(\frac{\rho}{\eta L}\,\big|_0^{1-(mL+d)}\right)\right] \qquad (4.28)$$

4.3.2.2 Asymptotic Analysis

Considering high SNR conditions, i.e. when $\rho\to\infty$, the MGF expression in equation (4.7) can be approximated as

$$M_\gamma(s) \approx \frac{1}{\exp(mkL)}\left(\frac{\rho s}{\eta L}\right)^{-mL} \qquad (4.29)$$

Substituting equation (4.29) into equation (4.26), we get

$$R(\rho\to\infty,\theta) \approx -\frac{1}{A}\log_2\left[\frac{1}{\Gamma(A)}\int_0^\infty s^{A-1}\exp(-s)\frac{1}{\exp(mkL)}\left(\frac{\rho s}{\eta L}\right)^{-mL}ds\right] \qquad (4.30)$$

Rearranging the terms, we get

$$R(\rho \to \infty, \theta) \approx -\frac{1}{A}\log_2\left[\frac{1}{\Gamma(A)}\frac{(\rho/\eta L)^{-mL}}{\exp(mkL)}\int_0^\infty s^{A-mL-1}\exp(-s)ds\right] \quad (4.31)$$

Solving the integral using equation (3.381.3) of [148], the expression of EC under high SNR regime can be approximated as

$$R(\rho \to \infty, \theta) \approx -\frac{1}{A}\log_2\left[\frac{1}{\Gamma(A)}\frac{\Gamma(A-mL)}{\exp(mkL)}\left(\frac{\rho}{\eta L}\right)^{-mL}\right] \quad (4.32)$$

4.4   Numerical Results and Discussions

In this section, we have presented the analytical results to study the impact of various system parameters on the performance of the effective rate.
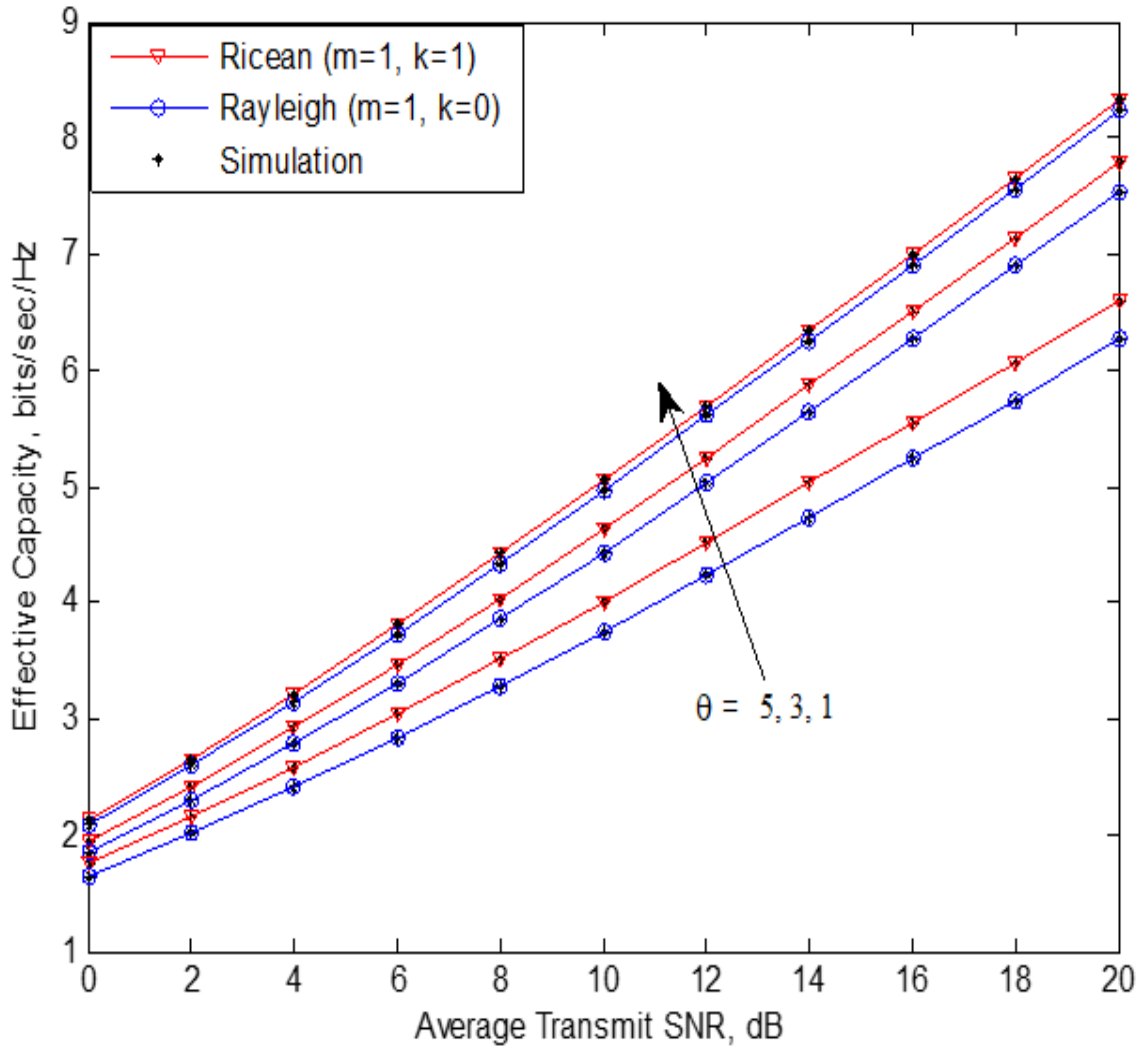
Figure 4.2 EC versus ρ for different values of Θ

The variation of effective rate versus ρ for different values of Θ and by keeping constant L=4, T=1, B=1 is shown in Figure 4.2. The effective rate increases with an increase in k and Θ values. It is noted that the effect of delay exponent on the system performance is more pronounced than the fading parameter k.
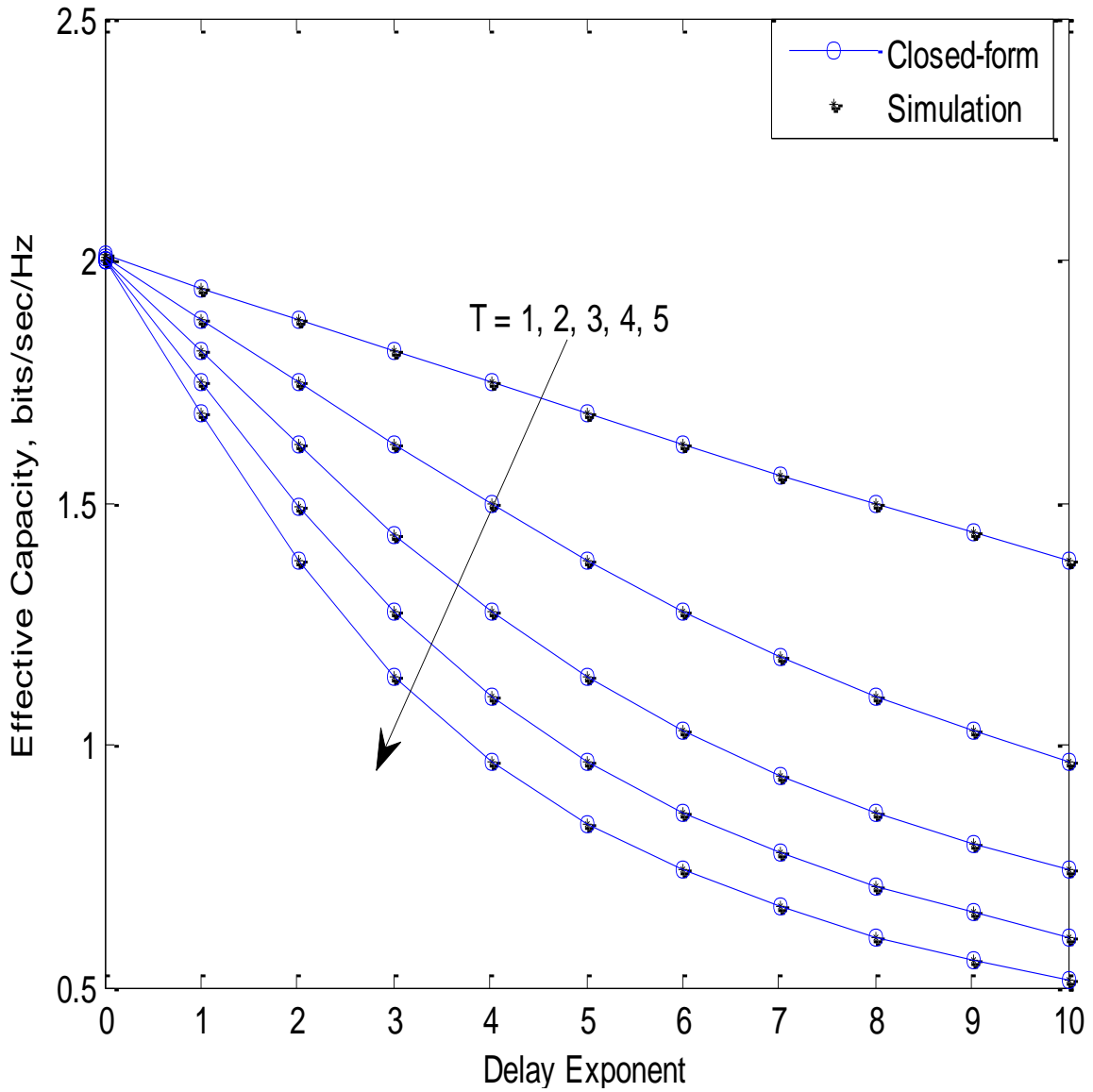
Figure 4.3 EC versus θ for various values of T

It is noted that the difference between the plots of delay exponent is less at lower average

transmitted SNR, and the plots depart away with an increase in average transmitted SNR.

It is observed that for a fixed value of *m*=1, *k*=0, the EC value is increased (from 1.6503

to 2.0908) by 27% when $\theta \rightarrow 5$ to 1 at $\rho = 0dB$, while EC value is increased (from

6.2643 to 8.2292) by 31% for $\theta \rightarrow 5$ to 1 at $\rho = 20dB$.
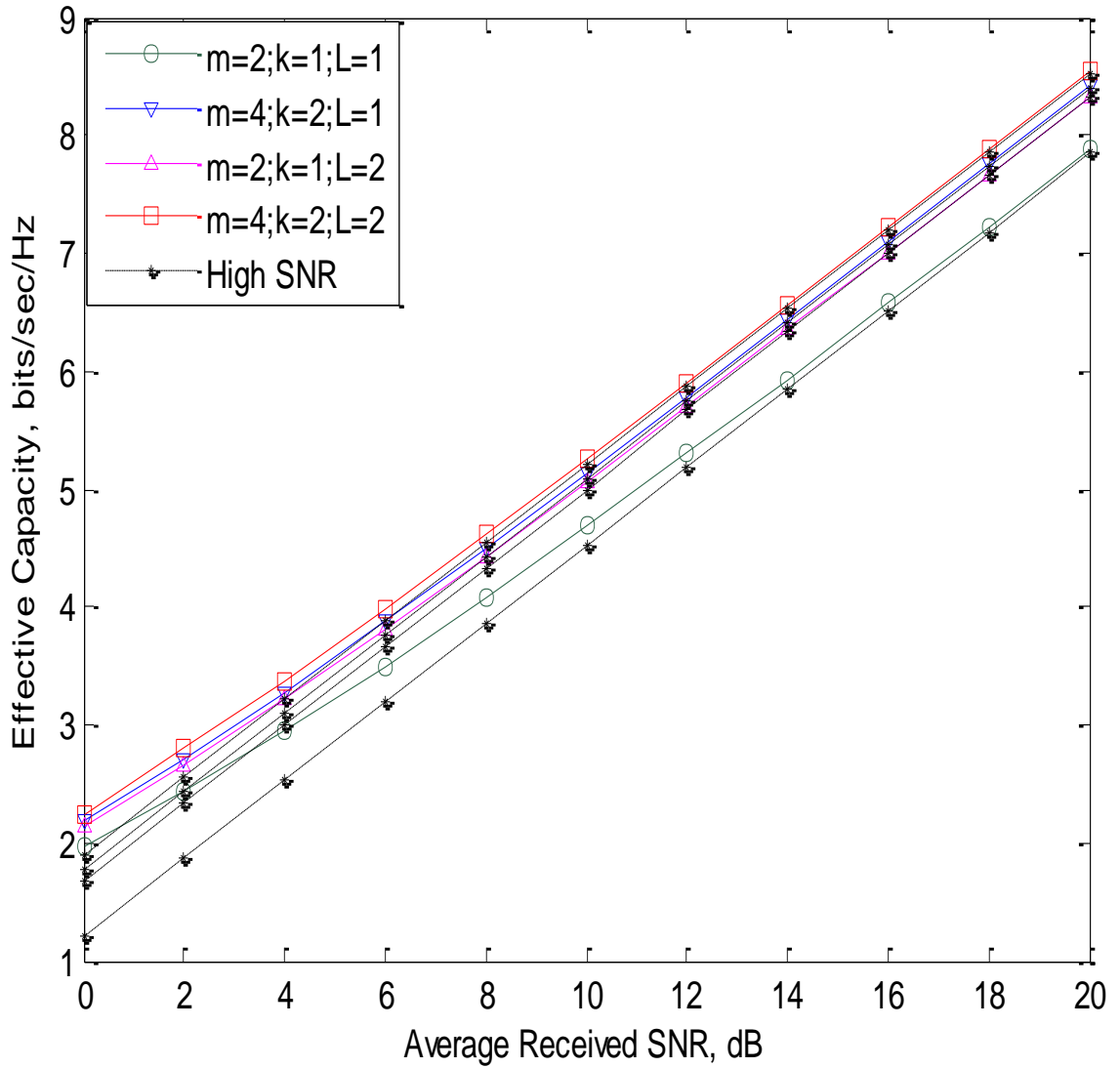
Figure 4.4 EC **versus** $\overline{\gamma}$ *for different values of m, k and L*
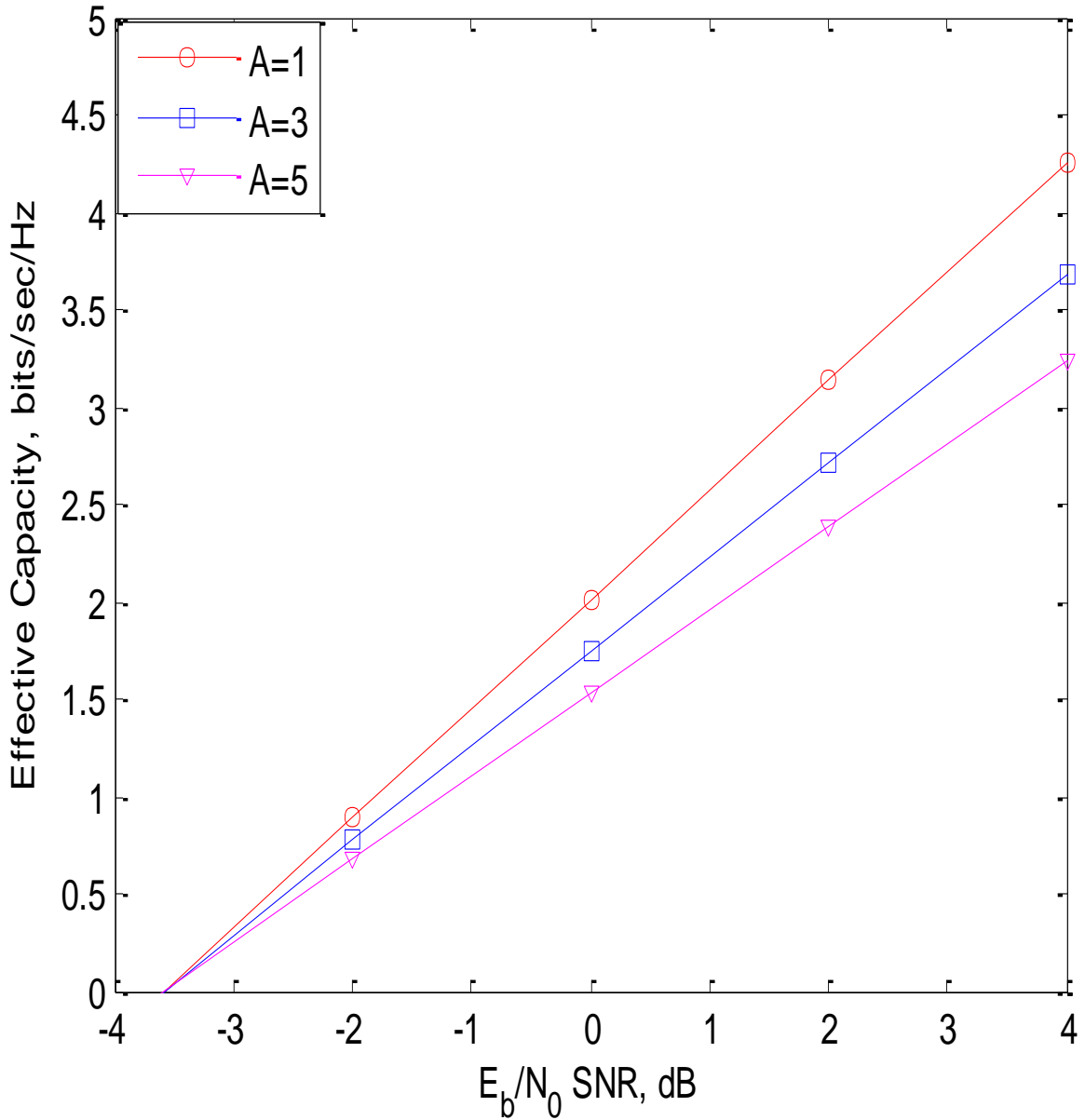
Figure 4.5 EC versus Eb/N0 at low SNR

The impact of T on the EC as a function of Θ is shown in Figure 4.3. It is observed from

the plots that the EC of the system was found to decrease with the increase in frame

duration and delay exponents. It is noted from the plots that for a fixed value of m=2,

k=2, L=2, B=1, ρ = 5dB and Θ =8, the EC value is reduced (from 2.4641 to 1.6835) by

32% when T is increased from 1 to 2, while EC is reduced (from 1.0195 to 0.8574) by

16% when T changes from 4 to 5. The combined effect of *m, k* and *L* on the EC as a

function of average received SNR is shown in Figure 4.4.
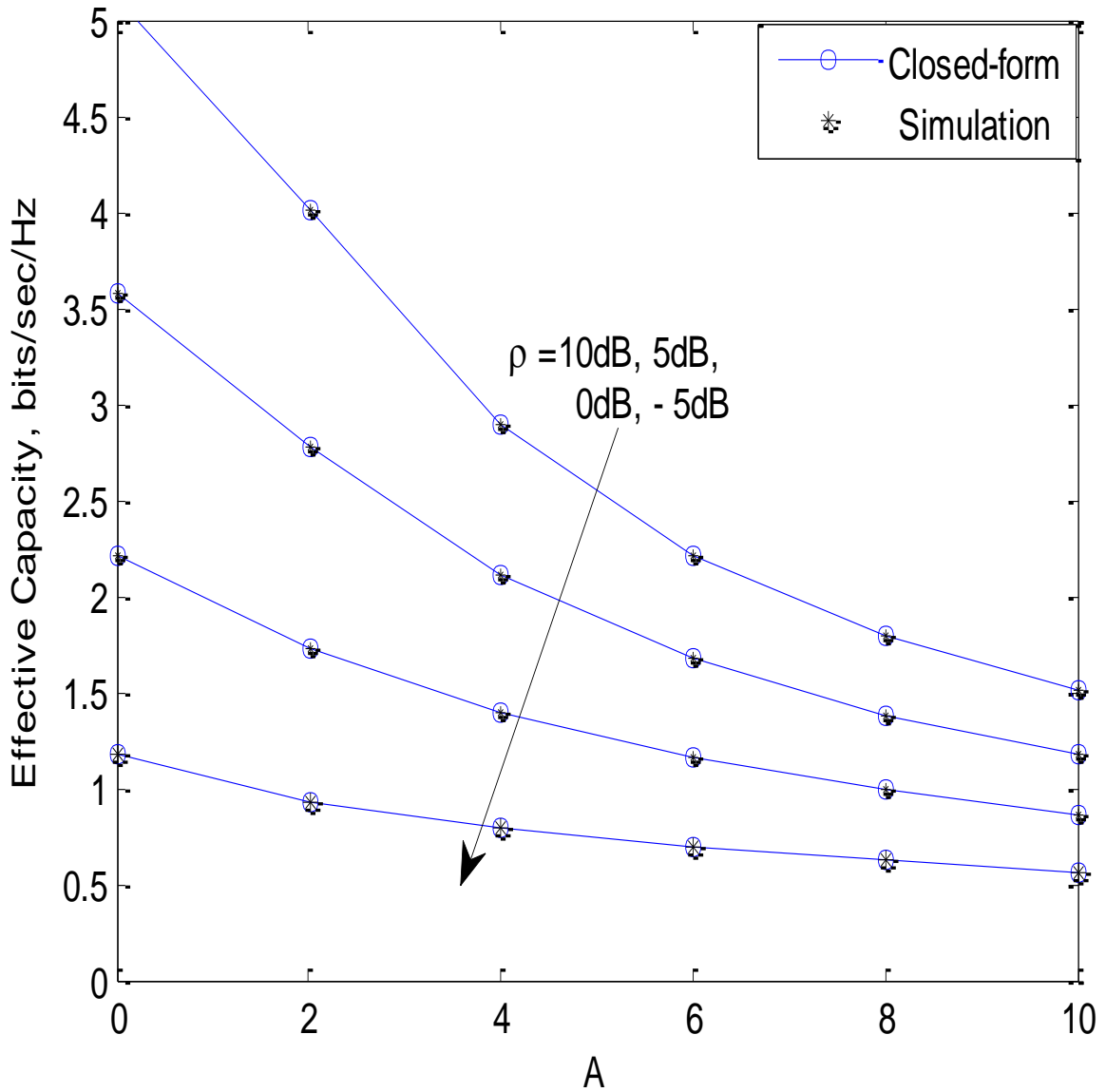
Figure 4.6 Effective throughput versus A for various values of ρ

. The asymptotic plots of the EC are also shown in this figure. The asymptotic plots are

seen to merge quickly with the analytical plots for higher values of fading parameters and

diversity order. In Figure 4.5, the results are drawn for EC in case of low SNR against

E_b/N_0 for various values of *A*, and fixed value of *m=2*, *k=2*, *L=3* with constant average

received SNR of 2 *dB*. From the figure, it can be demonstrated that in the case of low

SNR the EC is increasing by reducing the delay parameter of the system. The impact of

delay constraint *A* on the effective throughput performance is illustrated in Figure 4.6.

From the figure, it is seen that the effective throughput considerably decreases when the

value of A changes from 0 to 10. Particularly, for a fixed value of *m=0.5*, *k=0.5* and *N=4*,

the EC value is increased (from 2.7727 to 4.0010) by 44% when $\rho \rightarrow 5$dB to 10dB at

A=2, while EC value is increased (from 1.1805 to 1.5090) by 28% when $\rho \rightarrow 5$dB to

10dB at A=10. Besides, at high ρ values, the system achieves higher effective

throughput, especially at a very low *A* regime. The results presented in this study can be

used in designing the communication systems for real-time applications in femtocells and

high-speed trains.

4.5   Significant Findings

We have derived the mathematical expression of effective rate performance of the system

over BX fading channel for multi-antenna system. High power and low power asymptotic

expressions of the maximum data rate are provided. It is concluded that the growing

demand of the high data rate with tighter delay constraints can be achieved by increasing

the number of diversity branches in the system. Simulation results are in close agreement

with the numerical results.

CHAPTER 5

PERFORMANCE ANALYSIS OF EC OVER FISHER-SNEDECOR *F* FADING CHANNEL WITH MRC RECEPTION

The EC performance of the delay sensitive communication system over FSF fading channel with MRC is studied. The closed-form mathematical expressions for the EC are derived in terms of Meijer G-function and the effect of different fading parameters on the effective throughput of the system is demonstrated. The simplified asymptotic expression for high SNR and low SNR regimes is provided to gain more insight in to the system. The effect of different system parameters on the EC performance is also demonstrated. Simulation results are corroborated along with the numerical results to verify the correctness of the formulation.

5.1   System and Channel Model

To encourage the effective support of QoS in next-generation wireless networks, it is essential to present a wireless channel in terms of connection-level QoS metrics. Using the physical-layer channel models, the performance evaluation of the delay-

limited applications can be complicated and unreliable in some cases [7]. With the

support of EC, the channel can be modeled in terms of link-layer QoS-metrics. To

evaluate the performance of real-time applications of the wireless communication

system under the QoS requirements such as delay, reliability, and efficiency, the EC

concept is introduced in [7]. FSF distribution is used to model the combined effect of

multipath fading and shadowing. This model is formed by the composition of

Nakagami-*m* and inverse Nakagami-*m* distributions. The PDF of the received SNR of

the l_{th} branch of MRC combiner over FSF distribution is given by [71] as

$$f_{\gamma_l}(\gamma) = \frac{m_l^{m_l}\left(m_{s_l}\overline{\gamma}_l\right)^{m_{s_l}}\gamma_l^{(m_l-1)}}{B\left(m_l,m_{s_l}\right)\left(m_l\gamma_l + m_{s_l}\overline{\gamma}_l\right)^{m_l+m_{s_l}}} \tag{5.1}$$

where $\overline{\gamma}_l$ is the average received SNR of the l_{th} branch, m_l is the fading parameter and

m_{s_l} is shadowing parameter of the l_{th} branch. The channel severity is inversely

proportional to the shadowing parameter. The *L* branch MRC combiner co-phased,

weighted and summed the individual branch SNRs and get the instantaneous SNR (γ)

at the output of the combiner using

$$\gamma = \sum_{l=1}^{L}\gamma_l \tag{5.2}$$

With the assumptions of *L* i.i.d. branches of MRC with equal average SNR in all the

branches i.e. $\overline{\gamma}_l = \overline{\gamma}$ for $l \in \{1,2,3,...L\}$, the mathematical expression for the PDF of

γ is given by [73] as

$$f_{\gamma}(\gamma) = \frac{\gamma^{(mL-1)}}{B\left(mL,m_sL\right)}\left(\frac{m}{Lm_s\overline{\gamma}}\right)^{mL}{}_2F_1\left((m+m_s)L,mL;mL,-\frac{m}{Lm_s\overline{\gamma}}\gamma\right)(5.3)$$

5.2 EC Performance Analysis

5.2.1 Exact Analysis

We derive the mathematical formulation of the effective rate of the system over FSF fading channel with L branch MRC combiner. Putting equation (5.3) in equation (1.11) and using [158], the EC expression is written as

$$
R(\theta) = -\frac{1}{A}\log_2 \left(\begin{array}{c} \dfrac{1}{\Gamma(A)\Gamma(mL)\Gamma(m_sL)}\left(\dfrac{m}{Lm_s\bar{\gamma}}\right)^{mL} \int_0^\infty \gamma^{(mL-1)} G_{1\ 1}^{1\ 1}\left[\gamma \left| \begin{array}{c}(1-A)\\0\end{array}\right.\right] \\ \times G_{2\ 2}^{1\ 2}\left[\dfrac{m}{Lm_s\bar{\gamma}} \left| \begin{array}{cc}(1-mL-m_sL) & (1-mL)\\0 & (1-mL)\end{array}\right.\right] d\gamma \end{array} \right)
$$

(5.4)

Using equation (07.34.21.0011.01) of [151] and after some mathematical manipulations, equation (5.4) can be further simplified as

$$
R(\theta) = -\frac{1}{A}\log_2\left(\frac{1}{\Gamma(A)\Gamma(mL)\Gamma(m_sL)} G_{2\ 2}^{2\ 2}\left[\frac{Lm_s\bar{\gamma}}{m}\left|\begin{array}{cc}(1-A) & (1-mL)\\0 & m_sL\end{array}\right.\right]\right)
$$

(5.5)

5.2.1.1 Special Cases of Fisher-Snedecor *F* channel

Nakagami-*m* and Rayleigh fading channels are special cases of FSF distribution. The EC of Nakagami-*m* can be obtained from equation (5.5) by putting $m_s \to \infty$ as

$$
R(\theta) = -\frac{1}{A}\log_2\left(\frac{1}{\Gamma(A)\Gamma(mL)}\underset{m_s\to\infty}{Lim}\frac{1}{\Gamma(m_s)} G_{2\ 2}^{2\ 2}\left[\frac{Lm_s\bar{\gamma}}{m}\left|\begin{array}{cc}(1-A) & (1-mL)\\0 & m_sL\end{array}\right.\right]\right)
$$

(5.6)

Using equation (8.2.2.12) of [159] , the closed-form expression of effective rate over Nakagami-*m* channel with diversity reception can be written as

$$R_{Nak}(\theta) = -\frac{1}{A}\log_2\left(\frac{1}{\Gamma(A)\Gamma(mL)}G_{2\ 1}^{1\ 2}\left[\frac{\bar{\gamma}}{m}\Big|\begin{array}{cc}(1-A)&(1-mL)\\0&\end{array}\right]\right) \quad (5.7)$$

Putting $m = 1$ in equation (5.7), one can easily find out the EC expression for Rayleigh fading channels with MRC diversity as

$$R_{Ray}(\theta) = -\frac{1}{A}\log_2\left(\frac{1}{\Gamma(A)\Gamma(L)}G_{2\ 1}^{1\ 2}\left[\bar{\gamma}\Big|\begin{array}{cc}(1-A)&(1-L)\\0&\end{array}\right]\right) \quad (5.8)$$

5.2.2 Asymptotic Analysis

In this section, we present a detailed asymptotic analysis of the effective throughput in both high and low SNR regimes. The aim of providing asymptotic analysis for system performance is to gain more physical insights and optimize system parameters accordingly [160]. In addition, the asymptotic result reduces the analytical complexity while designing the system.

5.2.2.1 High SNR Approximation

High power analysis provides intuitive insight as how the system performance behaves with respect to channel fading parameters at high SNR. The expression of EC at high SNR can be written using $(1+\gamma)^{-A} \cong \gamma^{-A}$ approximation in equation (1.11) as

$$R(\rho \to \infty, \theta) = -\frac{1}{A}\log_2(I) \quad (5.9)$$

where I is written as

$$I = \int_0^\infty \frac{\gamma^{(mL-A-1)}}{B(mL,m_sL)}\left(\frac{m}{Lm_s\bar{\gamma}}\right)^{mL}{}_2F_1\left((m+m_s)L,mL;mL;-\frac{m}{Lm_s\bar{\gamma}}\gamma\right)d\gamma \quad (5.10)$$

Using equation (2.21.1.1) of [159] and simplifying, the above equation can be written as

$$I = \left(\frac{m}{Lm_s\bar{\gamma}}\right)^A \frac{\Gamma(mL-A)\Gamma(m_sL+A)}{\Gamma(mL)\Gamma(m_sL)} \qquad (5.10)$$

Putting equation (5.10) in equation (5.9), we can get the final expression of EC as

$$R(\rho \to \infty, \theta) = -\frac{1}{A}\log_2\left(\left(\frac{m}{Lm_s\bar{\gamma}}\right)^A \frac{\Gamma(mL-A)\Gamma(m_sL+A)}{\Gamma(mL)\Gamma(m_sL)}\right) \qquad (5.11)$$

Similarly, the high-power EC expressions for Nakagami-m and Rayleigh can be derived by using $\underset{a\to\infty}{Lim}\left[a^{-b}\Gamma(a+b)/\Gamma(a)\right]=1$ in equation (5.11) and simplified as

$$R_{Nak}(\rho \to \infty, \theta) = -\frac{1}{A}\log_2\left(\left(\frac{m}{\bar{\gamma}}\right)^A \frac{\Gamma(mL-A)}{\Gamma(mL)}\right) \qquad (5.12)$$

$$R_{Ray}(\rho \to \infty, \theta) = -\frac{1}{A}\log_2\left(\left(\frac{1}{\bar{\gamma}}\right)^A \frac{\Gamma(L-A)}{\Gamma(L)}\right) \qquad (5.13)$$

5.2.2.2 Low SNR Approximation

It is required to derive an approximation of equation (5.5) in the low-SNR regime. The effective rate performance for the fading channel is investigated for a low-power regime by considering that channel information is known to the Rx only where Tx may have either no channel information or imperfect channel information. By following the second order Taylor expansion of the EC at $\rho \to 0^+$, as per below equation:

$$R(\rho, \theta) = R'(0, \theta)\rho + R''(0, \theta)\frac{\rho^2}{2} + o(\rho^2) \qquad (5.14)$$

where $R'(0,\theta)$ and $R''(0,\theta)$ are the first and second-order derivatives of $R(\rho,\theta)$ with respect to average transmitting SNR, ρ at $\rho = 0$. Note that in the low-SNR regime, analysis based on ρ would lead to misleading conclusions. The capacity analysis should be better conducted using the transmitted normalized energy per information bit (E_b/N_0) rather than the average SNR ρ [161]. Following the same method as in [161], the effective rate in the low-SNR regime can be approximated as equation (4.19). The parameters of equation (4.19) are defined in equations (4.20) and (4.21).

Putting equation (5.3) in the definition of ith moment i.e., $E\left[\gamma^i\right] = \int_0^\infty \gamma^i f_\gamma(\gamma) d\gamma$, we get

$$E\left[\gamma^i\right] = \int_0^\infty \frac{\gamma^{(mL+i-1)}}{B(mL,m_sL)}\left(\frac{m}{Lm_s\bar{\gamma}}\right)^{mL} {}_2F_1\left((m+m_s)L,mL;mL,-\frac{m}{Lm_s\bar{\gamma}}\gamma\right)d\gamma \tag{5.15}$$

Using the relationship between hypergeometric function and Meijer G function and using (7.811.4) of [148] we get

$$E\left[\gamma^i\right] = \frac{\Gamma(mL+i)\Gamma(m_sL-i)}{\Gamma(mL)\Gamma(m_sL)}\left(\frac{m}{m_sL\bar{\gamma}}\right)^{-i} \tag{5.16}$$

The expressions of $E[\gamma]$ and $E\left[\gamma^2\right]$ can be easily calculated using equation (5.16) as

$$E[\gamma] = \frac{\Gamma(mL+1)\Gamma(m_sL-1)}{\Gamma(mL)\Gamma(m_sL)}\left(\frac{m}{m_sL\bar{\gamma}}\right)^{-1} \tag{5.17}$$

$$E\left[\gamma^2\right] = \frac{\Gamma(mL+2)\Gamma(m_sL-2)}{\Gamma(mL)\Gamma(m_sL)}\left(\frac{m}{m_sL\bar{\gamma}}\right)^{-2} \tag{5.18}$$

89

Putting the value of $E[\gamma]$ and $E[\gamma^2]$ from equations (5.17) and (5.18) into equation

(4.21), the expressions for $R'(0,\theta)$ and $R''(0,\theta)$ can be obtained as

$$R'(0,\theta) = \frac{\Gamma(mL+1)\Gamma(m_sL-1)}{\ln(2)\Gamma(mL)\Gamma(m_sL)}\left(\frac{m}{m_sL\bar{\gamma}}\right)^{-1} \tag{5.19}$$

$$R''(0,\theta) = \frac{1}{\ln(2)}\left[\begin{array}{l} A\left\{\dfrac{\Gamma(mL+1)\Gamma(m_sL-1)}{\Gamma(mL)\Gamma(m_sL)}\left(\dfrac{m}{m_sL\bar{\gamma}}\right)^{-1}\right\}^2 \\[3mm] -(A+1)\left\{\dfrac{\Gamma(mL+2)\Gamma(m_sL-2)}{\Gamma(mL)\Gamma(m_sL)}\left(\dfrac{m}{m_sL\bar{\gamma}}\right)^{-2}\right\} \end{array}\right] \tag{5.20}$$

Now putting equation (5.19) and equation (5.20) in equation (4.20), we get the

expressions of $(E_b/N_0)_{min}$ and S_0. Further, applying these results in equation (4.19), we

get the final expression of EC for low SNR regime.

5.3   Numerical Results and Discussions

In this section, we have presented the analytical results to study the impact of various

system parameters on the performance of the effective rate. The variation of effective

rate versus received SNR for different diversity order and fading parameters are

shown in figure 5.1. The effective rate increases with an increase in *m* and *L* values. It

is noted that the effect of diversity order on the system performance is more

pronounced for lower values of the fading parameters.
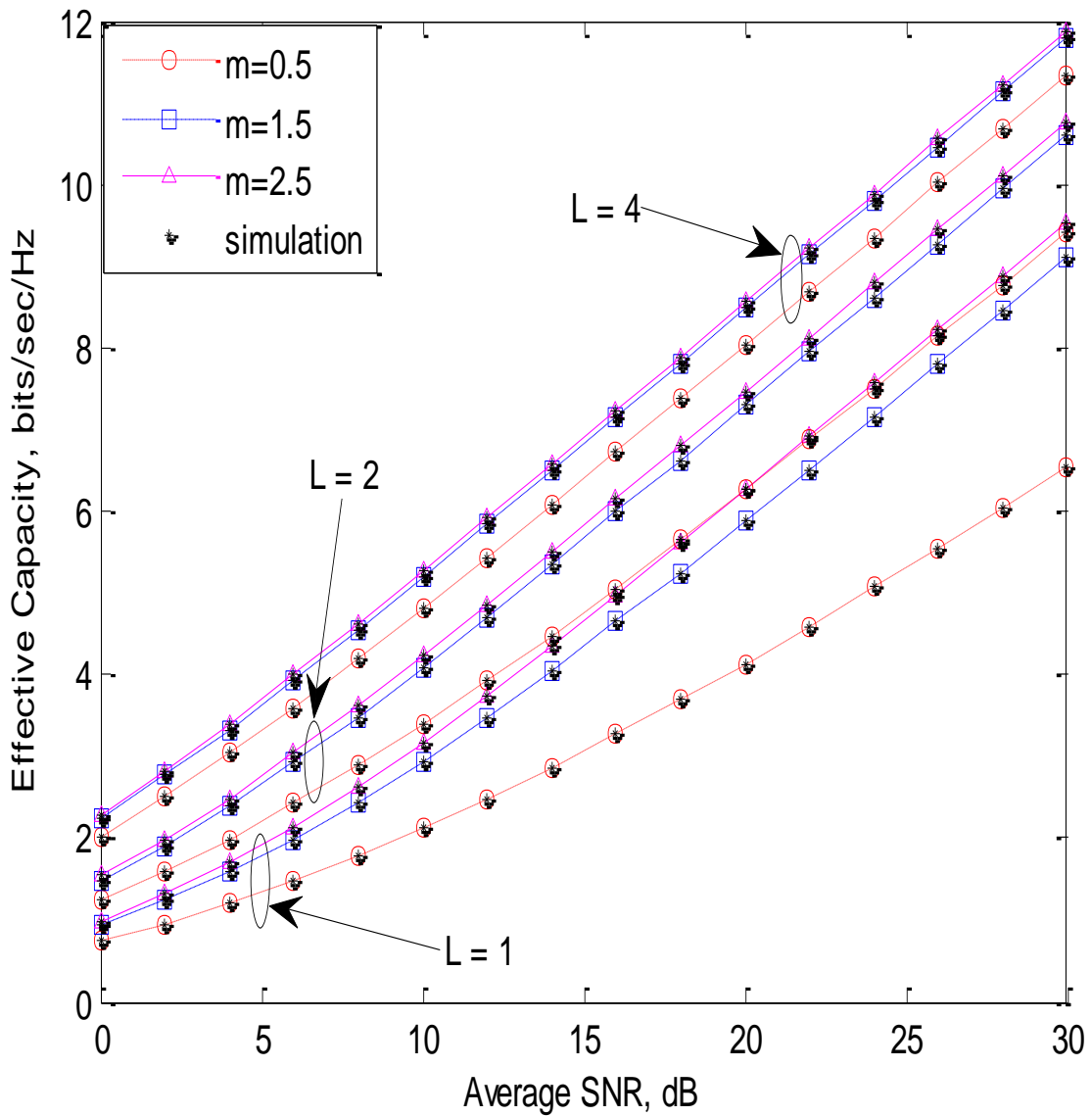
Figure 5.1 EC versus average SNR for various values of fading parameters and diversity order

The impact of delay constraint and average SNR on the EC as a function of diversity

order is shown in figure 5.2. It is clearly observed from the plots that the effect of

higher delay constraints can be compensated with the higher diversity order. It is

noted that the difference between the plots of delay constraints is more at lower

diversity order and the plots come closer with the further increase in diversity order.
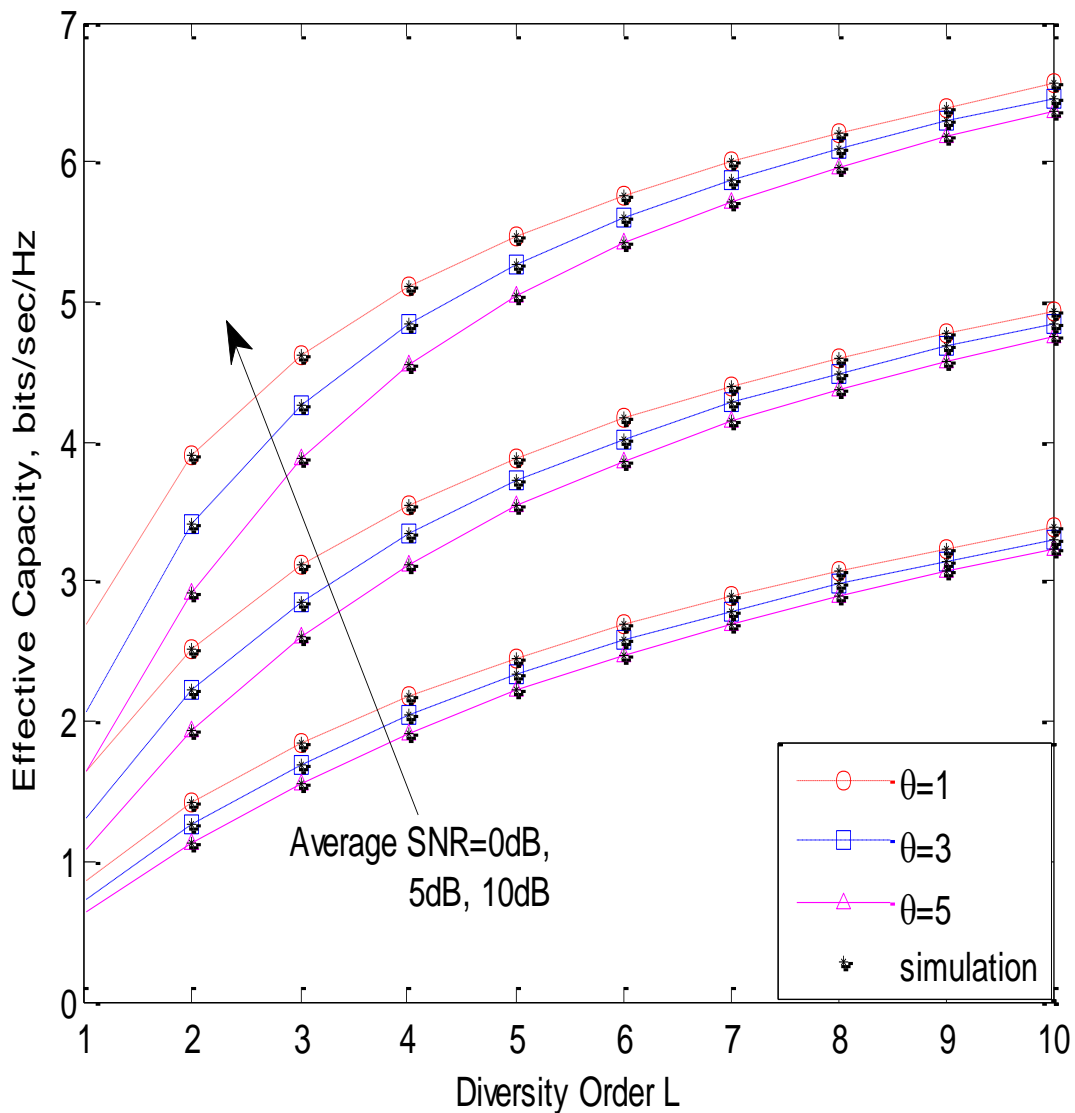
Figure 5.2 EC versus L for different values of delay constraint and average SNR

The effective throughput versus the QoS exponent θ is plotted in figure 5.3. Overall, the results show that the performance of the system degrades with a large QoS exponent, which implies that as the delay constraints become large, the less throughput system can handle. However, it is also seen that when QoS exponent is sufficiently small, further increase in θ can only pose slight impact on the effective throughput performance of the system.
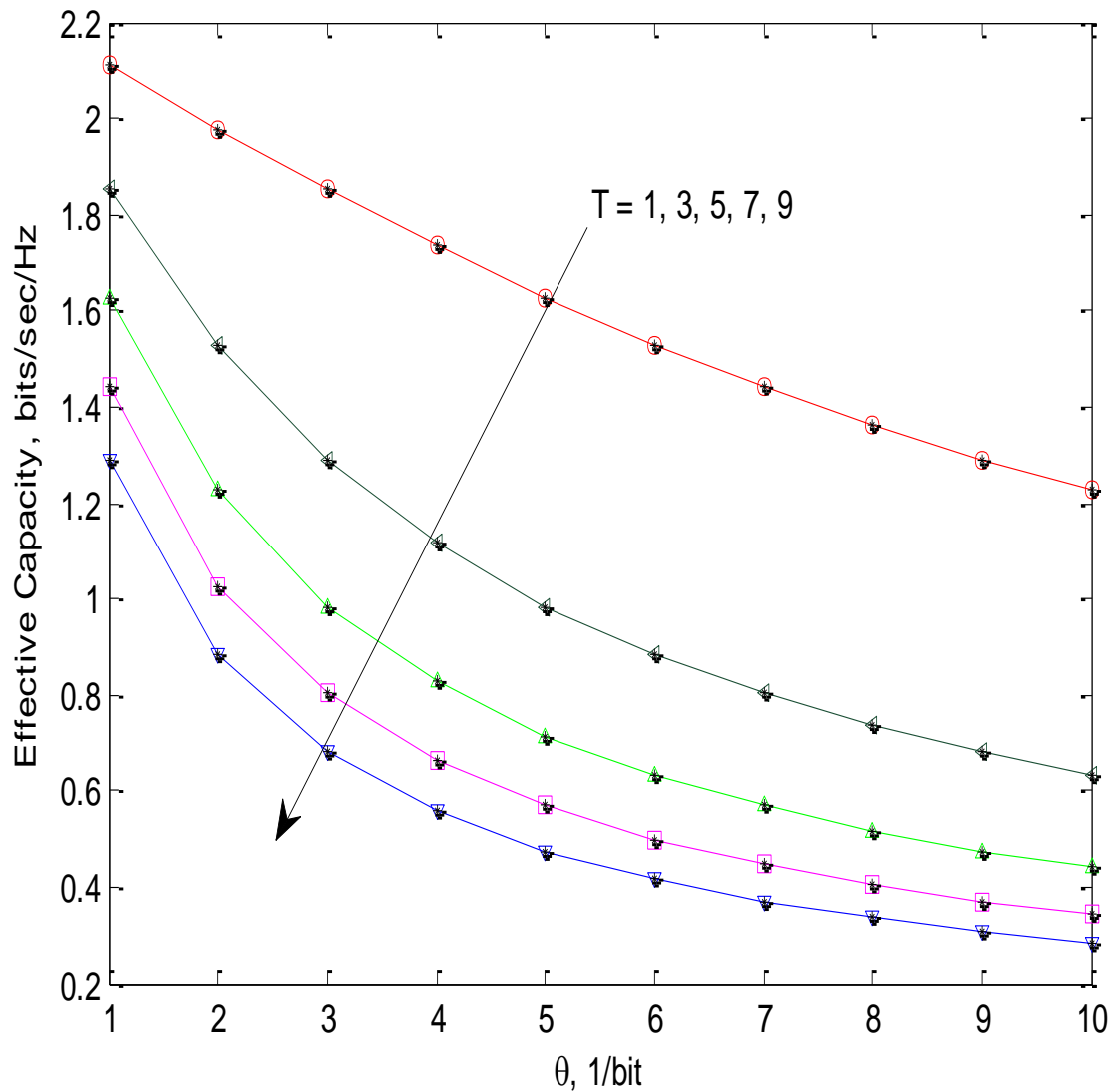
Figure 5.3 Effective throughput versus the QoS exponent parameter

The asymptotic performance of the system in terms of high SNR approximation for different diversity order and shadowing parameters are depicted in figure 5.4. The asymptotic plots merge quickly with the analytical plots for higher values of shadowing parameter and diversity order. In figure 5.5, the results are drawn for EC in case of low SNR against Eb/N0 for various values of diversity order and fixed values of A=1, m=1 and ms=30.
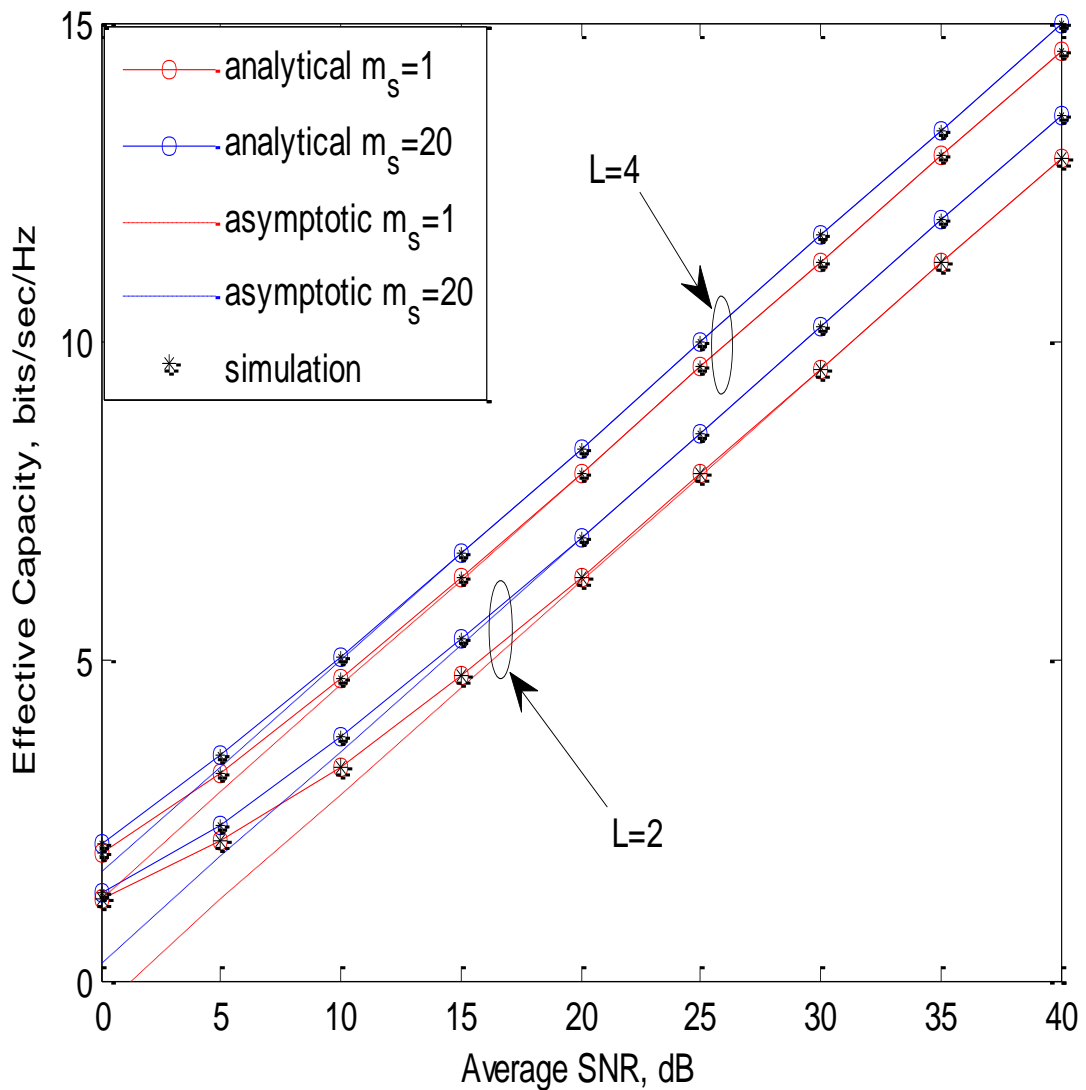
Figure 5.4 Impact of diversity order on the asymptotic performance for various values of shadowing parameter

From the figure, it can be inferred that with the increase of diversity order, the effective rate of the system also increases. The results produced here can be directly applied for designing the communication systems for the real time applications where the channel characteristics are modeled in the form of FSF distribution.
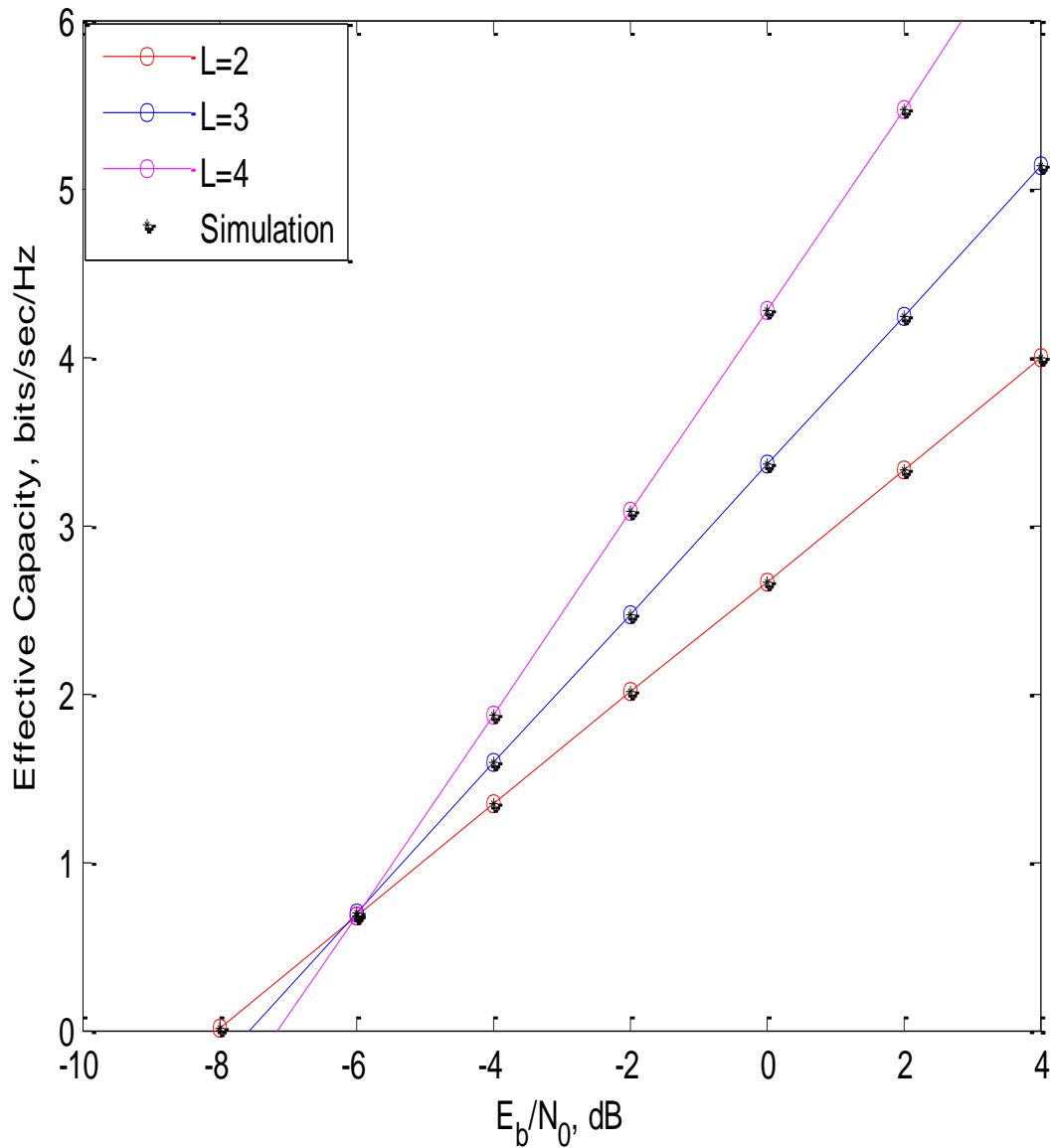
Figure 5.5 Low SNR EC versus average transmit SNR for fixed

5.4 Significant Findings

We have derived the mathematical expression of effective rate performance of the system over FSF fading channel with MRC reception. The impact of system parameters on the EC performance is studied in details. These results have extended and complimented the existing research of effective rate analysis. High power and

low power asymptotic expressions of the maximum data rate are provided and the importance of the approximation for MRC diversity is depicted. It is concluded that the growing demand of the high data rate with tighter delay constraints can be achieved by increasing the number of diversity branch in the system. Simulation results are also provided to verify the correctness of the proposed methodology.

CHAPTER 6

RIS–AIDED THROUGHPUT ANALYSIS OVER FISHER-SNEDECOR *F* AND BEAULIEU-XIE FADING CHANNELS

With the demanding need for next-generation wireless networks and the emergence of RIS in wireless communications, data rate performance over these systems is being researched for different fading channels. This chapter looked into the throughput analysis of the BX fading channel and FSF composite fading channel for RIS-assisted wireless systems. The MGF-based approach is used to derive the expressions of the system throughput for the aforementioned systems. The system performance in terms of the channel parameters and the number of reflecting elements is thoroughly examined and discussed. The accuracy of the inferred theoretical expressions is confirmed by the results of the Monte-Carlo simulation.

6.1   IRS-aided system

The evolution of wireless communication appears intriguing, given the possibility for new use cases and the demanding needs of 5G/6G wireless networks [18], [162]. The signal propagation in wireless scenario is indeterministic due to the dynamic position of surrounding objects with respect to the Tx and Rx [75], [123]. RIS have been emerged as a technology where the network operators can modify the electromagnetic radiation to remove the detrimental effects of fading in wireless propagation [163], [164].

The RIS-aided system design has been extensively researched in different wireless communication sectors as a newer technology. The integration of RIS into various emerging technologies, such as NOMA scheme was discussed in [165], energy receivers in SWIPT networks was discussed in [166], and secrecy performance in PLS networks was discussed in [167], has become increasingly important in next-generation wireless systems [168]. In [169], the authors have used an IRS for FSO-RF dual-hop system to enhance the system performance. Other work related to IRS-based study into the UAV can be found in [170]. Recently in [171], the performance analysis of the IRS-assisted mobile network in terms of the P_{out}, ABER over FSF distribution has been analyzed. In most of the new applications not only the throughput, but also delay should be addressed as a QoS requirement for these real-time applications [7], [70].

Table 6.1 Work on IRS-equipped communication system using MGF-based approach

S. No.	Year	Reference	Performance parameters	Fading Channel
1	2019	[173]	SER	Rayleigh
2	2020	[174]	SER	Rayleigh
3	2021	[175]	coverage analysis	Nakagami-m
4	2021	[49]	average/effective throughput, average BER/SER	$k-\mu$
5	2021	[176]	effective throughput	BX

Table 6.2 Work on IRS-equipped communication system using PDF-based

approach

S. No.	Year	Reference	Performance parameters	Fading Channel
1	2020	[177]	P_{out}, BER/SER	Rayleigh
2	2020	[178]	CC	Rayleigh
3	2020	[179]	P_{out}, SER, CC	Rayleigh
4	2020	[180]	P_{out}, CC, BER	Rayleigh
5	2020	[181]	P_{out}, CC	Rician
6	2020	[182]	BER	double-Nakagami
7	2021	[183]	P_{out}, CC, BER	Nakagami-*m*
9	2020	[184]	P_{out}, CC	Generalized Fox's H
10	2021	[185]	EC	$\alpha - \mu$
11	2021	[186]	P_{out}, BER	FTR
12	2020	[187]	P_{out}, CC	FTR channel with antenna misalignment/ hardware impairments.
13	2021	[188]	P_{out}, BER	Rayleigh/Gamma-Gamma

In light of the foregoing discussion, the throughput performance analysis of RIS-assisted communication systems is the need of the hour [172]. The performance of RIS-aided systems over various fading channels has been studied by a number of researchers. The PDF-based approach and the MGF-based approach are employed in the literature for the throughput study of RIS-aided systems. Both the methodologies have advantages and disadvantages; thus, they are utilized as needed depending on the system's design complexity and the time required to analyze performance metrics. Tables 1 and 2 show a literature review of the PDF-based strategy and the MGF-based approach, as well as the performance metrics evaluated and the channel employed in the study. It is clear from table 1 and table 2 that RIS study is the need of the hour in the development of next generation networks.

Similarly, the error probability and throughput analysis of RIS-aided system over the generalized κ-μ fading channel has been presented in [49]. Because of the importance of FSF composite fading channel in the D2D communication system [71], some new research has been performed on it, including the MRC diversity study.

6.2   IRS-aided Point-to-Point system

Consider an IRS-aided system consisting of a Tx, an IRS module equipped with N passive reflecting elements and a Rx as shown in Figure 6.1. For this system, it is assumed that link between Tx and IRS is not affected by fading and IRS is having CSI so that it can modulate the phase of the reflecting element to maximize the instantaneous SNR at the Rx.
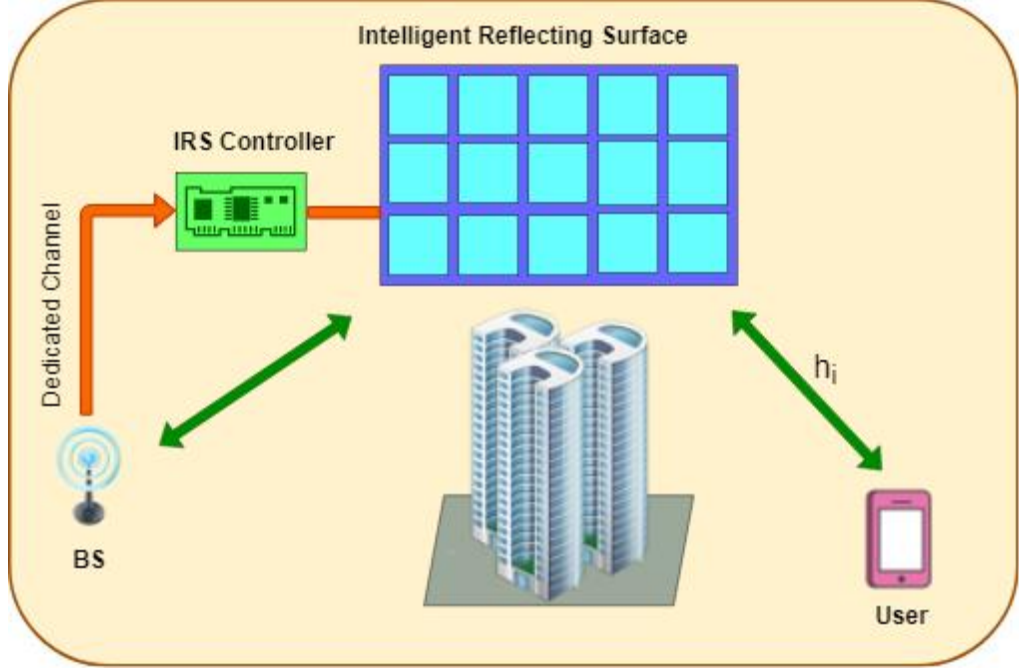
Figure 6.1 IRS-aided wireless system

The received signal at the Rx can be expressed as

$$y_d = \sqrt{P_s}\left[\sum_{i=1}^{N} h_i e^{j\phi_i}\right]x + n \tag{6.1}$$

where $h_i = a_i e^{j\theta_i}$ represents the fading channel coefficient between i_{th} passive reflector to the Rx, where a_i and θ_i denotes the magnitude and phase of h_i respectively. ϕ_i is the induced phase at each reflecting element, at $\phi_i = -\theta_i$, Rx yields the maximum SNR. Using equation (6.1), the SNR received by the user from the N reflecting elements can be expressed as

$$\gamma_d = \rho\gamma \tag{6.2}$$

where $\rho = P_s/N_0$ and $\gamma = \sum_{i=1}^{N}|h_i|^2$.

Using equation (6.2) and equation (4.4), the MGF expression can be written as

$$M_{\gamma_d}(s) = E\left[\exp(-s\gamma_d)\right] = \int_0^\infty \exp(-s\rho\gamma)f_\gamma(\gamma)d\gamma \tag{6.3}$$

6.3 Throughput Analysis over Fisher-Snedecor *F* composite channel

6.3.1 Average Throughput

The PDF of the sum of received SNR for *N* branches over FSF distribution is given by equation (5.3). One of the most crucial parameters to consider while developing a communication system is system throughput. In this part, we will calculate the average and effective throughputs of the RIS-assisted system over FSF composite channel. The average throughput of a fading channel can be defined as

$$C = E[\log_2(1 + \gamma_D)] \tag{6.4}$$

As per [49] , the average throughput in terms of MGF can be expressed as

$$C = \frac{1}{\ln(2)} \int_0^\infty E_i(-s)M'_{\gamma_D}(s)ds \tag{6.5}$$

here M'_{γ_D} is defined as

$$\frac{\partial}{\partial s}M_{\gamma_D}(s) = \frac{\partial}{\partial s}E[\exp(-\rho s\gamma)] = -\rho\int_0^\infty \gamma\exp(-\rho s\gamma)f_\gamma(\gamma)d\gamma \tag{6.6}$$

Putting equation (5.3) in the above equation, we get

$$\frac{\partial}{\partial s} M_{\gamma_D}(s) = -\frac{\rho}{B(mN + m_s N)} \left(\frac{m}{m_s \bar{\gamma} N} \right)^{mN} \int_0^\infty \gamma^{mN} \exp(-\rho s \gamma)$$

$$\times {}_2F_1 \left((m + m_s)N, mN; mN, -\frac{m}{m_s \bar{\gamma} N} \gamma \right) d\gamma \tag{6.7}$$

Using [158], the Gauss hypergeometric function can be represented in the form of

Meijer-G function and equation (6.7) becomes

$$\frac{\partial}{\partial s} M_{\gamma_D}(s) = \frac{-\rho}{\Gamma(mN)\Gamma(m_s N)} \left(\frac{m}{m_s \bar{\gamma} N} \right)^{mN+1} \int_0^\infty \gamma^{(mN+2)-1}$$

$$\times \exp(-\rho s \gamma) G_{2\,2}^{1\,2} \left(\frac{m\gamma}{m_s \bar{\gamma} N} \left| \begin{matrix} -mN - m_s N & -mN \\ -1 & -mN \end{matrix} \right. \right) d\gamma \tag{6.8}$$

Expressing the exponential term of equation (6.8) into its equivalent Meijer-G

function using 07.34.03.0228.01 of [151] we get

$$\frac{\partial}{\partial s} M_{\gamma_D}(s) = \frac{-\rho}{\Gamma(mN)\Gamma(m_s N)} \left(\frac{m}{m_s \bar{\gamma} N} \right)^{mN+1} \int_0^\infty \gamma^{(mN+2)-1} G_{0\,1}^{1\,0} \left(\rho s \gamma \left| \begin{matrix} \\ 0 \end{matrix} \right. \right)$$

$$\times G_{2\,2}^{1\,2} \left(\frac{m\gamma}{m_s \bar{\gamma} N} \left| \begin{matrix} -mN - m_s N & -mN \\ -1 & -mN \end{matrix} \right. \right) d\gamma \tag{6.9}$$

Solving the integral using equation (07.34.21.0011.01) of [151], equation (6.9) can be

simplified as

$$\frac{\partial}{\partial s} M_{\gamma_D}(s) = -\frac{s^{-(mN+2)}}{\Gamma(mN)\Gamma(m_s N)} \left(\frac{m}{\rho m_s \bar{\gamma} N} \right)^{mN+1}$$

$$\times G_{3\,2}^{1\,3} \left(\frac{m}{\rho m_s \bar{\gamma} Ns} \left| \begin{matrix} -mN - m_s N & -mN & -(mN+1) \\ 1 & -mN & \end{matrix} \right. \right) \tag{6.10}$$

Putting the above result in equation (6.5) and using equation (8.4.11.1) of [159] i.e.,

$$E_i(-x) = -G_{1\,2}^{2\,0} \left(x \left| \begin{matrix} 1 \\ 0 & 0 \end{matrix} \right. \right) \text{, we have}$$

$$C = \frac{1}{\ln(2)} \frac{1}{\Gamma(mN)\Gamma(m_s N)} \left(\frac{m}{\rho m_s \bar{\gamma} N}\right)^{mN+1} \int_0^\infty s^{-(mN+2)} G_{1\ 2}^{2\ 0}\left(s \left|\begin{matrix} 1 \\ 0 \quad 0 \end{matrix}\right.\right)$$
$$\times G_{3\ 2}^{1\ 3}\left(\frac{m}{\rho m_s \bar{\gamma} N s} \left|\begin{matrix} -mN - m_s N & -mN & -(mN+1) \\ 1 & -mN \end{matrix}\right.\right) ds \tag{6.11}$$

Using $G_{p\ q}^{m\ n}\left(\left.\frac{a_p}{b_q}\right| z\right) = G_{q\ p}^{n\ m}\left(\left.\frac{1-b_q}{1-a_p}\right| z^{-1}\right)$, property of Meijer-G function and equation

(07.34.21.0011.01) of [151] and after some manipulations the above equation can be

written as

$$C = \frac{1}{\ln(2)} \frac{1}{\Gamma(mN)\Gamma(m_s N)} \left(\frac{m}{\rho m_s \bar{\gamma} N}\right)^{mN+1}$$
$$\times G_{4\ 4}^{3\ 3}\left(\frac{\rho m_s \bar{\gamma} N}{m} \left|\begin{matrix} 0 & mN+2 & mN+2 & mN+1 \\ 1+mN+m_s N & mN+1 & mN+2 & mN+1 \end{matrix}\right.\right) \tag{6.12}$$

Using the property of Meijer-G, equation (6.11) can be further simplified as

$$C = \frac{1}{\ln(2)} \frac{1}{\Gamma(mN)\Gamma(m_s N)} \left(\frac{m}{\rho m_s \bar{\gamma} N}\right)^{mN+1}$$
$$\times G_{3\ 3}^{2\ 3}\left(\frac{\rho m_s \bar{\gamma} N}{m} \left|\begin{matrix} 2 & mN+2 & mN+2 \\ 1+mN+m_s N & mN+2 & mN+1 \end{matrix}\right.\right) \tag{6.13}$$

6.3.2 Effective Throughput:

The EC model, a link-layer channel model, was created to address the connection-

level QoS metrics like throughput, latency, and delay-violation probability in next-

generation wireless networks [7]. For a block fading channel, the EC can be expressed

as equation (1.11). The definition of EC in terms of MGF can be given as

$$R(\rho,\theta) = -\frac{1}{A} \log_2 \left[\frac{1}{\Gamma(A)} \underbrace{\int_0^\infty s^{A-1} \exp(-s) M_\gamma\left(\frac{\rho s}{N}\right) ds}_{I_1} \right] \tag{6.14}$$

The MGF of equation (6.14) can be evaluated using

$$M(s) = \frac{1}{B(mN + m_s N)} \left(\frac{m}{m_s \bar{\gamma} N} \right)^{mN} \int_0^\infty \gamma^{(mN-1)} \exp(-s\gamma) \times {}_2F_1 \left((m + m_s)N, mN; mN, -\frac{m}{m_s \bar{\gamma} N} \gamma \right) d\gamma$$

(6.15)

Using [158], the Gauss hypergeometric function can be represented in the form of Meijer-G function and equation (6.15) can be calculated as

$$M(s) = \frac{1}{\Gamma(mN)\Gamma(m_s N)} \left(\frac{m}{m_s \bar{\gamma} N} \right)^{mN+1} \int_0^\infty \gamma^{mN} \exp(-s\gamma) \times G_2^{1\,2} \left(\frac{m\gamma}{m_s \bar{\gamma} N} \left| \begin{matrix} -mN - m_s N & -mN \\ -1 & -mN \end{matrix} \right. \right) d\gamma$$

(6.16)

Applying the conversion of exponential function into Meijer-G using equation (07.34.03.0228.01) of [151] and then solving the integral using equation (07.34.21.0011.01) of [151] in equation (6.16), we get

$$M(s) = \frac{1}{\Gamma(mN)\Gamma(m_s N)} \left(\frac{m}{m_s \bar{\gamma} Ns} \right)^{mN+1} \times G_3^{1\,3} \left(\frac{m}{m_s \bar{\gamma} Ns} \left| \begin{matrix} -mN & -mN - m_s N & -mN \\ -1 & -mN \end{matrix} \right. \right)$$

(6.17)

Applying the change of variable in equation (6.17), as required in equation (6.14), it becomes

$$M_\gamma \left(\frac{\rho s}{N} \right) = \frac{s^{-(mN+1)}}{\Gamma(mN)\Gamma(m_s N)} \left(\frac{m}{\rho m_s \bar{\gamma}} \right)^{mN+1} \times G_3^{1\,3} \left(\frac{m}{\rho m_s \bar{\gamma} s} \left| \begin{matrix} -mN & -mN - m_s N & -mN \\ -1 & -mN \end{matrix} \right. \right)$$

(6.18)

Using $G_p^{m\,n} \left(\frac{a_p}{b_q} \left| z \right. \right) = G_q^{n\,m} \left(\frac{1 - b_q}{1 - a_p} \left| z^{-1} \right. \right)$ property of Meijer-G function, equation (6.18) can be rewritten as

$$M_\gamma\left(\frac{\rho s}{N}\right) = \frac{s^{-(mN+1)}}{\Gamma(mN)\Gamma(m+m_s)}\left(\frac{m}{\rho m_s \bar{\gamma}}\right)^{mN+1} \times G_{2\ 3}^{3\ 1}\left(\frac{\rho m_s \bar{\gamma}}{m} s \middle| \begin{matrix} 2 & & 1+mN \\ 1+mN & 1+mN+m_s N & 1+mN \end{matrix}\right)$$

(6.19)

Using equation (6.19), I_1 can be evaluated as

$$I_1 = \frac{1}{\Gamma(mN)\Gamma(m_s N)}\left(\frac{m}{\rho m_s \bar{\gamma}}\right)^{mN+1}$$

$$\times \int_0^\infty s^{(A-mN-2)}\exp(-s) \times G_{2\ 3}^{3\ 1}\left(\frac{\rho m_s \bar{\gamma}}{m} s \middle| \begin{matrix} 2 & & 1+mN \\ 1+mN & 1+mN+m_s N & 1+mN \end{matrix}\right)ds$$

(6.20)

Applying the conversion of exponential function into Meijer-G using equation (07.34.03.0228.01) of [151] in the above, we get

$$I_1 = \frac{1}{\Gamma(mN)\Gamma(m_s N)}\left(\frac{m}{\rho m_s \bar{\gamma}}\right)^{mN+1}$$

$$\times \int_0^\infty s^{(A-mN-1)-1} G_{0\ 1}^{1\ 0}\left(s \middle| \begin{matrix} \\ 1 \end{matrix}\right) \times G_{2\ 3}^{3\ 1}\left(\frac{\rho m_s \bar{\gamma}}{m} s \middle| \begin{matrix} 2 & & 1+mN \\ 1+mN & 1+m+m_s & 1+mN \end{matrix}\right)ds$$

(6.21)

The integral part in equation (6.21) can be solved using equation (07.34.21.0011.01) of [151] and it becomes

$$I_1 = \frac{1}{\Gamma(mN)\Gamma(m_s N)}\left(\frac{m}{\rho m_s \bar{\gamma}}\right)^{mN+1} \times G_{3\ 3}^{3\ 2}\left[\frac{\rho m_s \bar{\gamma}}{m}\middle| \begin{matrix} 2 & (2+mN-A) & 1+mN \\ 1+mN & 1+mN+m_s N & 1+mN \end{matrix}\right]$$

(6.22)

Further putting equation (6.22) in equation (6.14) and doing some simplification, we get the final expression of EC as

$$R(\rho,\theta) = -\frac{1}{A}\log_2\left\{\frac{1}{\Gamma(A)\Gamma(mN)\Gamma(m_s N)}\left(\frac{m}{\rho m_s \bar{\gamma}}\right)^{mN+1} G_{2\ 2}^{2\ 2}\left[\frac{\rho m_s \bar{\gamma}}{m}\middle| \begin{matrix} 2 & (2+mN-A) \\ 1+mN & 1+mN+m_s N \end{matrix}\right]\right\}$$

(6.23)

6.4   EC analysis for IRS-assisted system over BX Fading channel

6.4.1   Effective Throughput

Using variable transformation $s = \rho s$ in equation (4.7), the MGF expression of IRS-aided system over BX fading channel can be evaluated as

$$M_{\gamma d}(s) = \frac{1}{\exp(mkN)} \sum_{d=0}^{\infty} \frac{(mkN)^d}{(d!)\Gamma(mN+d)} G_{11}^{11}\left(\frac{\rho s}{\eta} \Big|_0^{1-(mL+d)}\right)$$

(6.24)

Putting equation (6.24) into equation (6.14) and using equation (07.34.03.0228.01) of [151], we get

$$R(\rho,\theta) = -\frac{1}{A}\log_2 \left[\begin{array}{l} \frac{1}{\Gamma(A)} \\ \times \int_0^{\infty} s^{A-1} \exp(-s) \frac{1}{\Gamma(mN)\exp(mkN)} \sum_{d=0}^{\infty} \frac{(mkN)^d}{(d!)\Gamma(mN+d)} G_{01}^{10}\left(s\Big|_0\right) G_{11}^{11}\left(\frac{\rho s}{\eta}\Big|_0^{1-(mL+d)}\right) ds \end{array} \right]$$

(6.25)

Using equation (07.34.21.0011.01) of [151], we get the closed-form expression for the EC of IRS-aided system as

$$R(\rho,\theta) = -\frac{1}{A}\log_2 \left[\frac{1}{\Gamma(A)\exp(mkN)} \sum_{d=0}^{\infty} \frac{(mkN)^d}{(d!)\Gamma(mN+d)} G_{21}^{12}\left(\frac{\rho}{\eta}\Big|_0^{1-(mN+d)}\right) \right]$$

(6.26)

6.4.2   Asymptotic Analysis

Considering high SNR conditions, applying $\rho \to \infty$ in equation (6.24), putting it in (6.14) and using equation (3.381.3) of [148], we get the final high-SNR approximation as

$$R\left(\rho \to \infty, \theta\right) \approx -\frac{1}{A}\log_2\left[\frac{1}{\Gamma\left(A\right)}\frac{\Gamma\left(A-mN\right)}{\exp(mkN)}\left(\frac{\rho}{\eta}\right)^{-mN}\right] \qquad (6.27)$$

6.5   **Numerical Results and Discussions**

Here, the graphs of the analytical expressions obtained in the preceding sections are illustrated. To establish the validity of the derived expressions, the results are verified using their Monte-Carlo equivalents (with a sufficiently large number of samples 10^6 generated). Figure 6.2 shows the average throughput versus the average transmits SNR for various fading parameters and special cases of the FSF composite channel. The average throughput is demonstrated to grow as the fading parameters values increase. Additionally, the simulation results overlap the analytical plots.
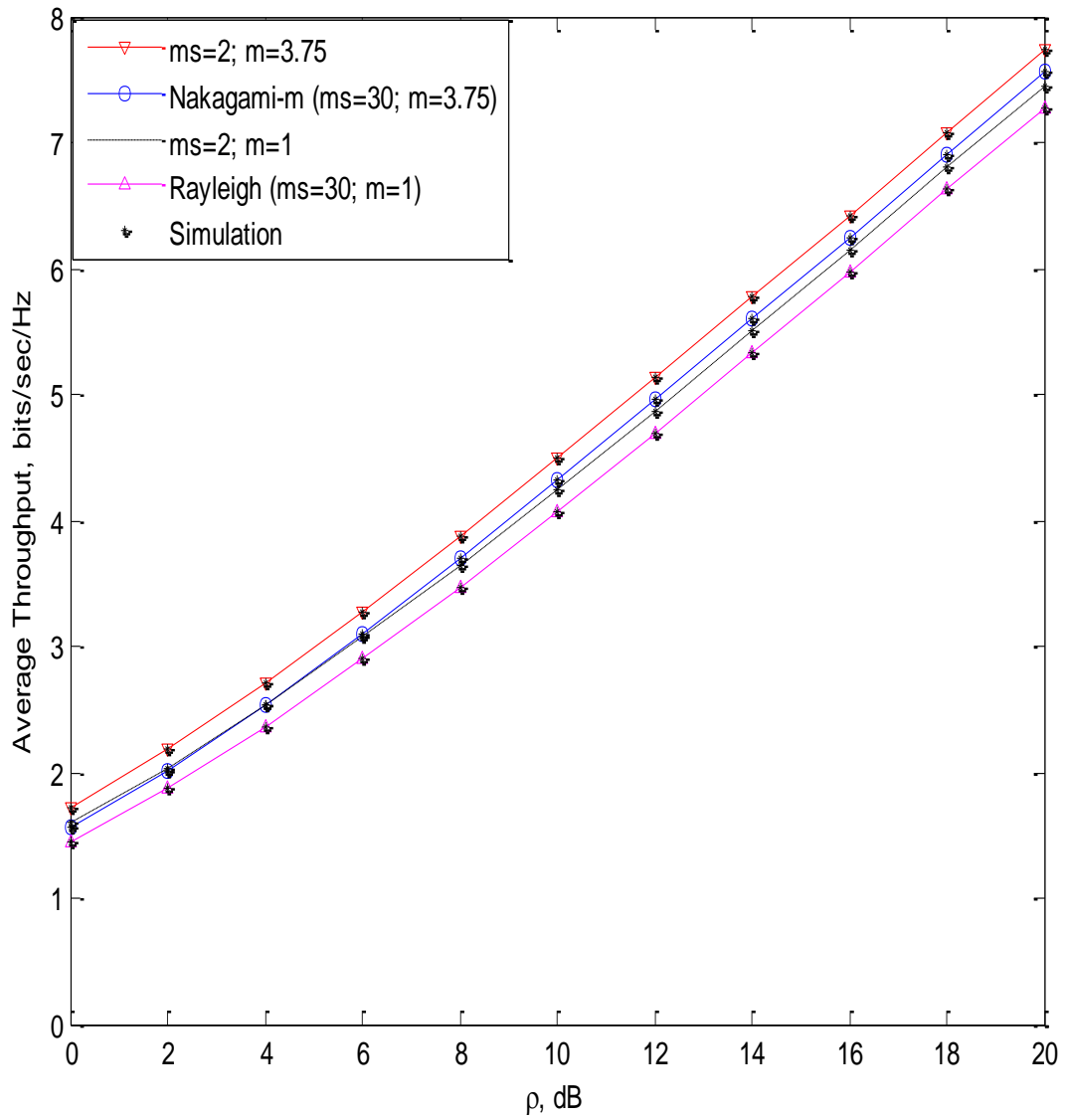
Figure 6.2 Average throughput versus average transmit SNR for various values of fading
parameters and special case of FSF composite channel
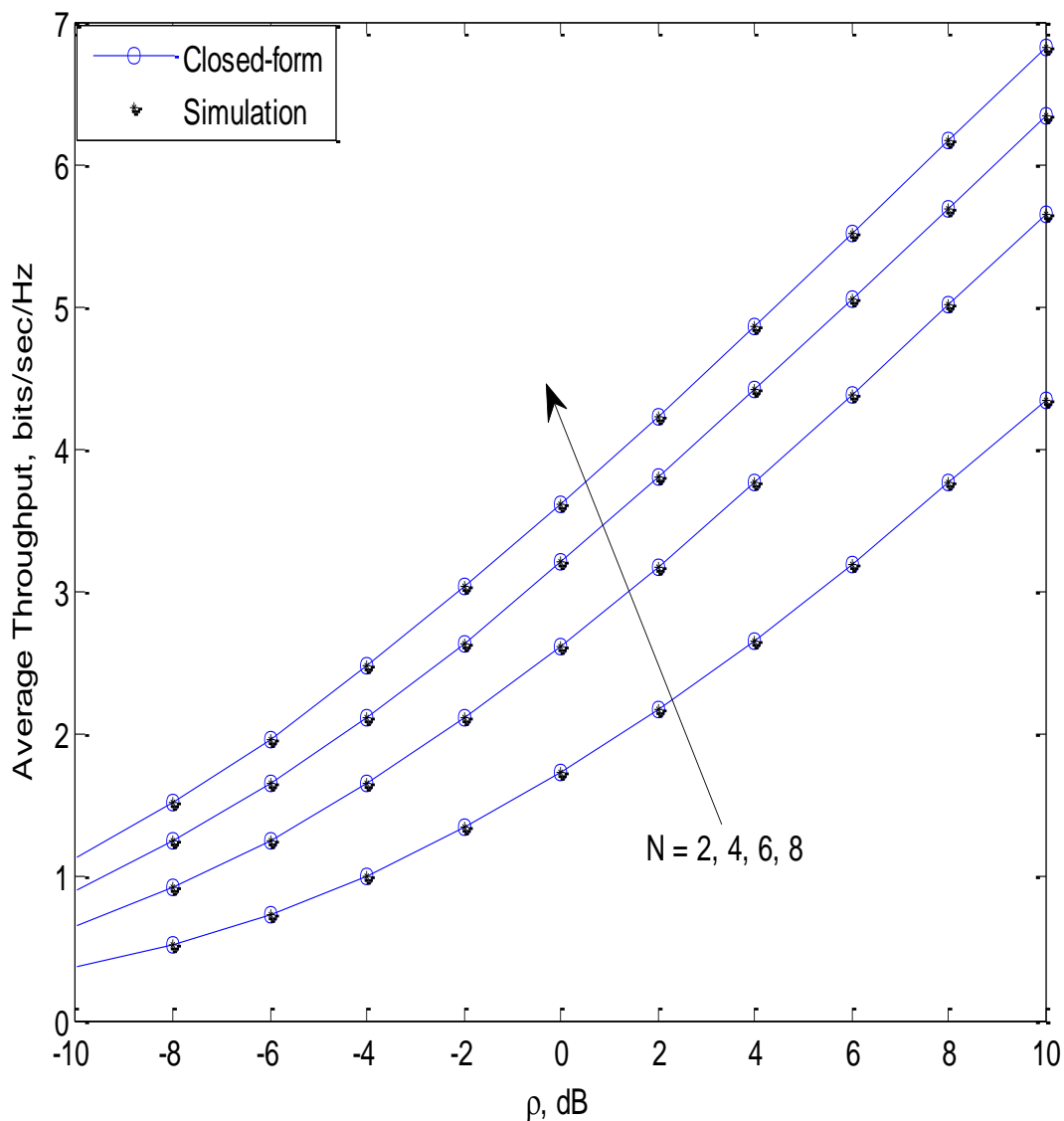
Figure 6.3 Average throughput versus average transmit SNR for some values of reflecting elements

Figure 6.3 depicts the average throughput versus the average transmit SNR for various values of reflecting element. The performance of the system improves as the number of reflecting elements increases. Figure 6.4 shows effective throughput as a function of average transmits SNR for various fading parameter values. The behaviour of fading parameters on system performance, as shown in figure 6.2 is also verified here.
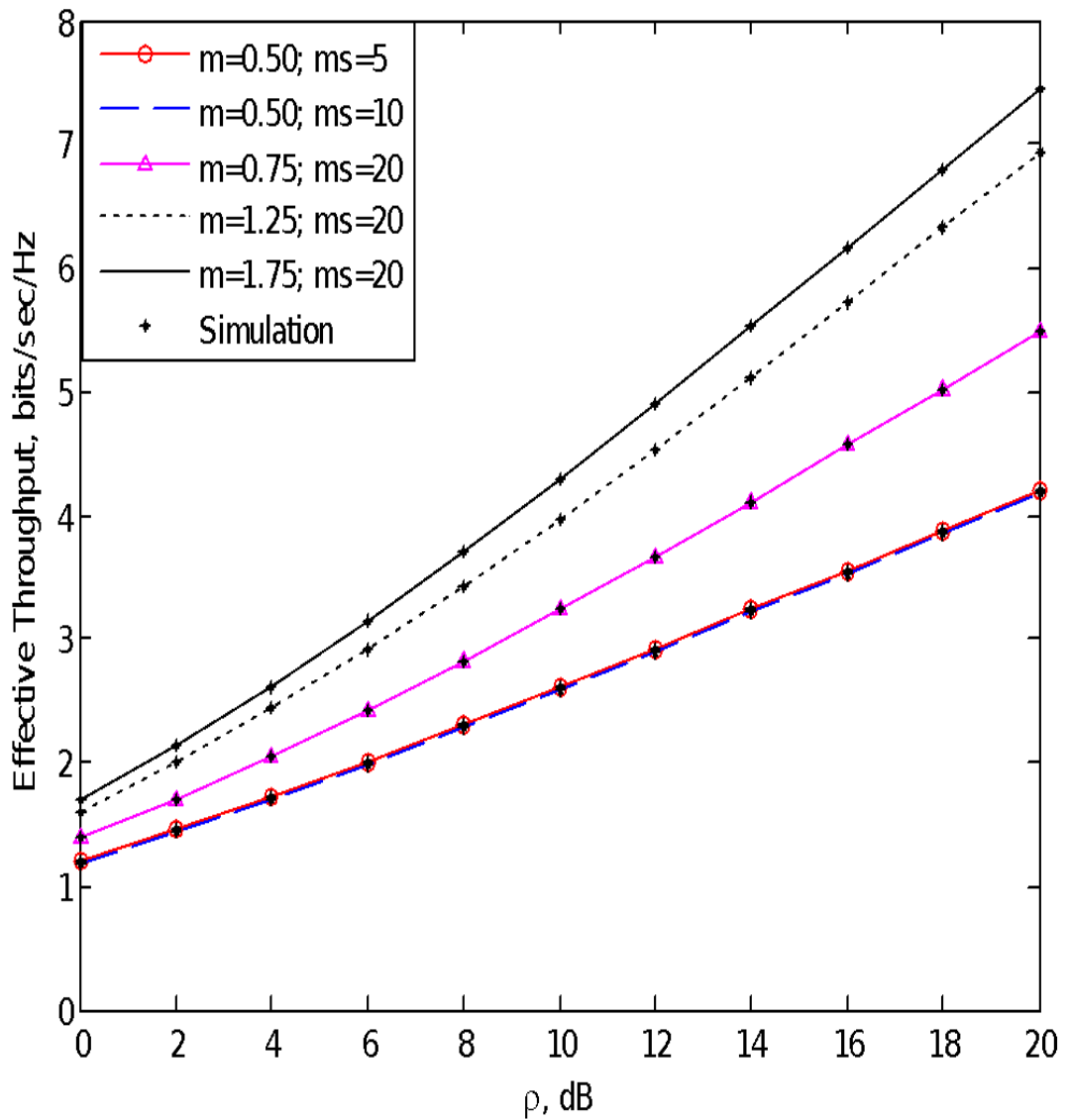
Figure 6.4 Effective throughput versus average transmit SNR for different values of fading
parameters

Figure 6.5 shows effective throughput as a function of A for various values of average

received SNR. It's worth noting that when the average received SNR value rises and

the A value falls, the system's data rate performance improves. For smaller values of

A, the effect on system performance is more noticeable than for higher values of A.
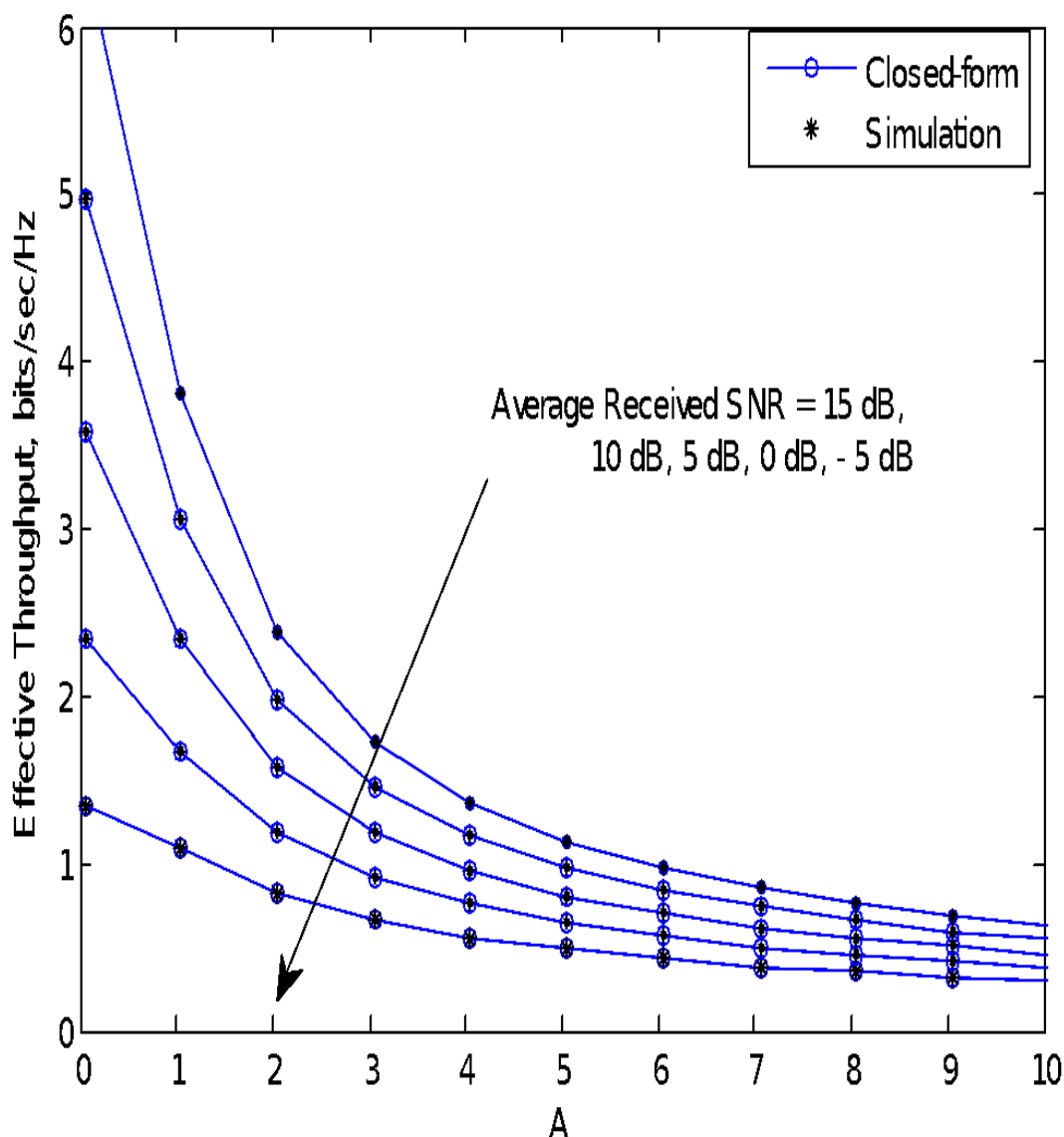
Figure 6.5 Effective throughput versus A for various values of average received SNR

Figure 6.6 shows effective throughput versus the number of reflecting elements for various average transmit SNR levels. Surprisingly, a considerable increase in the N value leads to a significant gain in system performance, which thereafter fades away. The conclusions obtained in this part are quite generic and can be used to design communication systems in which signal propagation is represented using a FSF composite fading channel and its special cases.
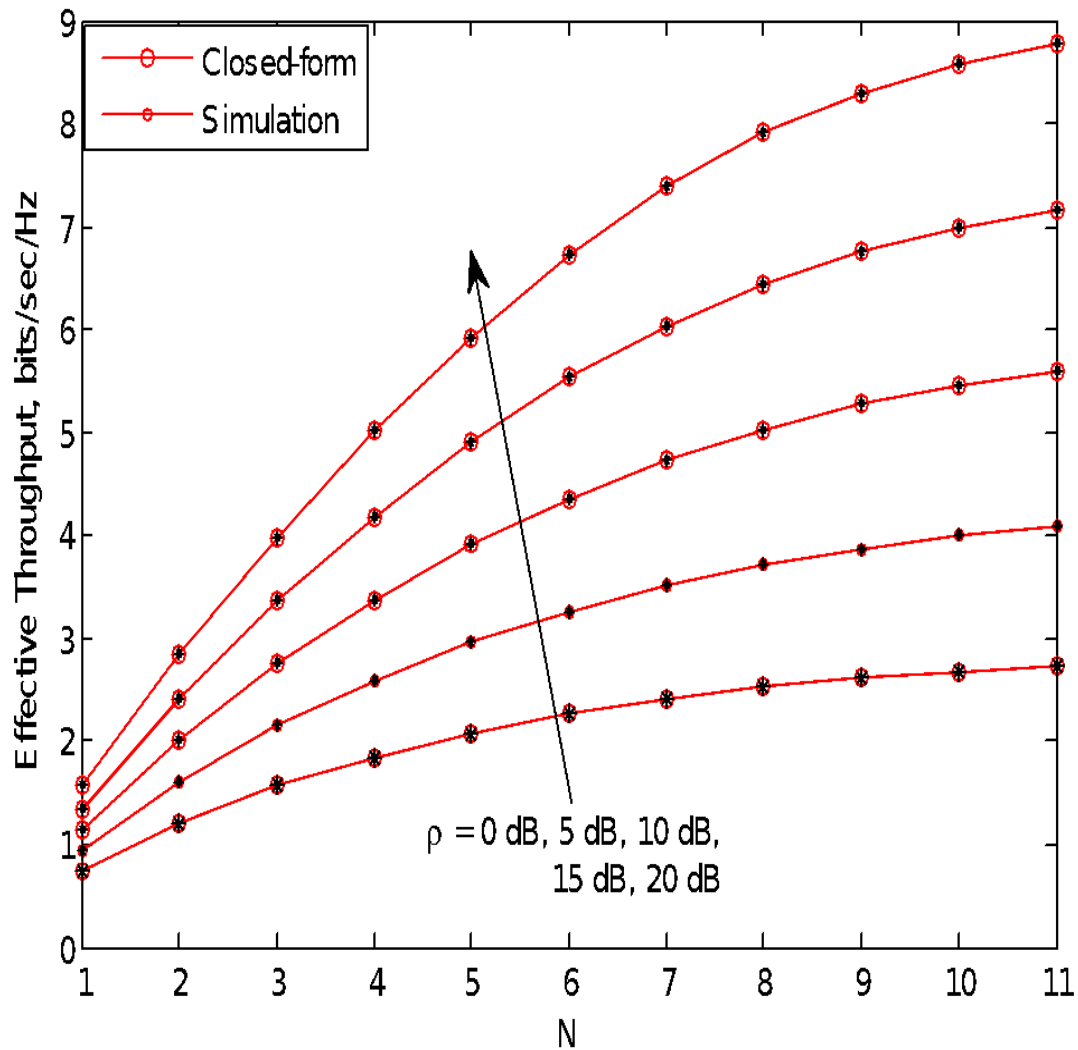
Figure 6.6 Effective throughput versus number of reflecting elements for various values of average transmit SNR

Figure 6.7 demonstrate the EC performance of the IRS-assisted system for BX fading channel under different system settings. The graph is plotted according to the results obtained from equations 6.28 and 6.29. The EC versus ρ is plotted by varying the values of fading parameters m and k, while the values of A & N is set to 6 and 2 respectively. As expected, increasing the value of m or/ and k improves the effective throughput significantly. Further, we can also see that the analytical results match perfectly with the

simulation results. Also at the high SNR regime, the asymptotic results are well

approximate to the exact values.
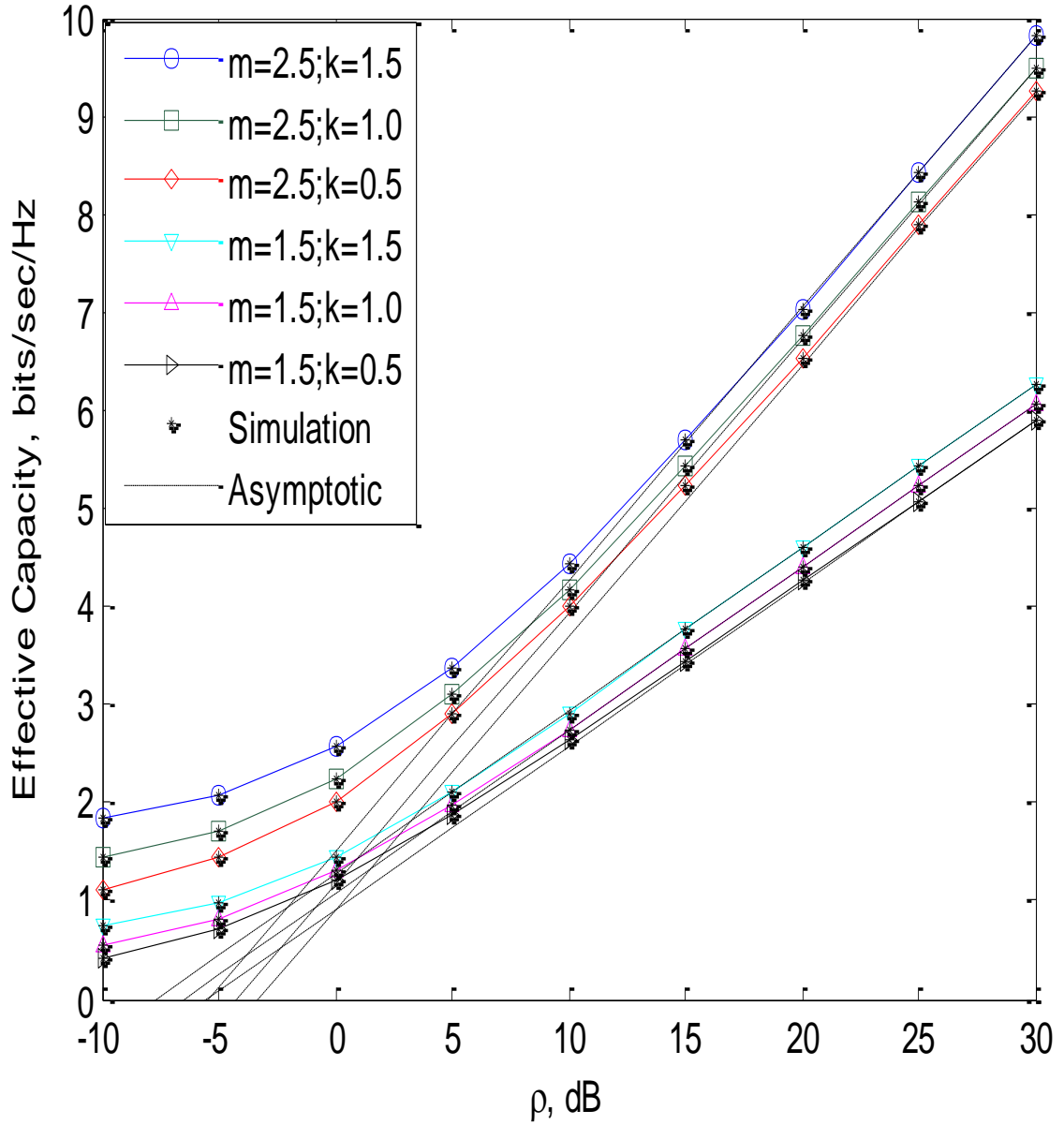
Figure 6.7 EC against ρ for various values of m and k with A=6 and N=2
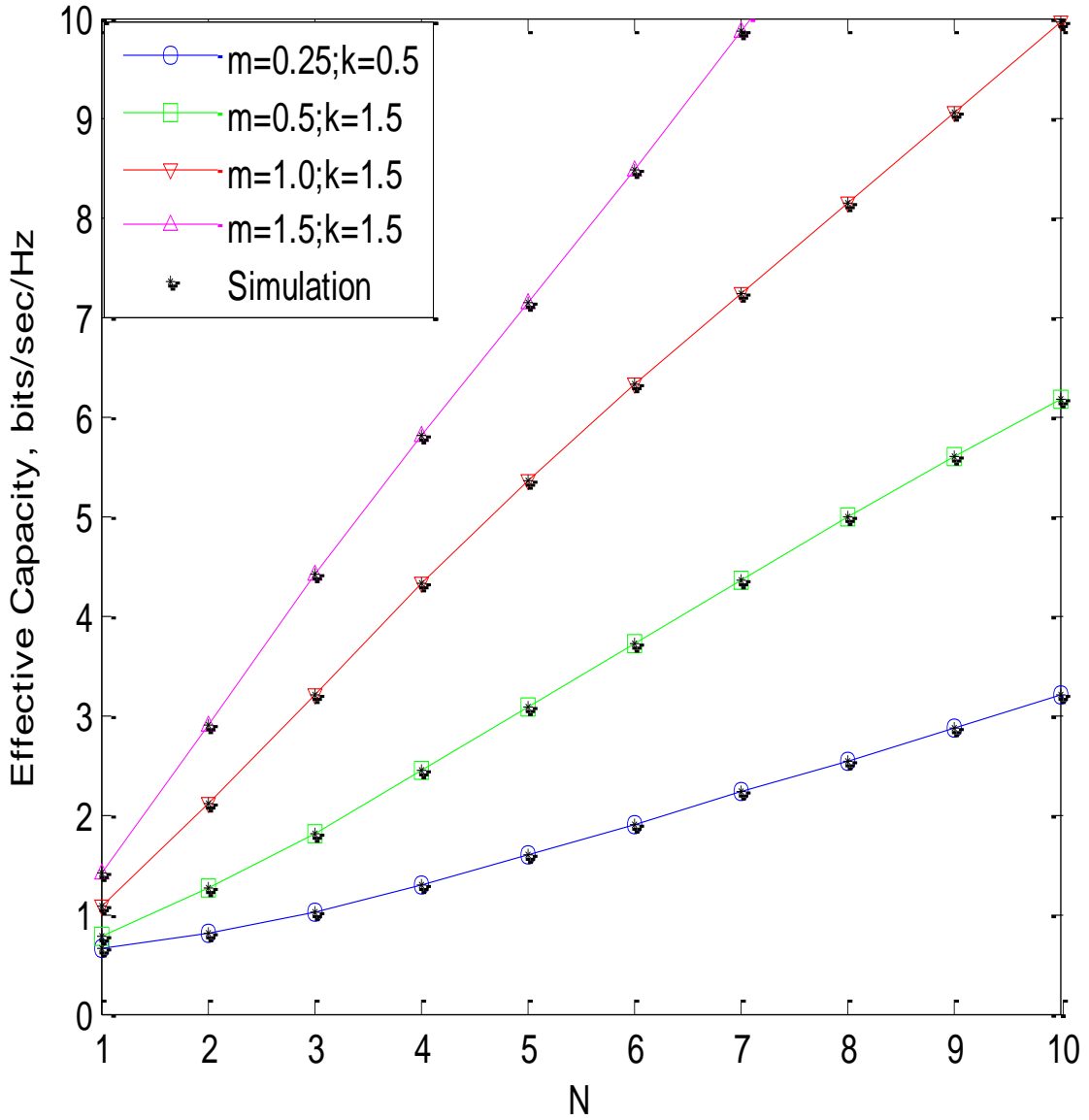
Figure 6.8 EC versus N with A=6 and ρ ***=10dB***

Figure 6.8 plots the EC versus N for BX Fading channel, considering the non-integer

values for m and k. From the figure, it is clear that for a given ρ , the effective system

throughput increased almost linearly as N increases. Also, the gain achieved due to

increasing the fading factor m and k is more significant when N is large.

6.6   Significant Findings

This research looked into the throughput study of the FSF and BX fading channel for RIS-assisted wireless systems. The expressions of the effective throughput and average throughput for the aforementioned FSF channel over the BX fading scenario are derived. The system performance in terms of the channel parameters and the number of reflecting elements is thoroughly examined and discussed. It is concluded that the growing demand of the high data rate with tighter delay constraints can be achieved by increasing the number of reflecting elements (*N*) in the IRS-assisted system. The accuracy of the results is verified by comparing them to their Monte-Carlo simulation counterparts. The results presented in this study can be used in the development of communication systems for real-time applications in next-generation wireless networks.

CHAPTER 7

CONCLUSION AND FUTURE SCOPE OF WORK

In this dissertation, performance evaluation of BX fading channel and FSF fading channel has been performed. The EC behaviour of the said channels with diversity reception is studied. The application of the proposed results for IRS-aided system for both the fading models is also studied. In this chapter, the major contributions, achievements, and future scope of work of the thesis are summarized.

7.1   Conclusion

The mathematical analysis for various performance measures over the BX fading channel and FSF fading channel have been obtained. The mathematically obtained expressions are numerically evaluated and the effect of different system parameters on the Rx performance is studied. The numerical results have been validated with the Monte-Carlo simulations results. The chapter wise main conclusions of this thesis are summarised as follows:

- The performance analysis over BX fading channel with MRC diversity is presented in chapter 3. The closed-form expressions of the P_{out}, AF, CC, and ASEP (coherent and non-coherent) are derived for the fading channel. The effect of diversity order and fading parameters on the system performance are analysed. It is observed that with the increase in the number of diversity branches the deteriorating effect of fading is reduced. Along with ORA, OPRA,

CIFR, and TIFR CC policies, P_{out} analysis is also performed. The unified analytical expressions for various coherent and non-coherent modulation schemes with MRC diversity are also derived and demonstrated.

- Chapter 4 analyse the EC performance of the multi-antenna system over the BX channel. The simplified high-SNR and low-SNR solutions are also derived. It is concluded that the growing demand for the high data rate with tighter delay constraints can be achieved by increasing the number of antennas in the MISO system.

- In chapter 5 the mathematical expression of effective rate performance of the system over FSF fading channel with MRC reception has been derived. The impact of system parameters on the EC performance is studied in details. These results have extended and complimented the existing research of effective rate analysis. High power and low power asymptotic expressions of the maximum data rate are provided and the importance of the approximation for MRC diversity is depicted. It is concluded that the growing demand of the high data rate with tighter delay constraints can be achieved by increasing the number of diversity branches in the system. Simulation results are to validate the accuracy of the proposed methodology and it is observed that the simulation results are in close agreement with the numerical results.

- Chapter 6 discusses the RIS-aided performance metric of the multi-antenna system over the BX fading channel and FSF fading channel. The expressions of the throughput for the aforementioned system are derived using an MGF-based technique. It is concluded that the growing demand for the high data rate with

tighter delay constraints can be achieved by increasing the number of reflecting elements in the IRS-assisted system. The accuracy of the results is verified by comparing them to their Monte-Carlo simulation counterparts.

The obtained expressions for performance measures are obtained in terms of gamma, incomplete gamma and hypergeometric functions.

7.2   Future Scope of Work

This thesis has addressed different problems that are related to performance analysis of fading channels. However, there are also other questions, which are being currently investigated and which have not been presented in this thesis. This research work gives rise to several possible improvements and future research directions.

- The validation of the proposed fading models was performed through Monte-Carlo simulation only and measurement validation still need to carried out to find the application to different practical scenarios. Throughout the thesis, communication system behaviour with fading models was examined with arbitrary parameters. Further, parameter estimations of the proposed models through measurement data can be considered to gain more practical insight.

- Analysis of the proposed composite models can be extended to examine the system behaviour under multi-hop, PLS, and for co-channel interference.

- To improve the performance of the system, various diversity combining techniques like MRC, SC and EGC are used in the literatures. The GSC diversity technique is less explored for the fading channels. For the considered channels

also, GSC performance is not explored till now, so all the performance matrices of BX fading channel and FSF fading channel for GSC diversity can be studied.

• The energy harvesting technique is a promising solution for the battery limited devices which is widely used in the real-world applications of 5G and beyond networks [189]. Limited work has been done in the literature to investigate the effect of energy harvesting on the data rate of the system. In energy harvesting channels [190], transmitter is powered by energy harvested from a random exogenous energy source. The closed-form expressions of the ergodic capacity and P_{out} for energy harvesting protocols is well explored in [191]. In [192], The authors have modeled the harvesting of energy in terms of gamma distribution and the expression of P_{out} and CC are derived. Similar study like [192], need to be carried out for BX and FSF fading channels.

References

[1]   M. K. Simon and M. S. Alouini, Digital Communications over Fading Channels: A
        Unified Approach to Performance Analysis, 2nd ed., NY: John Wiley & Sons,
        2004.

[2]   M. Mirahmadi, A. Al-Dweik and A. Shami, "Interference modeling and
        performance evaluation of heterogeneous cellular networks," *IEEE Transactions on
        Communication,* vol. 62, no. 6, p. 2132–2144, 2014.

[3]   N. C. Beaulieu and X. Jiandong, "A novel fading model for channels with multiple
        dominant specular components," *IEEE Wireless Communications Letters,* vol. 4,
        no. 1, pp. 54-57, 2015.

[4]   J. Karmeshu and R. Agrawal, "On efficacy of Rayleigh-inverse Gaussian
        distribution over K-distribution for wireless fading channels," *Wireless
        Communications & Mobile Computing,* vol. 7, no. 1, p. 1–7, 2006.

[5]   T. S. Rappaport, Wireless Communication-Principle and Practice., Upper saddle
        River, New Jersy,: Prantice Hall PTR, 1996.

[6]   R. Singh, S. K. Soni, P. K. Verma and S. Kumar, "Performance Analysis of MRC
        Combiner Output in Log Normal Shadowed Fading, Proceeding of IEEE
        International Conference on Computing, Communication and Automation (ICCCA
        - 2015)".

[7]   D. Wu and R. Negi, "Effective capacity: A wireless link model for support of

quality of service," *IEEE Trans. Wireless Commun.,* vol. 2, no. 4, p. 630–643, 2003.

[8]   J. Singh, O. Dabeer and U. Madhow, "Capacity of the discrete-time AWGN channel under output quantization," in *IEEE International Symposium on Information Theory*, Toronto, ON, 2008.

[9]   C. Ling and J. C. Belfiore, "Achieving AWGN Channel Capacity With Lattice Gaussian Coding," *IEEE Transactions on Information Theory,* vol. 60, no. 10, pp. 5918-5929, 2014.

[10] M. S. Alouini and A. Goldsmith, "Capacity of Nakagami multipath fading channels," in *IEEE Veh. Technol.*, Phoenix, 97.

[11] W. C. Lee, "Estimate of channel capacity in Rayleigh fading environment," *IEEE Trans. Veh. Technol,* vol. 39, pp. 187-190, Aug. 1990.

[12] S. Kumar, S. K. Soni and P. Jain, "Micro-Diversity Analysis of Error Probability and Channel Capacity over Hoyt/Gamma Fading," *Radioengineering,* vol. 26, no. 4, pp. 1096-1103, 2027.

[13] S. Kumar, S. Soni and P. Jain, "Performance analysis of Hoyt-lognormal composite fading channel," in *International Conference on Wireless Communications, Signal Processing and Networking (WiSPNET)*, Chennai,India, 2017.

[14] P. M. Shankar, Fading and shadowing in wireless systems, 1st ed., NY: Springer,

2012.

[15] P. S. Chauhan, S. Kumar, S. K. Soni, V. K. Upaddhyay and D. Pant, "Average channel capacity over mixture Gamma distribution," in *International conference on Electrical & Electronics Engineering (ICE3-2020)*, 2020.

[16] R. Chile, S. Sawant and M. Chavan, "Multipath Fading Channel Modeling and Performance Comparison of Wireless Channel Models," *International Journal of Electronics and Communication Engineering.,* vol. 4, no. 2, pp. 189-203, 2011.

[17] L. Musavian, M. Rehmani and M. Amjad, "Effective Capacity in Wireless Networks: A Comprehensive Survey," *IEEE Communications Surveys & Tutorials, vol. 21, no. 4, pp. 3007-3038, Fourthquarter 2019, doi: 10.1109/COMST.2019.2929001..*

[18] P. Yadav, S. Kumar and R. Kumar, "A Comprehensive Survey of Physical-layer Security over Fading Channels: Classifications, Applications, and Challenges.," *Transaction on Emerging Telecommunication Technology,* p. e4270., 2021.

[19] A. Khisti, C. Xiao, G. Caire, K. Wong, X. Gao and Y. Wu, "A Survey of Physical Layer Security Techniques for 5G Wireless Networks and Challenges Ahead," *IEEE Journal on Selected Areas in Communications,* vol. 36, no. 4, pp. 679-695, April 2018.

[20] H. Chen, L. Wang and Y. Liu, "Physical layer security for next generation wireless networks: Theories, technologies, and challenges," *IEEE Commun. Surveys Tuts.,*

vol. 19, no. 1, p. 347–376, First Quarter 2017.

[21] A. Kak, S. Nie and I. Akyildiz, "6G and Beyond: The Future of Wireless Communications Systems," *IEEE Access,* vol. 8, pp. 133995-134030, 2020.

[22] D. Kwan Ng, W. Yu, E. G. Larsson, N. Al-Dhahir and R. Schober X.Chen, "Massive Access for 5G and Beyond," *arXiv:2002.03491,* 2020.

[23] P. S. Chauhan, V. Rana, S. Kumar, S. K. Soni and D. Pant, "Performance Analysis of Wireless Communication system over Non-identical Cascaded Generalised Gamma Fading Channels," *International Journal of Communication Systems,* vol. 32, no. 13, 2019.

[24] I. Ansari and M. Alouini, "Asymptotic Ergodic Capacity Analysis of Composite Lognormal Shadowed Channels," in *IEEE 81st Vehicular Technology Conference (VTC Spring)*, Glasgow, 2015.

[25] A. Laourine, S. Affes and A. Stephenne I. Trigui, "The Inverse Gaussian Distribution in Wireless Channels: Second-Order Statistics and Channel Capacity," *IEEE Transactions on Communications,* vol. 60, no. 11, pp. 3167-3173, 2012.

[26] P. Chauhan, S. Soni and D. Pant, "Error probability and channel capacity analysis of wireless system over inverse gamma shadowed fading channel with selection diversity," *International journal of communication system,* vol. 32, no. 16, p. e4083, 2019.

[27] A. Stephenne and S. Affes A. Laourine, "On the capacity of log-normal fading channels," *IEEE Transactions on Communications,* vol. 57, no. 6, pp. 1603-1607, 2009.

[28] I. M. Kostic, "Analytical approach to performance analysis for channel subject to shadowing and fading," *IEE Proceedings - Communications,* vol. 152, no. 6, pp. 821-827, 2005.

[29] M. S. Alouini, S. Affes, A. Stephenne and A. Laourine, "On the Performance Analysis of Composite Multipath/Shadowing Channels Using the G-Distribution," in *IEEE International Conference on Communications*, Beijing, 2008.

[30] M. Shu, Y. Wang, C. Zhang and C. Chen, "Outage probability analysis for MRC in κ-μ shadowed fading channels with co-channel interference," in *IEEE International Conference on Information and Automation (ICIA)*, Ningbo, 2016.

[31] H. Al-Hmood, "A mixture gamma distribution based performance analysis of switch and stay combining scheme over α-κ-μ shadowed fading," in *Proc. IEEE Annual Conf. on New Trends in Info. & Commun*, 2017.

[32] D. B. D. Costa and M. D. Yacoub, "Average Channel Capacity for Generalized Fading Scenarios," *IEEE Communications Letters,* vol. 11, no. 12, pp. 949-951, Dec 2007.

[33] G. Tombras, G. Karagiannidis and N. Sagias, "New results for the Shannon channel capacity in generalized fading channels," *IEEE Communications Letters,* vol. 9, no.

2, pp. 97-99, Feb 2005.

[34] A. M. Magableh and M. M. Matalgah, "Closed-form expressions for the average channel capacity of the α-µ Fading model under different adaptive transmission protocols," *Wireless communications and Mobile Computing,* vol. 15, no. 1, pp. 1-9, 2015.

[35] F. Yilmaz and M. Alouini, "A new simple model for composite fading channels: Second order statistics and channel capacity," in *7th International Symposium on Wireless Communication Systems*, 2010, pp. 676-680,.

[36] S. Soni, R. Raw, S. Kumar and R. Singh, "A New Approximate Closed-Form Distribution and Performance Analysis of a Composite Weibull/Log-Normal Fading Channel," *Wireless Pers Commun,* vol. 92, p. 883–900, 2017.

[37] T. Berger and J. Cheng, "Capacity of Nakagami-q (Hoyt) fading channels with channel side information," *International Conference on Communication Technology Proceedings ICCT,* vol. 2, pp. 1915-1918, 2003.

[38] P. Das, R. Ahmed, R. Subadar and N. Barman, "Channel Capacity of Adaptive Transmission Techniques over Rice (Nakagami-n) Fading Channels," *Advanced Research in Electrical and Electronic Engineering,* vol. 2, no. 13, pp. 18-21, 2015.

[39] P. C. Sofotasios and et al., "Capacity analysis under generalized composite fading conditions," in *International Conference on Advanced Communication Technologies and Networking (CommNet)*, Marrakech, 2018.

[40] A. Magableh, S. Mater and O. Badarneh T. Aldalgamouni, "Capacity analysis of $\alpha - \eta - \mu$ channels over different adaptive transmission protocols," *IET Communications,* vol. 11, no. 7, pp. 1114-1122, 2017.

[41] D. Da Costa, F. Lopez-Martinez and R. A. A. D. Souza J. M. Moualeu, "On the Performance of $\alpha - \eta - \kappa - \mu$ Fading Channels," *IEEE Communications Letters,* vol. 23, no. 6, pp. 967-970, 2019.

[42] M. Matthaiou, Z. Tan and H. Wang J. Zhang, "Performance Analysis of Digital Communication Systems Over Composite η–μ/Gamma Fading Channels," *IEEE Transactions on Vehicular Technology,* vol. 61, no. 7, pp. 3114-3124, 2012.

[43] N. Ermolova, V. Aalo and G. Efthymoglou, "Channel capacity and average error rates in generalised-K fading channels," *IET Communications,* vol. 4, no. 11, pp. 1364-1372, 2010.

[44] P. Chauhan, S. Soni, S. Naithani and D. Pant, "Channel Capacity Analysis of Wireless System under ORA scheme over κ–μ/Inverse Gamma and η–μ/Inverse Gamma Composite Fading Models," in *International Conference on Electrical and Electronics Engineering (ICE3)*, Gorakhpur, 2020.

[45] M. S. Alouini and A. J. Goldsmith, "Capacity of rayleigh fading channels under different adaptive transmission and diversity- combining techniques," *IEEE Transactions on Vehicular Technology,* vol. 48, no. 4, pp. 1165-1181, 1999.

[46] S. H. Oh, K. H. Li and W. S. Lee, "Performance of BPSK pre-detection MRC

systems over two-wave with diffuse power fading channels," *IEEE Transactions on Wireless Communications,* vol. 6, no. 8, p. 2772–2775, 2007.

[47]   M. Milisic, M. Hamza and M. Hadziliac, "BEP/SEP and outage performance analysis of L-branch maximal-ratio combiner for k-μ fading," *International Journal of Digital Multimedia Broadcasting,* pp. 1-8, 2009.

[48]   A. D. Singh and R. Subadar, "Capacity analysis of MRC receiver with adaptive transmitters over TWDP fading channels," in *IEEE International Symposium on Advance Computing and Communication (ISSAC)*, 2015.

[49]   M. Kaur and R. K. Yadav, "Performance analysis of Beaulieu-Xie fading channel with MRC diversity reception," *Transactions on Emerging Telecommunication Technologies,* vol. 31, no. 7, p. e3949, 2020.

[50]   S. Kumar, S. K. Soni and P. Jain, "Performance of MRC receiver over Hoyt-lognormal Composite Fading Channel," *Internation Journal of Electronics,* vol. 105, no. 9, pp. 1433-1450, 2018.

[51]   S. Kumar, S. Soni and P. Chauhan, "New approximate expressions of average symbol error probability, probability of detection and AUC with MRC over generic and composite fading channels," *AEU - International Journal of Electronics and Communications,* vol. 99, pp. 119-129, 2019.

[52]   D. Milovic, A. Mitic, M. Jakovljevic and M. Stefanovic, "Performance analysis of system with selection combining over correlated Weibull fading channels in the

presence of cochannel interference.," *AEU - Int. J. Electron. Communication,* vol. 62, no. 9, pp. 695-700, 2008.

[53] P. Mathiopoulos, S. Kotsopoulos and P. Bithas, "Diversity reception over generalized-K (KG) fading channels," *IEEE Transactions on Wireless Communications,* vol. 6, no. 12, pp. 4238-4243, Dec 2007.

[54] E. Salahat and M. Qasaimeh, "Unified Analytical Modeling of the Error Rates and the Ergodic Channel Capacity in η-μ Generalized Fading Channels with Integer μ and Maximal Ratio Combining Receiver," *https://arxiv.org/abs/1511.03039: Accessed Sep 2020.*

[55] M. D. Trott, S. Shamai and I. C. Abou-Faycal, "The capacity of discrete-time memoryless Rayleigh fading channels," *IEEE Trans. Inform. Theory,* pp. 1290-1301, 2001.

[56] M. Chowdhury and A. Goldsmith, "Capacity of block Rayleigh fading channels without CSI," *IEEE Int. Symp. Info. Theory,* pp. 1884-1888, July 2016.

[57] T. Marzetta and B. Hochwald, "Capacity of a mobile multiple-antenna communication link in Rayleigh flat fading," *IEEE Trans. Inf. Theory,* vol. 45, no. 1, pp. 139-157, 1999.

[58] X. Yang, "Capacity of Fading Channels without Channel Side Information," *https://arxiv.org/pdf/1903.12360.pdf,* 2019.

[59] A. Goldsmith and P. Varaiya, "Capacity of Fading Channels with Channel Side Information," *IEEE Transactions on Information Theory,* vol. 43, no. 6, pp. 1986-1992, 1997.

[60] J. Paris and D. Morales-Jimenez, "Outage probability analysis for Nakagami-q (Hoyt) fading channels under rayleigh interference," *IEEE Transactions on Wireless Communications,* vol. 9, no. 4, pp. 122-1276, April 2010.

[61] Chin Choy Chai and X. Dong Tjeng Thiang Tjhung, "Outage probability for lognormal-shadowed Rician channels," *IEEE Transactions on Vehicular Technology,* vol. 46, no. 2, pp. 400-407, 1997.

[62] A. Olutayo, H. Ma, J. Cheng and J. F. Holzman, "Level Crossing Rate and Average Fade Duration for the Beaulieu-Xie Fading Model," *IEEE Wireless Commun. Lett,* vol. 6, no. 3, pp. 326-329, 2017.

[63] P. S. Chauhan, S. Kumar and S. K. Soni, "On the Physical Layer Security over Beaulieu-Xie Fading Channel," *International Journal of Electronics and Communications,* vol. 113, no. 2020, p. 152940, 2020.

[64] A. Olutayo, J. Cheng and J. F. Holzman, "Asymptotically tight performance bounds for equal-gain combining over a new correlated fading channel," in *15th Canadian Workshop on Information Theory (CWIT)*, Quebec City, 2017.

[65] A. Olutayo, J. Cheng and J. F. Holzman, "Asymptotically tight performance bounds for selection diversity over Beaulieu-Xie fading channels with arbitrary

correlation," in *IEEE International Conference on Communications (ICC)*, Paris, 2017.

[66] D. Singh and H. D. Joshi, "Generalized MGF based analysis of line-of-sight plus scatter fading model and its applications to MIMO-OFDM systems," *AEU - International Journal of Electronics and Communications,* vol. 91, pp. 110-117, 2018.

[67] V. Kansal and S. Singh, "Analysis of effective capacity over Beaulieu-Xie fading model," in *IEEE International WIE Conference on Electrical and Computer Engineering (WIECON-ECE)*, Dehradun,, 2017.

[68] D. Singh and H. D. Joshi, "Error Probability Analysis of STBC-OFDM Systems with CFO and Imperfect CSI over Generalized Fading Channels," *International Journal of Electronics and Communications,* pp. 156-163, 2019.

[69] P. Yadav, S. Kumar and R. Kumar, "Analysis of EC over Gamma shadowed α–η–μ fading channel," in *IOP Conference series: Material Science & Engineering*, Nirjuli, India, 2021.

[70] P. Yadav, R. Kumar and S. Kumar, "Effective capacity analysis over α–κ–μ/Gamma composite fading channel," in *IEEE Internatational conference on advances in computing,communication control and networking (ICACCCN)*, Greater Noida, India, 2020.

[71] S. K. Yoo, S. Cotton, P. Sofotasios, M. Matthaiou, M. Valkama and G.

Karagiannidis, "The Fisher-Snedecor F distribution: A simple and accurate composite fading model," *IEEE Communication Letters,* vol. 21, no. 7, p. 1661–1664, 2017.

[72] H. Zhao, L. Yang, A. S. Salem and M. S. Alouini, "Ergodic Capacity Under Power Adaption Over Fisher-Snedecor F Fading Channels," *IEEE Communications Letters,* 2019.

[73] O. S. Badarneh, D. B. da Costa, P. C. Sofotasios, S. Muhaidat and S. L. Cotton, "On the Sum of Fisher–Snedecor F Variates and Its Application to Maximal-Ratio Combining," *IEEE Wireless Communications Letters,* vol. 7, no. 6, pp. 966-969, 2018.

[74] M. Kaur and R. K. Yadav, "Effective capacity analysis over Fisher-Snedecor F fading channels with MRC reception," *Wireless Personal Communications,* vol. 121, p. 693–1705, 2021.

[75] S. Kumar, "Energy Detection in Hoyt-Gamma Fading Channel with Micro-Diversity Reception," *Wireless Personal Communications,* vol. 101, no. 2, pp. 723-734, 2018.

[76] P. Yadav, S. Kumar and R. Kumar, "Effective capacity analysis over generalized lognormal shadowed composite fading channels," *Internet Technology Letters,* vol. 3, no. 5, p. e171, 2020.

[77] P. S. Chauhan, S. K. Kumar, V. K. Upadhayay and S. K. Soni, "Unified approach

to effective capacity for generalised fading channels," *Physical Communication,* vol. 45, p. 101278, 2021.

[78] F. Benkhelifa, Z. Rezki and M. S. Alouini, "Effective capacity of nakagami-m fading channels with full channel state information in the low power regime," in *IEEE 24th Annual Int Symp Personal, Indoor, and Mobile Radio Commun (PIMRC)*, 2013.

[79] S. K. Yoo, S. Cotton, P. Sofotasios, S. Muhaidat and G. Karagiannidis, "Effective capacity analysis over generalized composite fading channels," *IEEE Access,* vol. 8, pp. 123756-123764, 2020.

[80] L. Liu and J. Chamberland, "On the effective capacities of multiple-antenna Gaussian channels," in *IEEE International Symposium on Information Theory*, Toronto, 2008.

[81] M. Matthaiou, G. C. Alexandropoulos, H. Q. Ngo and E. G. Larsson, "Analytic framework for the effective rate of MISO fading channels," *IEEE Trans. Commun.,* vol. 60, no. 6, p. 1741–1751, 2012.

[82] Z. Ji, C. Dong, Y. Wang and J. Lu, "On the analysis of effective capacity over generalized fading channels," in *IEEE Int. Conf. Commu.(ICC)*, Sydney, 2014.

[83] X. B. Guo, L. Dong and H. Yang, "Performance analysis for effective rate of correlated MISO fading channels," *Electronics Letters,* vol. 48, no. 24, p. 1564–1565, 2012.

[84] M. You, H. Sun, J. Jiang and J. Zhang, "Effective rate analysis in Weibull Fading Channels," *IEEE Wireless Communication Letters,* vol. 5, no. 4, p. 340–343, 2016.

[85] J. Zhang, L. Dai, Z. Wang, D. Ng and W. Gerstacke, "Effective rate analysis of MISO systems over α-μ fading channels," in *Proc.Global Communications Conference (GLOBECOM)*, San Diego, CA, 2015.

[86] F. Yilmaz and M. Alouini, "A unified MGF-based capacity analysis of diversity combiners over generalized fading channels," *IEEE Trans.Commun.,* vol. 60, no. 3, p. 862–875, 2012.

[87] S. Y. Lien, C. C. Tseng, K. C. Chen and C. W. Su, "Cognitive radio resource management for QoS guarantees in autonomous femtocell networks," in *IEEE International Conference on Communications (ICC)*, 2010.

[88] S. Glisic, Z. Nikolic, N. Milosevic and P. Pirinn, "Effective capacity of advanced wireless cellular," *IEEE 16th International Symposium on Personal Indoor and Mobile Radio Communications,* vol. 4, p. 2771–2780, 2005.

[89] S. Xiangquna and C. Qingxin, "Effective capacity of cognitive radio systems in asymmetric fading channels," *The Journal of China Universities of Posts and Telecommunications,* vol. 22, no. 3, pp. 18-25, June 2015.

[90] M. J. Piran, Q. Pham, S. Riazul Islam, S. Cho, B. Bae, D. Suh and Z. Han, "Multimedia communication over cognitive radio networks from QoS/QoE perspective: A comprehensive survey," *Journal of Network and Computer*

Applications, vol. 172, 2020.

[91] X. Zhang and Q. Du, "Cross-layer modeling for QoS-driven multimedia multicast/broadcast over fading channels in advances in mobile multimedia," *IEEE Communications Magazine,* vol. 45, no. 8, pp. 62-75, 2007.

[92] A. Khalek and Z. Dawy, "Energy-efficient cooperative video distribution with statistical QoS provisions over wireless networks," *IEEE Trans.Mobile Comput.,* vol. 11, no. 7, p. 1223–1236, 2012.

[93] A. Balasubramanian and S. Miller, "The effective capacity of a time division downlink scheduling system," *IEEE Trans. Commun.,* vol. 58, no. 1, p. 73–78, 2010.

[94] S. Agarwal, S. De, S. Kumar and H. Gupta, "QoS-aware downlink cooperation for cell-edge and handof users," *IEEE Trans. Veh. Technol.,* vol. 64, no. 6, p. 2512–2527, 2015.

[95] D. Qiao, M. Gursoy and S. Velipasalar, "Effective capacity of two hop wireless communication systems," *IEEE Trans. Inf. Theory,* vol. 59, no. 2, p. 873–885, 2013.

[96] Q. Wang, P. Fan, D. O. Wu and K. B. Letaief, "End-to-end delay constrained routing and scheduling for wireless sensor networks," in *IEEE International Conference on Communications (ICC)*, 2011.

[97] Y. Chen and I. Darwazeh, "End-to-end delay performance analysis in IEEE 802.16j mobile multi-hop relay (mmr) networks," *International Conference on Telecommunications,,* pp. 488-492, 2011.

[98] Q. Du, Y. Huang, P. Ren and C. Zhang, "Statistical Delay Control and QoS-Driven Power Allocation over Two-Hop Wireless Relay Links," in *IEEE Global Telecommunications Conference - GLOBECOM*, Houston, TX, USA, 2011.

[99] Y. Chen and I. Darwazeh, "An estimator for delay distributions in distributions in packet-based wireless digital communication systems,," in *An estimator for d IEEE Wireless Communications and Networking Conference (WCNC)*, Shanghai, 2013.

[100] X. Zhang and J. Wang, "Heterogeneous QoS-Driven Resource Allocation over MIMO-OFDMA Based 5G Cognitive Radio Networks," in *IEEE Wireless Communications and Networking Conference (WCNC)*, San Francisco, CA, 2017.

[101] J. Wang and X. Zhang, "Statistical QoS-driven cooperative power," in *Wireless Communications and Networking Conference (WCNC), 2017,pp. 1-6.*

[102] Y. Chen, I. Darwazeh, N. Philip and R. Istepanian, "End-to-end delay distributions in wireless tele-ultrasongraphy medical systems," in *IEEE Global Communications Conference*, GA, USA, 2013.

[103] M. You, X. Mou and H. Sun, "Effective capacity analysis of smart grid communication networks," in *International workshop on computer aided modelling and design of communication links and networks*, Guildford, UK, 2015.

[104] W. Liang, Z. Li, H. Zhang, S. Wang and R. Bie, "Vehicular Ad Hoc Networks: Architectures, Research Issues, Methodologies, Challenges, and Trends," *International Journal of Distributed Sensor Networks,* vol. 11, no. 8, pp. 1-4, 2014.

[105] V. Khairnar and K. Kotecha, "Performance of Vehicle-to-Vehicle Communication using IEEE 802.11p in Vehicular Ad-hoc Network Environment," *International Journal of Network Security & Its Applications (IJNSA),* vol. 5, no. 2, pp. 143-170, Mar 2013.

[106] O. A. Saraereh, A. Ali, I. Khan and K. Rabie, "Interference Analysis for Vehicle-to-Vehicle Communications at 28 GHz," *Electronics,* vol. 262, no. 9, 2020.

[107] R. Verdone, "Outage probability analysis for short-range communication systems at 60 GHz in ATT urban environments," *IEEE Transactions on Vehicular Technology,* vol. 46, no. 4, pp. 1027-1039, Nov,1997.

[108] X. He, W. Shi and T. Luo, "Transmission Capacity Analysis for Vehicular Ad Hoc Networks," *IEEE Access,* vol. 6, pp. 30333-30341, 2018.

[109] K. Eshteiw, G. Kaddoum, K. B. Fredj and E. Soujer, "Performance Analysis of Full-Duplex Vehicle Relay-Based Selection in Dense Multi-Lane Highways," *IEEE Access,* vol. 7, pp. 61581-61595, 2019.

[110] C. Valdivieso, F. Novillo, J. Gomez and D. Dik, "Performance Evaluation of Channel Capacity in Wireless Sensor Networks using ISM band in Dense Urban Scenarios," in *IEEE Ecuador Technical Chapters Meeting (ETCM)*, Ecuador, 2016.

[111] D. Hassan, Y. Kirsal and S. Redif, "Channel capacity improvement for cooperative MIMO wireless sensor networks via adaptive MIMO-SVD," in *2016 HONET-ICT, pp. 49-53*, 2016.

[112] M. Ahmad, E. Dutkiewicz and X. Huang, "Performance analysis of MAC protocol for cooperative MIMO transmissions in WSN," in *Proceedings of International Symposium on Personal, Indoor and Mobile Radio Communications*, France, 2008.

[113] V. K. Sachan, S. A. Imam and M. T. Beg, "Performance analysis of STBC encoded cooperative MIMO system for wireless sensor networks," in *IEEE International Conference on Signal Processing, Computing and Control*, Waknaghat Solan, 2012.

[114] D. Puccinelli and M. Haenggi, "Multipath fading in wireless sensor networks: measurements and interpretation," in *Proceedings of the International Conference on Wireless Communications and Mobile Computing, IWCMC 2006, July 3-6, 2006*, Vancouver, British Columbia, Canada, 2016.

[115] T. Shi and X. Lv, "Transmission performance analysis of wireless sensor networks under complex railway environment," *29th Chinese Control And Decision Conference (CCDC),* pp. 2970-2947, 2017.

[116] M. Torabi and D. Haccoun, "Capacity Analysis of Opportunistic Relaying in Cooperative Systems with Outdated Channel Information," *IEEE Communications Letters,,* vol. 14, no. 12, pp. 1137-1139, Dec 2010.

[117] N. C. Beaulieu and J. Hu, "A closed-form expression for the outage probability of decode-and-forward relaying in dissimilar Rayleigh fading channels," *EEE Communications Letters,* vol. 10, no. 12, pp. 813-815, Decm 2006.

[118] I. Lee and D. Kim, "BER analysis for decode-and-forward relaying in dissimilar Rayleigh fading channels," *IEEE Communications Letters,* vol. 11, no. 1, pp. 52-54, Jan 2007.

[119] Z. Sun, I. F. Akyildiz and G. P. Hancke, "Capacity and Outage Analysis of MIMO and Cooperative Communication Systems in Underground Tunnels," *IEEE Transactions on Wireless Communication,* vol. 10, no. 11, pp. 3793-3803, Nov 2011.

[120] W. Gheth, A. Alfitouri, K. Rabie, B. Adebisi and K. Hamdi, "Performance Analysis of Cooperative Diversity in Multi-user Environments," in *8th International Conference on Modeling Simulation and Applied Optimization (ICMSAO), Manama, Bahrain, 2019,*.

[121] I. Dimitriou and N. Pappas, "Performance Analysis of a Cooperative Wireless Network with Adaptive Relays," [Online]. Available: https://arxiv.org/abs/1710.05748. [Accessed Sep 2020].

[122] T. R. Rasethuntsa, M. Kaur, S. Kumar, P. S. Chauhan and K. Singh, "On the performance of DF-based multi-hop system over $\alpha - \kappa - \mu$ and $\alpha - \kappa - \mu$-extreme fading channels," *Digital Signal Processing,* vol. 109, p. 102909, 2021.

[123] T. R. Rasethuntsa, M. Kaur and S. Kumar, "On the Outage probability and BER of a DF based multi-hop system over α–κ–µ and α–κ–µ Extreme Fading Channels," *International Journal of Electronics and Communications,* vol. 124, p. 153324, 2020.

[124] H. Venkataraman and G.-M. Muntean, Cognitive Radio and its Application for Next Generation Cellular and Wireless Networks, Springer Netherlands, 2012.

[125] M. Premkumar and M. Chitra, "Analysis of Cognitive Radio Capacity in Fading Channels," *International Journal of Wireless Communications and Mobile Computing,* vol. 6, no. 1, pp. 31-36, 2018.

[126] M. Khoshafa and S. Al-Ahmadi, "On the Capacity of Underlay Cognitive Radio Networks Over Shadowed Multipath Fading Channels," *Arabian Journal for Science and Engineering,* vol. 42, p. 5191–5199, 2017.

[127] S. Kumar, "Performance of ED based spectrum sensing over α–η–µ fading channel," *Wireless Personal Communications,* vol. 100, no. 4, pp. 1845-1857, 2018.

[128] P. S. Chauhan, S. Kumar, V. K. Upaddhyay, R. Mishra, B. Kumar and S. K. Soni, "Performance Analysis of ED over Air-to-Ground and Ground-to-Ground Fading Channels: A Unified and Exact Solution," *International Journal of Electronics and Communications,* p. 153839, 2021.

[129] T. R. Rasethuntsa and S. Kumar, "An Integrated Performance Evaluation of ED-

Based Spectrum Sensing over α–κ–μ and α–κ–μ Extreme Fading Channels," *Transaction on Emerging Telecommunication Technology,* vol. 30, no. 5, p. e3569, 2019.

[130] S. Kumar, P. S. Chauhan, P. Raghuwanshi, M. Kaur and K. Singh, " ED performance over α–η–μ/IG and α–κ–μ/IG generalized fading channels with diversity reception and cooperative sensing," *A unified approach International Journal of Electronics and Communications,* vol. 97, pp. 273-279, 2018.

[131] S. Kumar, M. Kaur, S. K. Singh, K. Singh and P. S. Chauhan, ", Energy Detection based Spectrum Sensing for Gamma Shadowed α–η–μ and α–κ–μ Fading Channels," *International Journal of Electronics and Communications,* vol. 93, pp. 26-31, 2018.

[132] S. Kumar, P. K. Verma, M. Kaur, S. K. Soni and P. Jain, "Performance Evaluation of Energy Detection over Hoyt/gamma Channel with MRC Reception," *Journal of Electromagnetic Waves and Applications,* vol. 32, no. 16, pp. 2157-2166, 2018.

[133] M. Kim and J. Lee, "Outage Probability of UAV Communications in the Presence of Interference," in *2018 IEEE Global Communications Conference (GLOBECOM)*, Abu Dhabi, United Arab Emirates, 2018.

[134] N. Goddemeier and C. Wietfeld, "Investigation of Air-to-Air Channel Characteristics and a UAV Specific Extension to the Rice Model," in *2015 IEEE Globecom Workshops (GC Wkshps)*, San Diego, CA, 2015.

[135] Z. Chen, Y. Hu and X. Gao, "Analysis of Unmanned Aerial Vehicle MIMO Channel Capacity Based on Aircraft Attitude," *WSEAS Transactions on Information Science and Applications,* vol. 10, no. 2, pp. 58-67, Feb 2013.

[136] M. Noori, M. Madani and M. Tarihi, "Improving the Performance of HALE UAV Communication Link Through MIMO Cooperative Relay Strategy," *Wireless Personal Communications,* vol. 113, p. 1051–1071, May 2020.

[137] H. Khalid, S. S. Muhammad and H. E. Nistazakis, "Performance Analysis of Hard-Switching Based Hybrid FSO/RF System over Turbulence Channels," *Computation,* vol. 7, no. 28, pp. 1-10, 2019.

[138] W. Shakir, "Performance evaluation of a selective combining scheme for the hybrid FSO/RF system," *IEEE Photonics ,* vol. 10, pp. 1-10, 2018.

[139] T. Rakia, H. Yang, M. Alouini and F. Gebali, "Outage analysisof practical FSO/RF hybrid system with adaptive combining," *IEEE Commun. Lett. 2015, 19, ,* vol. 19, p. 1366–1369., 2015.

[140] M. A. Amirabadi, "Performance Analysis of a Novel Hybrid FSO/RF Communication System," [Online]. Available: https://arxiv.org/ftp/arxiv/papers/1802/1802.07160.pdf..

[141] A. A. Thabit, M. S. Mahmoud and A. Alkhayyatand, "Energy harvesting Internet of Things health-based paradigm: Towards outage probability reduction through inter–wireless body area network cooperation," *Internation Journal of Distributed*

Sensor Networks, vol. 15, no. 10, pp. 1-12, 2019.

[142] A. Guidotti, B. Evans and M. Renzo, "Integrated satellite-terrestrial networks in future wireless systems," *International Journal of Satellite Communication and Networking,* vol. 37, no. 2, pp. 73-75, 2019.

[143] Y. Zhao, L. Xie, H. Chen and K. Wang, "Ergodic channel capacity analysis of the hybrid satellite-terrestrial single frequency network," in *IEEE 26th Annual International Symposium on Personal, Indoor, and Mobile Radio Communications (PIMRC)*, Hong Kong, 2015.

[144] Z. Lin, M. Lin, Q. Huang, J. Ouyung and G. Cheng, "Outage Probability Analysis for Hybrid Satellite and Terrestrial Network with Different Combining Schemes," *WiSATS , LNICST,* vol. 281, p. 488–496, 2019.

[145] K. An, J. Ouyang, M. Lin and T. Liang, "Outage analysis of multi-antenna cognitive hybrid satellite-terrestrial relay networks with beamforming.," *IEEE Commun. Letter,* vol. 19, no. 7, pp. 1157-1160, 2015.

[146] N. I. Miridakis, D. D. Vergados and A. Michalas, "Dual-hop communication over a satellite relay and shadowed Rician channels," *IEEE Trans. Vehicular Technology,* vol. 64, no. 9, p. 4031–4040, 2015.

[147] L. Zhao, T. Liang and K. An, "Performance Optimization of Hybrid Satellite-Terrestrial Relay Network Based on CR-NOMA," *Sensors (Basel).,* vol. 20, no. 18, pp. 1-14, Sep 2020.

[148] I. S. Gradshteyn and I. M. Ryzhik, Table of Integrals, Series, and Products, 7th ed., Elsevier: Academic Press, 2007.

[149] M. Abramowitz and I. Stegun, Handbook of Mathemathical Functions with Formulas, Graphs and Mathematical Tables, 10th ed. ed., Dover Publications, 1972.

[150] J. Paris, "Statistical characterization of κ–μ shadowed fading.," *IEEE Trans Veh Technol.,* vol. 63, no. 2, pp. 518-526, 2014.

[151] Wolfram, Dec. 2021. [Online]. Available: http://functions.wolfram.com/PDF/MeijerG.pdf.

[152] T. R. Rasethuntsa, S. Kumar and M. Kaur, "A comprehensive performance evaluation of a DF-based multi-hop system Over α–κ–μ and α–κ–μ-extreme fading channels," 2019. [Online]. Available: https://arxiv.org/abs/1903.09353. [Accessed December 30,2019].

[153] V. Khandelwal and Karmeshu, "A New Approximation for Average Symbol Error Probability over Log-Normal Channels," *IEEE Wireless Communications Letters,* vol. 3, no. 1, pp. 58-61, Feb. 2014.

[154] R. Subadar and A. D. Singh, "Performance of M-MRC receivers over TWDP fading channels," *International Journal of Electronics and Communications,* vol. 68, p. 569–572, 2014.

[155] A. P. Prudnikov, Y. A. Brychkov and O. I. Marichev, Integrals and series: more special functions, vol. 3 ed., New York: Gordon & Breach Sci. Publ., 1990.

[156] M. Kang and M. Alouini, "Capacity of MIMO Rician channels," *IEEE Transactions on wireless communications,* vol. 5, no. 1, pp. 112-122, 2006.

[157] M. You, H. Sun, J. Jiang and J. Zhang, "Unified Framework for the Effective Rate Analysis of Wireless Communication Systems Over MISO Fading Channels," *IEEE Transactions on Communications,* vol. 65, no. 4, pp. 1775-1785, 2017.

[158] V. Adamchik and O. Marichev, "The algorithm for calculating integrals of hypergeometric type functions and its realization in REDUCE system," in *International Conference on Symbolic and Algebraic Computation*, New York (USA), 1990.

[159] A. P. Prudnikov and Y. A. Brychkov, Integrals and Series Volume 3, More Special Functions, 1st ed., Amsterdam: Gordon and Breach Science Publishers, 1986.

[160] P. S. Chauhan, S. Kumar and I. S. Ansari, "On the Integral and Derivative Identities of Bivariate Fox H-Function: Application in Wireless System Performance Analysis," arXiv, 2022. [Online]. Available: 10.48550/arXiv.2208.08642. [Accessed 20 9 2022].

[161] M. Matthaiou and C. Zhong, "Low-SNR analysis of MIMO Weibull fading channel," *IEEE Communications Letters,* vol. 16, no. 5, pp. 694-697, 2012.

[162] P. Yadav, S. Kumar and R. Kumar, "A Review of Transmission Rate over Wireless Fading Channels: Classifications, Applications, and Challenges," *Wireless Personal Communications,* vol. 122, p. 1709–1765, 2022.

[163] E. Larsson, O. Edfors, F. Tufvesson and T. Marzetta, "Massive MIMO for next generation wireless systems," *IEEE Communications Magazine,* vol. 52, no. 2, p. 186–195, 2014.

[164] Q. Wu and R. Zhang, "Towards smart and reconfigurable environment: Intelligent reflecting surface aided wireless network," *IEEE Communications Magazine,* vol. 58, no. 1, p. 106–112, 2019.

[165] T. Hou, Y. Liu, Z. Song, X. Sun, Y. Chen and L. Hanzo, "Reconfigurable intelligent surface aided NOMA networks," *IEEE Journal on Selected Areas in Communications,* vol. 38, no. 11, p. 2575–2588, 2020.

[166] C. Pan, H. Ren, K. Wang, M. Elkashlan, A. Nallanathan, J. Wang and L. Hanzo, "Intelligent reflecting surface aided MIMO broadcasting for simultaneous wireless information and power transfer," *IEEE Journal on Selected Areas in Communications,* vol. 38, no. 8, p. 1719–1734, 2020.

[167] L. Yang, J. Yang, W. Xie, M. Hasna, T. Tsiftsis and M. Di Renzo, "Secrecy performance analysis of RIS-aided wireless communication systems," *IEEE Transactions on Vehicular Technology,* vol. 69, no. 10, p. 12296–12300, 2020.

[168] S. Kumar, P. Yadav, M. Kaur and R. Kumar, "A survey on IRS NOMA Integrated

Communication Networks," *Telecommunication Systems,* vol. 80, p. 277–302, 2022.

[169] L. Yang, W. Guo and I. Ansari, "Mixed dual-hop FSO-RF communication systems through reconfigurable intelligent surface," *IEEE Communications Letters,* vol. 24, no. 7, p. 1558–1562, 2020.

[170] S. Li, B. Duo, X. Yuan, Y.-C. Liang and M. Di Renzo, "Reconfigurable intelligent surface assisted UAV communication: Joint trajectory design and passive beamforming," *IEEE Wireless Communications Letters,* vol. 9, no. 5, p. 716–720, 2020.

[171] K. Odeyemi, P. A. Owolawi and O. O. Olakanmi, "Reconfigurable intelligent surface assisted mobile network with randomly moving user over fisher-snedecor fading channel.," *Physical Communication,* vol. 43, p. 101186, 2020.

[172] E. Basar, M. Renzo, J. Rosny, M. Debbah, M. Alouini and R. Zhang, "Wireless Communications Through Reconfigurable Intelligent Surfaces,," *IEEE Access,* vol. 7, pp. 116753-116773, 2019.

[173] E. Basar, "Reconfigurable Intelligent Surface-Based Index Modulation: A New Beyond MIMO Paradigm for 6G," *IEEE Transactions on Communications,* vol. 68, no. 5, pp. 3187-3196, 2020.

[174] H. Ibrahim, H. Tabassum and U. Nguyen, "Exact coverage analysis of intelligent reflecting surfaces with Nakagami-m channels," *IEEE Trans. Veh. Technol.,* vol.

70, no. 1, p. 1072–1076, 2021.

[175] M. Kaur and R. Yadav, "EC Analysis of Multi-Antenna system over 5G and beyond networks and its Application to IRS-Assisted Wireless systems," *Wireless Pers Commun,* vol. accepted, 2022.

[176] D. Kudathanthirige, D. Gunasinghe and G. Amarasuriya, "Performance analysis of intelligent reflective surfaces for wireless communication," in *ICC 2020-2020 IEEE Int. Conf. Commun. (ICC)*, 2020.

[177] A. Boulogeorgos and A. Alexiou, "Ergodic capacity analysis of reconfigurable intelligent surface assisted wireless systems," in *2020 IEEE 3rd 5G World Forum (5GWF)*, 2020.

[178] A. Boulogeorgos and A. Alexiou, "Performance analysis of reconfigurable intelligent surface-assisted wireless systems and comparison with relaying," *IEEE Access,* vol. 8, p. 94 463–94 483, 2020.

[179] L. Yang, F. Meng, D. Wu, D. Benevides da Costa and M. Alouini, "Accurate closed-form approximations to channel distributions of RIS-aided wireless systems," *IEEE Wireless Commun.Lett.,* vol. 9, no. 11, p. 1985–1989, 2020.

[180] Q. Tao, J. Wang and C. Zhong, "Performance analysis of intelligent reflecting surface aided communication systems," *IEEE Commun. Lett.,* vol. 24, no. 11, p. 2464–2468, 2020.

[181] R. Ferreira, M. Facina, F. A. Figueiredo, G. Fraidenraich and E. De Lima, "Bit error probability for large intelligent surfaces under double-Nakagami fading channels," *IEEE Open J. Commun. Society,* vol. 1, p. 750–759, 2020.

[182] D. Selimis, K. Peppas, G. Alexandropoulos and F. Lazarakis, "On the performance analysis of RIS-empowered communications over Nakagami-m fading," *IEEE Commun. Lett.,* vol. 25, no. 7, pp. 2191-2195, 2021.

[183] W. Trigui, Ajib and W.-P. Zhu, *A comprehensive study of reconfigurable intelligent surfaces in generalized fading,* arXiv: 2004.02922, 2020.

[184] L. Kong, Y. Ai, S. Chatzinotas and B. Ottersten, "Effective rate evaluation of RIS-assisted communications using the sums of cascaded a-u random variates," *IEEE Access,* vol. 9, p. 5832–5844, 2021.

[185] H. Du, J. Zhang, J. Cheng, Z. Lu and B. Ai, "Millimeter wave communications with reconfigurable intelligent surfaces: Performance analysis and optimization," *IEEE Trans. Commun.,* vol. 69, no. 4, pp. 2752–2768,, 2021.

[186] H. Du, J. Zhang, K. Guan, B. Ai and K. Thomas, "Reconfigurable intelligent surface aided TeraHertz communications under misalignment and hardware impairments," 2020. [Online]. Available: arXiv: 2012.00267.

[187] A. Salhab and L. Yang, "Mixed RF/FSO Relay Networks: RIS-Equipped RF Source vs RIS-Aided RF Source," *IEEE Wireless Communications Letters,* vol. 10, no. 8, pp. 1712-1716, 2021.

[188] M. Kaur and R. Yadav, "Data rate over different applications in 5G and beyond Networks," in *Second International Conference on Electronics and Sustainable Communication Systems (ICESC)*, 2021.

[189] S. Kumar and P. Yadav, "Energy Harvesting–Based Architecture in IoT," *Energy Harvesting,* pp. 1-18, doi:10.1201/9781003218760-1, 2022.

[190] J. Gómez-Vilardebó, "Competitive Design of Energy Harvesting Communications in Wireless Fading Channels," *IEEE/ACM Transactions on Networking,* vol. 25, no. 6, pp. 3863-3872, 2017.

[191] K. Rabie, A. Salem, E. Alsusa and M. Alouini, "Energy-harvesting in cooperative AF relaying networks over log-normal fading channels," in *IEEE International Conference on Communications (ICC)*, Kuala Lumpur, 2016.

[192] I. Castro, L. Landesa and A. Serna, "Modeling the Energy Harvested by an RF Energy Harvesting System Using Gamma Processes," *Mathematical Problems in Engineering,* vol. 2019, pp. 1-12, 2019.

AUTHOR BIOGRAPHY

Manpreet KAUR received her B. Tech. in Electronics and Communication Engineering from Punjab Technical University, Punjab, India in 2005 and Master of Engineering in Electronics and Communication from Thapar University, Patiala, India in 2007. She has completed her PhD. From Delhi Technological University, Delhi, India in 2023. She is currently working as Member (Senior Research Staff) at Central Research Laboratory, Bharat Electronics Limited, Ghaziabad. She has more than 15 years of experience in the field of research and development. She has received various awards and certificates of appreciation for her research activities. She is serving as a reviewer for IEEE, Elsevier and Springer journals etc. She has also served as a technical chair and member of technical programme committee of various reputed international conferences. Her research interest includes the wireless communication and cognitive radios networks and 5G and beyond technologies and AI-enabled communication systems etc.